SYNTHESIS OF CATALYTICALLY IMPORTANT MANGANESE OXIDE NANO-PARTICLES AND THEIR DISPERSION INTO A POLYMERIC MATRIX
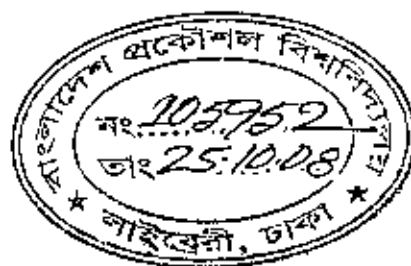
BY

MD SHAFIUL AZAM

SUBMITTED IN PARTIAL FULFILLMENT OF THE
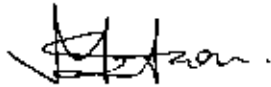REQUIREMENT FOR THE DEGREE OF
M.PHIL. IN CHEMISTRY

DEPARTMENT OF CHEMISTRY

BANGLADESH UNIVERSITY OF ENGINEERING AND
TECHNOLOGY (BUET)
DHAKA-1000, BANGLADESH
MAY 2008

Candidate's Declaration

It is hereby declared that this thesis or any part of it has not been submitted elsewhere for the award of any degree or diploma.
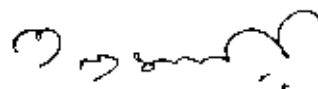
_____

Signature of the Candidate

Md. Shafiul Azam

Name of the Candidate

CERTIFICATE

This is to certify that the research work embodying in this thesis has been carried out under my supervision. The work presented herein is original. This thesis has not been submitted elsewhere for the award of any other degree or diploma in any university or institution.

Dr. Al-Nakib Chowdhury
(Supervisor)
Professor
Department of Chemistry
BUET, Dhaka
Bangladesh

Acknowledgement

During the preparation and completion of this thesis I had the distinctive opportunity to work under the supervision of Dr. Al-Nakib Chowdhury, Professor, Department of Chemistry, Bangladesh University of Engineering & Technology (BUET), Dhaka, to whom I owe my profound gratitude for his stimulating inspiration, astute guidance, keen interest, worthy criticism and wise advices. His deep concern and valuable suggestions throughout this research work inspired me to face problems with confidence.

My gratitude and thanks are also to Prof. Dr. Md. Wahab Khan, Head, Department of Chemistry, BUET, for his kind assist and encouragement in all respects. I am also thankful to Dr. Md. Abdur Rashid, Professor, Dr. Md. Nazrul Islam, Assistant Professor, and Mr. Nurul Islam, Retired Assistant Professor, Department of Chemistry, BUET, Dr Qamrul Ahsan, Professor, Department MME, BUET, Professor Munirul Alam, ICDDR,B, Dhaka and Dr. Sheikh Manjura Haque, Atomic Energy Centre, Dhaka, for their kind help and constant co-operation in different stages of my research work. My thanks to Mr. Md. Yousuf Khan, Instrument Engineer, Department of MME, BUET for his tireless cooperation in taking SEM of my samples. I am also grateful to other teachers and staff of Chemistry department, BUET, Dhaka.

It will not be out of place to put on record the love, friendliness and care that I received from my wife whose sacrifices and inspiration came to my succor in all-trying moments during the completion of this work. Special mention is made of my

parents, sisters, brothers and other relatives for their generous support, constant inspiration and encouragement during the progress of my research work.

I would like to extent my thanks to Mr. Abdur Rahim, Mr. Saiful Islam, Ms Hoore Jannat, Ms Kamrunnahar, Mr Yousuf Jamal and other fellows who shared me to solve all the problems confronted in the whole thesis period.

I am grateful to the authority of BUET for providing financial support for this research work.

Let me end by paying unqualified tribute to my creator whose directions and blessings had been with me throughout the completion of this work as in all matters of my life and so praise be to Allah, the most beneficent and the merciful.

<div align="right">

Md. Shafiul Azam
Author

</div>

Bangladesh University of Engineering and Technology, Dhaka
Department of Chemistry

Certification of Thesis
A thesis on

"SYNTHESIS OF CATALYTICALLY IMPORTANT MANGANESE OXIDE NANO-PARTICLES AND THEIR DISPERSION INTO A POLYMERIC MATRIX"
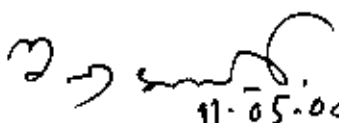
BY
MD SHAFIUL AZAM

has been accepted as satisfactory in partial fulfillment of the requirements for the degree of Master of Philosophy (M.Phil) in Chemistry and certify that the student has demonstrated a satisfactory knowledge of the field covered by this thesis in an oral examination held on May 11, 2008.

Board of Examiners

1. **Dr. Al-Nakib Chowdhury**
   Professor
   Department of Chemistry
   BUET, Dhaka

   _11·05·08_
   Supervisor & Chairman
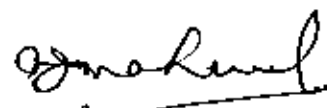
2. **Dr. Md. Wahab Khan**
   Professor & Head
   Department of Chemistry
   BUET, Dhaka

   _11. 5. 08_
   Member (Ex-officio)

3. **Dr. Md. Manwarul Islam**
   Professor
   Department of Chemistry
   BUET, Dhaka

   _11. 05. 08_
   Member

4. **Dr. Abu Jafar Mahmood**
   Supernumerary Professor
   Department of Chemistry
   University of Dhaka, Dhaka

   Member (External)

Contents

LIST OF TABLES

LIST OF FIGURES

ABSTRACT

Mn_3O_4 nanoparticles were prepared by forced hydrolysis of aqueous manganese(II) acetate, $Mn(OOCCH_3)_2$, solution. Starch was used as capping agent to prevent the agglomeration of the nanoparticles thus formed in the colloidal mixture. 0.4 M $Mn(OOCCH_3)_2$ precursor in saturated aqueous solution of starch was aged for 2, 6, and 12 h at a temperature 80 °C . The nanoparticles were then collected by reducing the volume of suspension on mild heating followed by ethanol extraction. The more uniform and well-dispersed particles were obtained by heating the reaction mixture for 2 h. The nanoparticles thus obtained were characterized by means of EDX, XRD, IR, and SEM. The results showed that the Mn_3O_4 nanoparticles were single phase, spherical, and uniformly dispersed. The average crystallite size was calculated from the XRD data to be approximately 10 nm.

Polyaniline (PANI) was synthesized from aniline by using potassium dichromate, $K_2Cr_2O_7$, as an oxidizing agent. The dispersion of the Mn_3O_4 nanoparticles into PANI matrix was achieved by the addition of nanoparticles suspension to the sediment of PANI. The conductivity of the PANI/Mn_3O_4 matrix was measured to be 20.82×10^{-6} Scm^{-1} and found to be higher than that of PANI, 3.72×10^{-6} Scm^{-1}.

Mn_3O_4 nanoparticles were tested to perform the polymerization of aniline instead of conventional chemical polymerization by an oxidant. The nanoparticles can effectively polymerize aniline to yield PANI. The PANI thus prepared was found to be more conductive because of its compact and modified morphology as seen from SEM.

The efficiency of the Mn_3O_4 nanoparticles on the decolorization of methylene blue (MB) dye has been studied in presence of H_2SO_4. Effect of MB concentration, amount of nanoparticles required, influence of acid concentration, and function of time on MB decolorization were also investigated by employing UV-Visible spectroscopy. It was found from these investigations that Mn_3O_4 nanoparticles can efficiently and rapidly decolorize MB in adequately acidic media.

The Mn_3O_4 nanoparticles was also successfully employed to decolorize another textile dye procion red (PR) and an industrial dye effluent. UV-Visible spectra of the solutions were taken in all cases to measure the extent of decolorization.

Sensitivity of the Mn_3O_4 nanoparticles suspension was tested on various pathogenic organisms at two different pH, 3.3 and 6.2. The nanoparticles were found to be sensitive against *Vibrio cholerae*, *Shigella sp.*, *Salmonella sp.*, and *Escherichi coli* bacteria, which are responsible for cholera, dysentery, typhoid, and diarrhoea diseases, respectively.

Chapter 1

INTRODUCTION

1.1 Nanomaterials
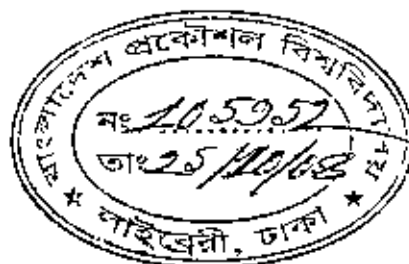
1.1.1 Fundamental Concepts

Nanotechnology is expected to be the basis of many of the main technological innovations of the 21st century. Research and development in this field is growing rapidly throughout the world. A major output of this activity is the development of new materials in the nanometer scale, including nanoparticles. A unique aspect of nanotechnology is the vastly increased ratio of surface area to volume present in many nanoscale materials which opens new possibilities in surface-based science, such as catalysis. A number of physical phenomena become noticeably pronounced as the size of the system decreases. These include statistical mechanical effects, as well as quantum mechanical effects, for example the "quantum size effect" where the electronic properties of solids are altered with great reductions in particle size. This effect does not come into play by going from macro to micro dimensions. However, it becomes dominant when the nanometer size range is reached.

Materials reduced to the nanoscale can suddenly show very different properties compared to what they exhibit on a macroscale, enabling unique applications. For instance, opaque substances become transparent (copper); inert materials become catalysts (platinum); stable materials turn combustible (aluminum); solids turn into liquids at room temperature (gold); insulators become conductors (silicon). Materials such as gold, which is chemically inert at normal scales, can serve as a potent chemical catalyst at nanoscales. Much of the fascination with nanotechnology stems from these unique quantum and surface phenomena that matter exhibits at the nanoscale.

A nanoparticle (which historically has included nanopowder, nanocluster, and nanocrystal) is a small particle with at least one dimension less than 100 nm. This definition can be fleshed out further in order to remove ambiguity from future nano nomemeclature. A nanoparticle is an amorphous or semicrystalline zero dimensional (0D) nano structure with at least one dimension between 10 and 100 nm and a relatively large ($\geq$ 15%) size dispersion [1].

1.1.2 Properties of Nanoparticles

Nanoparticles are of great scientific interest as they are effectively a bridge between bulk materials and atomic or molecular structures. A bulk material should have constant physical properties regardless of its size, but at the nano-scale this is often not the case. Size-dependent properties are observed such as quantum confinement in semiconductor particles, surface plasmon resonance in some metal particles and superparamagnetism in magnetic materials.

The properties of materials change as their size approaches the nanoscale and as the percentage of atoms at the surface of a material becomes significant. For bulk materials larger than one micrometre the percentage of atoms at the surface is minuscule relative to the total number of atoms of the material. The interesting and sometimes unexpected properties of nanoparticles are partly due to the aspects of the surface of the material dominating the properties in lieu of the bulk properties.

Nanoparticles exhibit a number of special properties relative to bulk material. For example, the bending of bulk copper (wire, ribbon, etc.) occurs with movement of copper atoms/clusters at about the 50 nm scale. Copper nanoparticles smaller than 50 nm are considered super hard

materials that do not exhibit the same malleability and ductility as bulk copper. The change in properties is not always desirable. Ferroelectric materials smaller than 10 nm can switch their magnetisation direction using room temperature thermal energy, thus making them useless for memory storage. Suspensions of nanoparticles are possible because the interaction of the particle surface with the solvent is strong enough to overcome differences in density, which usually result in a material either sinking or floating in a liquid. Nanoparticles often have unexpected visible properties because they are small enough to confine their electrons and produce quantum effects. For example gold nanoparticles appear deep red to black in solution.

Nanoparticles have a very high surface area to volume ratio. This provides a tremendous driving force for diffusion, especially at elevated temperatures. Sintering can take place at lower temperatures, over shorter time scales than for larger particles. This theoretically does not affect the density of the final product, though flow difficulties and the tendency of nanoparticles to agglomerate complicates matters. The large surface area to volume ratio also reduces the incipient melting temperature of nanoparticles [2].

1.1.3 Classification

At the small end of the size range, nanoparticles are often referred to as clusters. Nanospheres, nanorods, and nanocups are just a few of the shapes that have been grown. Metal, dielectric, and semiconductor nanoparticles have been formed, as well as hybrid structures (e.g., core-shell nanoparticles). Nanoparticles made of semiconducting material may also be labeled quantum dots if they are small enough (typically sub 10

TARIQUL ISLAM, Md.
Application of
public administrati...
Md. Tariqul Islam -
of Engineering and :
xi,123p.
Includes biblio
10586(REF)

nm) that quantization of electronic energy levels occurs. Such nanoscale particles are used in biomedical applications as drug carriers or imaging agents.

Semi-solid and soft nanoparticles have been manufactured. A prototype nanoparticle of semi-solid nature is the liposome. Various types of liposome nanoparticles are currently used clinically as delivery systems for anticancer drugs and vaccines.

1.1.4 Characterization

Nanoparticle characterization is necessary to establish understanding and control of nanoparticle synthesis and applications. Characterization is done by using a variety of different techniques, mainly drawn from materials science. Common techniques are Electron Microscopy [TEM,SEM], Atomic Force Microscopy [AFM], Dynamic Light Scattering [DLS], X-ray Photoelectron Spectroscopy [XPS], powder X-ray Diffractometry [XRD], and Fourier Transform Infrared Spectroscopy [FTIR].

Whilst the theory has been known for over a century, the technology for Nanoparticle Tracking Analysis (NTA) allows direct tracking of the Brownian motion and this method therefore allows the sizing of individual nanoparticles in solution.

1.1.5 Fabrication of Nanoparticles

There are several methods for creating nanoparticles; attrition and pyrolysis are common methods. In attrition, macro or micro scale particles are ground in a ball mill, a planetary ball mill, or other size

reducing mechanism. The resulting particles are air classified to recover nanoparticles.

In pyrolysis, an organic precursor (liquid or gas) is forced through an orifice at high pressure and burned. The resulting ash is air classified to recover oxide nanoparticle.

A thermal plasma can also deliver the energy necessary to cause evaporation of small micrometre size particles. The thermal plasma temperatures are in the order of 10000 K, so that solid powder easily evaporates. Nanoparticles are formed upon cooling while exiting the plasma region. The main types of the thermal plasmas torches used to produce nanoparticles are dc plasma jet, dc arc plasma and radio frequency (RF) induction plasmas. In the arc plasma reactors, the energy necessary for evaporation and reaction is provided by an electric arc which forms between the anode and the cathode. For example, silica sand can be vaporized with an arc plasma at atmospheric pressure. The resulting mixture of plasma gas and silica vapour can be rapidly cooled by quenching with oxygen, thus ensuring the quality of the fumed silica produced. In RF induction plasma torches, energy coupling to the plasma is accomplished through the electromagnetic field generated by the induction coil. The plasma gas does not come in contact with electrodes, thus eliminating possible sources of contamination and allowing the operation of such plasma torches with a wide range of gases including inert, reducing, oxidizing and other corrosive atmospheres. The working frequency is typically between 200 kHz and 40 MHz. Laboratory units run at power levels in the order of 30-50 kW while the large scale industrial units have been tested at power levels up to 1 MW. As the residence time of the injected feed droplets in the plasma is very short it is important that the droplet sizes are small enough in order to obtain

complete evaporation. The RF plasma method has been used to synthesize different nanoparticle materials, for example synthesis of various ceramic nanoparticles such as oxides, carbours/carbides and nitrides of Ti and Si.

Inert-gas aggregation is frequently used to make nanoparticles from metals with low melting points. The metal is vaporized in a vacuum chamber and then supercooled with an inert gas stream. The supercooled metal vapor condenses in to nanometer-sized particles, which can be entrained in the inert gas stream and deposited on a substrate or studied in situ.

1.1.6 Nanoparticle Morphology

Scientists have taken to naming their particles after the real world shapes that they might represent. Nanospheres [3], nanoreefs [4], nanoboxes [5] and more have appeared in the literature. These morphologies sometimes arise spontaneously as an effect of a templating or directing agent present in the synthesis such as micellular emulsions or anodized alumina pores, or from the innate crystallographic growth patterns of the materials themselves [6]. Some of these morphologies may serve a purpose, such as long carbon nanotubes being used to bridge an electrical junction, or just a scientific curiosity like the stars shown at left.

1.1.7 Application of Nanoparticles

A.   Medicine

The biological and medical research communities have exploited the unique properties of nanomaterials for various applications (e.g., contrast

agents for cell imaging and therapeutics for treating cancer). Terms such as *biomedical nanotechnology*, *bionanotechnology*, and *nanomedicine* are used to describe this hybrid field. Functionalities can be added to nanomaterials by interfacing them with biological molecules or structures. The size of nanomaterials is similar to that of most biological molecules and structures; therefore, nanomaterials can be useful for both in vivo and in vitro biomedical research and applications. Thus far, the integration of nanomaterials with biology has led to the development of diagnostic devices, contrast agents, analytical tools, physical therapy applications, and drug delivery vehicles.

i)   *Diagnostics*: Nanotechnology-on-a-chip is one more dimension of lab-on-a-chip technology. Biological tests measuring the presence or activity of selected substances become quicker, more sensitive and more flexible when certain nanoscale particles are put to work as tags or labels. Magnetic nanoparticles, bound to a suitable antibody, are used to label specific molecules, structures or microorganisms. Gold nanoparticles tagged with short segments of DNA can be used for detection of genetic sequence in a sample. Multicolor optical coding for biological assays has been achieved by embedding different-sized quantum dots into polymeric microbeads. Nanopore technology for analysis of nucleic acid converts strings of nucleotides directly into electronic signatures.

ii)   *Drug delivery*: The overall drug consumption and side-effects can be lowered significantly by depositing the active agent in the morbid region only and in no higher dose than needed. This highly selective approach reduces costs and human suffering. An example can be found in dendrimers and nanoporous materials. They could hold small drug molecules transporting them to the desired location. Another vision is based on small electromechanical systems; NEMS are being investigated

for the active release of drugs. Some potentially important applications include cancer treatment with iron nanoparticles or gold shells. A targeted or personalized medicine reduces the drug consumption and treatment expenses resulting in an overall societal benefit by reducing the costs to the public health system. Nanotechnology is also opening up new opportunities in implantable delivery systems, which are often preferable to the use of injectable drugs, because the latter frequently display first-order kinetics (the blood concentration goes up rapidly, but drops exponentially over time). This rapid rise may cause difficulties with toxicity, and drug efficacy can diminish as the drug concentration falls below the targated range.

iii)   Tissue engineering: Nanotechnology can help to reproduce or to repair damaged tissue. This so called "tissue engineering" makes use of artificially stimulated cell proliferation by using suitable nanomaterial-based scaffolds and growth factors. Tissue engineering might replace today's conventional treatments like organ transplants or artificial implants. On the other hand, tissue engineering is closely related to the ethical debate on human stem cells and its ethical implications.

B.   Chemistry and Environment

Chemical catalysis and filtration techniques are two prominent examples where nanotechnology already plays a role. The synthesis provides novel materials with tailored features and chemical properties: for example, nanoparticles with a distinct chemical surrounding (ligands), or specific optical properties. In this sense, chemistry is indeed a basic nanoscience. In a short-term perspective, chemistry will provide novel "nanomaterials" and in the long run, superior processes such as "self-assembly" will enable energy and time preserving strategies. In a sense, all chemical synthesis can be understood in terms of nanotechnology, because of its ability to manufacture certain molecules. Thus, chemistry forms a base

for nanotechnology providing tailor-made molecules, polymers, etcetera, as well as clusters and nanoparticles.

i)   Catalysis: Chemical catalysis benefits especially from nanoparticles, due to the extremely large surface to volume ratio. The application potential of nanoparticles in catalysis ranges from fuel cell to catalytic converters and photocatalytic devices. Catalysis is also important for the production of chemicals.

ii)   Filtration: A strong influence of nanochemistry on waste-water treatment, air purification and energy storage devices is to be expected. Mechanical or chemical methods can be used for effective filtration techniques. One class of filtration techniques is based on the use of membranes with suitable hole sizes, whereby the liquid is pressed through the membrane. Nanoporous membranes are suitable for a mechanical filtration with extremely small pores smaller than 10 nm ("nanofiltration") and may be composed of nanotubes. Nanofiltration is mainly used for the removal of ions or the separation of different fluids. On a larger scale, the membrane filtration technique is named ultrafiltration, which works down to between 10 and 100 nm. One important field of application for ultrafiltration is medical purposes as can be found in renal dialysis. Magnetic nanoparticles offer an effective and reliable method to remove heavy metal contaminants from waste water by making use of magnetic separation techniques. Using nanoscale particles increases the efficiency to absorb the contaminants and is comparatively inexpensive compared to traditional precipitation and filtration methods.

C.   Energy

The most advanced nanotechnology projects related to energy are: storage, conversion, manufacturing improvements by reducing materials

and process rates, energy saving (by better thermal insulation for example), and enhanced renewable energy sources.

i)   *Reduction of energy consumption*: A reduction of energy consumption can be reached by better insulation systems, by the use of more efficient lighting or combustion systems, and by use of lighter and stronger materials in the transportation sector. Currently used light bulbs only convert approximately 5% of the electrical energy into light. Nanotechnological approaches like light-emitting diodes (LEDs) or quantum caged atoms (QCAs) could lead to a strong reduction of energy consumption for illumination.

ii)   *Increasing the efficiency of energy production*: Today's best solar cells have layers of several different semiconductors stacked together to absorb light at different energies but they still only manage to use 40 percent of the Sun's energy. Commercially available solar cells have much lower efficiencies (15-20%). Nanotechnology could help increase the efficiency of light conversion by using nanostructures with a continuum of bandgaps. The degree of efficiency of the internal combustion engine is about 30-40% at the moment. Nanotechnology could improve combustion by designing specific catalysts with maximized surface area.

iii)   *The use of more environmentally friendly energy systems*: An example for an environmentally friendly form of energy is the use of fuel cells powered by hydrogen, which is ideally produced by renewable energies. Probably the most prominent nanostructured material in fuel cells is the catalyst consisting of carbon supported noble metal particles with diameters of 1-5 nm. Suitable materials for hydrogen storage contain a large number of small nanosized pores. Therefore many nanostructured materials like nanotubes, zeolites or alanates are under investigation. Nanotechnology can contribute to the further reduction of combustion

engine pollutants by nanoporous filters, which can clean the exhaust mechanically, by catalytic converters based on nanoscale noble metal particles or by catalytic coatings on cylinder walls and catalytic nanoparticles as additive for fuels.

iv)   Recycling of batteries: Because of the relatively low energy density of batteries the operating time is limited and a replacement or recharging is needed. The huge number of spent batteries and accumulators represent a disposal problem. The use of batteries with higher energy content or the use of rechargeable batteries or supercapacitors with higher rate of recharging using nanomaterials could be helpful for the battery disposal problems.

D.   Information and Communication

Current high-technology production processes are based on traditional top down strategies, where nanotechnology has already been introduced silently. The critical length scale of integrated circuits is already at the nanoscale (50 nm and below) regarding the gate length of transistors in CPUs or DRAM devices.

i)   Novel semiconductor devices: An example of such novel devices is based on spintronics. The dependence of the resistance of a material (due to the spin of the electrons) on an external field is called magnetoresistance. This effect can be significantly amplified (GMR - Giant Magneto-Resistance) for nanosized objects, for example when two ferromagnetic layers are separated by a nonmagnetic layer, which is several nanometers thick (e.g. Co-Cu-Co). The GMR effect has led to a strong increase in the data storage density of hard disks and made the gigabyte range possible. The so called tunneling magnetoresistance (TMR) is very similar to GMR and based on the spin dependent tunneling of electrons through adjacent ferromagnetic layers. Both GMR and TMR

effects can be used to create a non-volatile main memory for computers, such as the so called magnetic random access memory or MRAM.

ii)   Novel optoelectronic devices: In the modern communication technology traditional analog electrical devices are increasingly replaced by optical or optoelectronic devices due to their enormous bandwidth and capacity, respectively. Two promising examples are photonic crystals and quantum dots. Photonic crystals are materials with a periodic variation in the refractive index with a lattice constant that is half the wavelength of the light used. They offer a selectable band gap for the propagation of a certain wavelength, thus they resemble a semiconductor, but for light or photons instead of electrons. Quantum dots are nanoscaled objects, which can be used, among many other things, for the construction of lasers. The advantage of a quantum dot laser over the traditional semiconductor laser is that their emitted wavelength depends on the diameter of the dot. Quantum dot lasers are cheaper and offer a higher beam quality than conventional laser diodes.

iii)   Nanologic: Nanoscale devices exhibit dominant nonlinearities that prevent their use as two-state devices in digital computers. The idea behind nanologic is to *exploit* these nonlinearities (rather than suppress them) to implement functions that correspond to mathematical sets: interval numbers, disjoint intervals, fuzzy numbers, fuzzy sets, etc. Simple nanoelectronic circuits can be designed that can represent sets and set operations, and an array of such devices constitutes a universal mathematical processor, able to solve any problem that can be expressed in set theory. Nanologic will find most value for human-meaningful problems involving uncertainty, ambiguity, error, under-specified and over-specified systems, and for approximate analysis of combinatorially intractable problems, including mathematical theorems.

iv)   Quantum computers: Entirely new approaches for computing exploit the laws of quantum mechanics for novel quantum computers, which enable the use of fast quantum algorithms. The Quantum computer will have quantum bit memory space termed qubit for several computations at the same time.

E.   Consumer Goods

Nanotechnology is already impacting the field of consumer goods, providing products with novel functions ranging from easy-to-clean to scratch-resistant. Modern textiles are wrinkle-resistant and stain-repellent; in the mid-term clothes will become "smart", through embedded "wearable electronics". Already in use are different nanoparticle improved products. Especially in the field of cosmetics, such novel products have a promising potential.

i)   Foods: Nanotechnology can be applied in the production, processing, safety and packaging of food. A nanocomposite coating process could improve food packaging by placing anti-microbial agents directly on the surface of the coated film. Nanocomposites could increase or decrease gas permeability of different fillers as is needed for different products. They can also improve the mechanical and heat-resistance properties and lower the oxygen transmission rate. Research is being performed to apply nanotechnology to the detection of chemical and biological substances for sensing biochemical changes in foods.

ii)   Household: The most prominent application of nanotechnology in the household is self-cleaning or "easy-to-clean" surfaces on ceramics or glasses. Nanoceramic particles have improved the smoothness and heat resistance of common household equipment such as the flat iron.

iii)   Optics: The first sunglasses using protective and antireflective ultrathin polymer coatings are on the market. For optics, nanotechnology

also offers scratch resistant surface coatings based on nanocomposites. Nano-optics could allow for an increase in precision of pupil repair and other types of laser eye surgery.

iv) *Textiles*: The use of engineered nanofibers already makes clothes water- and stain-repellent or wrinkle-free. Textiles with a nanotechnological finish can be washed less frequently and at lower temperatures. Nanotechnology has been used to integrate tiny carbon particles membrane and guarantee full-surface protection from electrostatic charges for the wearer.

v) *Cosmetics*: One field of application is in sunscreens. The traditional chemical UV protection approach suffers from its poor long-term stability. A sunscreen based on mineral nanoparticles such as titanium dioxide offer several advantages. Titanium oxide nanoparticles have a comparable UV protection property as the bulk material, but lose the cosmetically undesirable whitening as the particle size is decreased.

1.2 Fundamental Aspects of Catalytic Process

In chemistry and biology, catalysis is a way of accelerating the rate of a chemical reaction by means of contacting the reactants with a substance called a catalyst, which itself is not consumed by the overall reaction. More generally, one may at times call anything that accelerates a process, a "catalyst". A catalyst provides an alternative route to products, the catalytic route being subject to lower activation energy than in the uncatalyzed reaction. A lowered activation energy increases the reaction rate. Catalysts generally change in the course of a reaction but are regenerated.

A good example of a catalyst usage is in the disproportionation of hydrogen peroxide to give water and oxygen.

$$2\ H_2O_2 \rightarrow 2\ H_2O + O_2$$
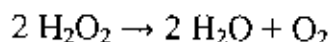
This reaction is slow but upon the addition of manganese dioxide to hydrogen peroxide, the reaction occurs rapidly as signaled by effervescence of oxygen. In demonstrations, the evolved oxygen is detectable by its effect on a glowing splint. The manganese dioxide may be recovered, and re-used indefinitely, thus it is a catalyst — it is not consumed by the reaction. (The H_2O_2 sold as a sterilizing agent in drugstores is too dilute for this to work dramatically.)

1.2.1 Mechanism of Catalytic Process

i)   General mechanism: Catalysts generally react with one or more reactants to form an intermediate that subsequently give the final reaction product, in the process regenerating the catalyst. The following is a typical reaction scheme, where C represents the catalyst, A and B are reactants, and D is the product of the reaction of A and B:

$$A + C \rightarrow AC \tag{1}$$

$$B + AC \rightarrow ABC \tag{2}$$

$$ABC \rightarrow CD \tag{3}$$

$$CD \rightarrow C + D \tag{4}$$
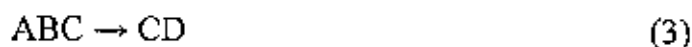
Although the catalyst (C) is consumed by reaction 1, it is subsequently produced by reaction 4, so for the overall reaction:

$$A + B \rightarrow D$$
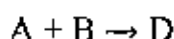
ii) *Catalytic cycles*: A catalytic cycle is another term for mechanism. Catalytic cycles are central to any discussion of catalysis, be it in biochemistry, organometallic chemistry, or solid state chemistry.

Often, a so-called sacrificial catalyst is also part of the reaction system with the purpose of regenerating the true catalyst in each cycle. As the name implies the sacrificial catalyst is not regenerated and is instead irreversibly consumed. This sacrificial compound is also known as a stoichiometric catalyst when added in stoichiometric quantities compared to the main reactant. Usually the true catalyst is an expensive and complex molecule and added in quantities as small as possible. The stoichiometric catalyst on the other hand should be cheap and abundant.

1.2.2 Catalysts and Reaction Energetics

Catalysts work by providing an alternative mechanism involving a different transition state and lower activation energy. The effect of this is that more molecular collisions have the energy needed to reach the transition state. Hence, catalysts can perform reactions that, albeit thermodynamically feasible, would not run without the presence of a catalyst, or perform them much faster, more specific, or at lower temperatures. This can be observed on a Boltzmann distribution and energy profile diagram. This means that catalysts reduce the amount of energy needed to start a chemical reaction. Figure 1.2.1 is a generic potential energy diagram showing the effect of a catalyst in an hypothetical exothermic chemical reaction. The presence of the catalyst opens a different reaction pathway (shown in dotted line) with a lower

activation energy. The final result and the overall thermodynamics are the same.
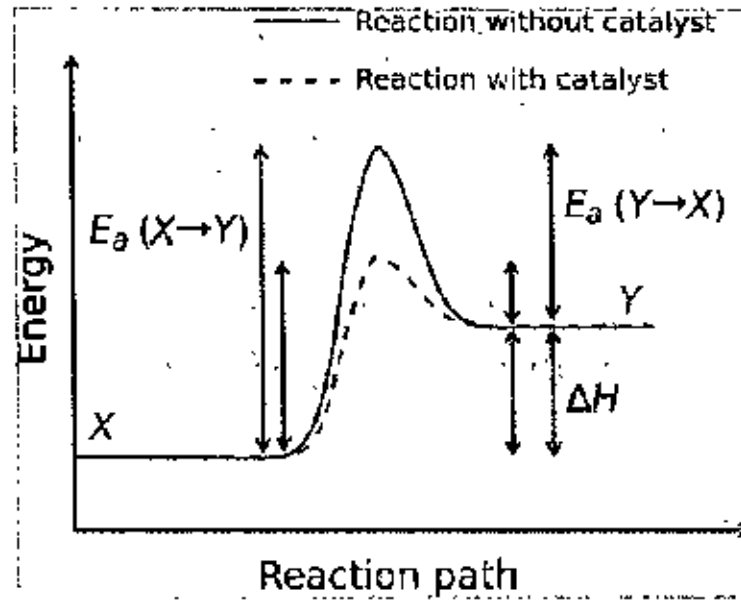
Fig. 1.2.1   Energy profile diagram showing the effect of a catalyst.

Catalysts *cannot* make energetically unfavorable reactions possible — they have *no* effect on the chemical equilibrium of a reaction because the rate of both the forward and the reverse reaction are eqnally affected (see also thermodynamics). The net free energy change of a reaction is the same whether a catalyst is used or not; the catalyst jnst makes it easier to activate.

The SI derived unit for measuring the catalytic activity of a catalyst is the katal, which is moles per second. The degree of activity of a catalyst can also be described by the Turn Over Number (TON) and the catalytic efficiency by the Turn Over Frequency (TOF). The biochemical equivalent is the Enzyme Unit.

1.2.3 Types of Catalysts

Catalysts can be either heterogeneous or homogeneous. Biocatalysts are often seen as a separate group. Heterogeneous catalysts are present in different phases from the reactants (for example, a solid catalyst in a liquid reaction mixture), whereas homogeneous catalysts are in the same phase (for example, a dissolved catalyst in a liquid reaction mixture).

i) *Heterogeneous catalysts*: A simple model for heterogeneous catalysis involves the catalyst providing a surface on which the reactants (or substrates) temporarily become adsorbed. Bonds in the substrate become weakened sufficiently for new bonds to be created. The bonds between the products and the catalyst are weaker, so the products are released. Different possible mechanisms for reactions on surfaces are known, depending on how the adsorption takes place.

For example, in the Haber process to manufacture ammonia, finely divided iron acts as a heterogeneous catalyst. Active sites on the metal allow partial weak bonding to the reactant gases, which are adsorbed onto the metal surface. As a result, the bond within the molecule of a reactant is weakened and the reactant molecules are held in close proximity to each other. In this way the particularly strong triple bond in nitrogen is weakened and the hydrogen and nitrogen molecules are brought closer together than would be the case in the gas phase, so the rate of reaction increases.

Other heterogeneous catalysts include vanadium(V) oxide in the contact process, nickel in the manufacture of margarine, alumina and silica in the cracking of alkanes and platinum, rhodium and palladium in catalytic converters. Mesoporous silicates have found utility in heterogeneous reaction catalysis because their large accessible surface area allows for high catalyst loading.

In car engines, incomplete combustion of the fuel produces carbon monoxide, which is toxic. The electric spark and high temperatures also allow oxygen and nitrogen to react and form nitrogen monoxide and nitrogen dioxide, which are responsible for photochemical smog and acid rain. Catalytic converters reduce such emissions by adsorbing CO and NO onto catalytic surface, where the gases undergo a redox reaction. Carbon dioxide and nitrogen are desorbed from the surface and emitted as relatively harmless gases:

$$2CO + 2NO \rightarrow 2CO_2 + N_2$$
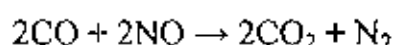
Many catalysts used in refineries and in petrochemical applications are regenerated and reused multiple times to save costs and energy and to reduce environmental impact from recycling or disposal of spent catalysts.

ii) *Homogeneous catalysts*: Homogeneous catalysts are in the same phase as the reactants. In homogeneous catalysis the catalyst is a molecule which facilitates the reaction. The catalyst initiates reaction with one or more reactants to form intermediate(s) and in some cases one or more products. Subsequent steps lead to the formation of remaining products and to the regeneration of the catalyst.

Examples of homogeneous catalysts are:

1) The ion $H^+(aq)$ which acts as a catalyst in esterification, as well as in the inverse reaction - hydrolysis of esters such as methyl acetate is catalysed by H^+

2) Chlorine free radicals in the break down of ozone. These radicals are formed by the action of ultraviolet radiation on chlorofluorocarbons (CFCs). They react with ozone to form oxygen molecules and regenerate

the catalyst radicals. This process destroys the thin layer of stratospheric ozone

$$Cl^\cdot + O_3 \rightarrow ClO^\cdot + O_2$$

$$ClO^\cdot + O^\cdot \rightarrow Cl^\cdot + O_2$$
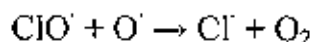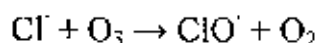
3) Oxides of nitrogen in the oxidation of sulphur dioxide to sulphur trioxide by dioxygen in the chamber process.

iii) *Biocatalysts*: In nature enzymes are catalysts in the metabolic pathway. In biochemistry catalysis is also observed with abzymes, ribozymes and deoxyribozymes. Biocatalysts can be thought of as a mixture of a homogenous and heterogeneous catalyst. This is because the enzyme is in solution itself, but the reaction takes place on the enzyme surface.

iv) *Electrocatalysis*: In the context of electrochemistry, specifically in fuel cell engineering, various metal-rich catalysts are used to promote the efficiency of a half reaction that occurs within the fuel cell. One common type of fuel cell electrocatalyst is based upon tiny nanoparticles of platinum which adorn slightly larger carbon particles. When this type of platinum electrocatalyst is in contact with one of the electrodes in a fuel cell, it increases the rate of the redox half reaction in which oxygen gas is reduced to water (or hydroxide or hydrogen peroxide).

1.2.4 Significance

Catalysis is of paramount importance in the chemical industry. The production of most industrially important chemicals involves catalysis. Two notable commercial processes are the Haber process for ammonia

synthesis and the Fischer-Tropsch synthesis. Research into catalysis is a major field in applied science, and involves many fields of chemistry, notably in organometallic chemistry, and physics. Catalysis is important in many aspects of environmental science, from the catalytic converter in automobiles to the alleged causes of the ozone hole. Catalytic, rather than stoichiometric reactions are preferred in environmentally friendly green chemistry due to the reduced amount of waste generated.

1.3 Catalytic Materials

1.3.1 Metals

Metals are crystalline solid materials consist of metal atoms distributed in a definite pattern resulting from their close packing. The types of close packing arrangement depend upon the size and electronic configuration of the atoms involved in the formation of crystal lattice. Since the metal atoms are all in direct contact with one another in the lattice and their valence electrons are in identical energy states, it is believed that the electrons are free to migrate between atoms. Metal atoms have an excess of low energy orbital vacancies. These vacancies enable valence electrons to move from near a certain nucleus to near any other nucleus where their position remains indistinguishable from the first. Thus, metals may be pictured as a collection of positive atomic cores embedded in a fluid of electrons or sea of electrons. For this fluid of electrons, metals are good conductors of electricity and heat. Metals have metallic luster; they are malleable, ductile and high melting points.

Metals have simple crystal lattices since metallic bonding envisages closest packing of atoms-one layer above another. Metals may have any

system of seven common crystal systems. Fe, Cu, Al, Ag, Au etc are the most common metals which are very useful to us.

1.3.2 Semiconductors

Semiconductors are special kind of materials which have the properties of semiconductivity is an electrical property of materials. A relatively small group of elements and compounds have an important electrical property, semiconduction in which they are neither good electrical conductors nor good electrical insulators. Instead, their ability to conduct electricity is intermediate. Si, Ge, impure ZnO, impure NiO are some examples of semiconductors.

The magnitude of conductivity in the simple semiconductors fall within the range 10^{-6} to 10^{-1} Ω^{-1} cm^{-1}. This intermediate range corresponds to band gaps of less then 2e V. Both conduction electrons and electron holes are charge carriers in a simple semiconductor.

In a semiconductor element, the energies of the valence electrons, which bind the crystal together, lie in the highest filled energy band, called the valence band. The empty band above, called the conduction band, is separated from the valence band by an energy gap. The magnitude of the energy gap or the width of the forbidden energy zoue is characteristic of the lattice alone and varies widely for different crystals.

The transfer of an electron from the valence band to the conduction band requires high excitation energy to overcome the potential barrier of the forbidden energy zone. Consequently, such elements behave like an insulator at low temperatures. The application of heat or light energy may give enough energy to some electrons in the valence band to excite them

across the forbidden zone into the conduction band. These electrons in the conduction band are now free to move and can carry electricity (Fig. 1.3.1).

Semiconductors are of two kinds such as

    (i)   Intrinsic semiconductor

    (ii)   Extrinsic semiconductor

(i) Intrinsic semiconductors: If a pure, elemental substance shows the semiconducting properties, it is called intrinsic semiconductor. Pure Si, Ge shows these semiconducting properties. This semiconduction results from the thermal promotion of electrons from a filled valence band to an empty conduction band. There, the electrons are negative charge carriers. The removal of electrons from the valence band produces electron holes which are positive charge carrier and identical to the conduction electrons (Fig. 1.3.1. a). This overall conduction scheme is possible because of the relatively small energy band gap between the valence and conduction bands in silicon. If δ is the conductivity of semiconductor then for intrinsic semiconductor, we can write:

$$\delta = \quad nq\,(\mu_e + \mu_n) \qquad\qquad\qquad 1.3.1$$

Where, $n \rightarrow$ density of conduction electron

           $q \rightarrow$ charge of single carrier

           $\mu_e \rightarrow$ carrier mobility of electron

           $\mu_n \rightarrow$ carrier mobility of hole

(ii) Extrinsic semiconductors: Extrinsic semiconduction result from impurity additions known as dopants, and the process of adding these components is called doping. These types of semiconductors are extrinsic semiconductors. At room temperature the conductivity of semiconductors results from electrons and holes introduced by impurities in the crystal.

The presence of an impurity lowers considerably the activation energy necessary to transfer an electron from the valence band to the conduction band. This indicates that the ground state energies of such easily excited electrons must lie in the forbidden energy region. Two such discrete energy levels, known as donor levels and acceptor levels, may be introduced into the forbidden energy zone at a small interval of energy below the conduction band or above the valance band (Fig.1.3.1. b). Donor levels give rise to electrons in the conduction band, whereas acceptor levels lead to the formation of holes in the valence band. Impurity of Si, with B, P, NiO, ZnO, are the examples of extrinsic semiconductors. Extrinsic semiconductors are of two kinds such as p-type extrinsic semiconductor and n-type extrinsic semiconductor.

p-type extrinsic semiconductors: The p-type semiconductor is obtained when the impurity atoms have fewer valence electrons than the silicon or germanium atoms of the original crystal. When a trivalent element such as B, Al, Ga, In is substituted for Si atom, the structure will be locally incomplete and the impurity atom will acquire an extra electron from a nearly bond in the lattice to approximate the tetrahedral cloud distribution of the lattice. This creates a positive hole localized near the impurity, which will attempt to neutralize itself by taking an electron from another neighboring bond.

Then again a hole is formed in place of this electron and it will neutralize itself by taking another electron from the next neighboring bond. Such way the positive holes carry electricity in the extrinsic semiconductor. So it is called p (i.e. positive) type semiconductor (Fig. 1.3.1 a) Cu_2O also p-type semiconductor.
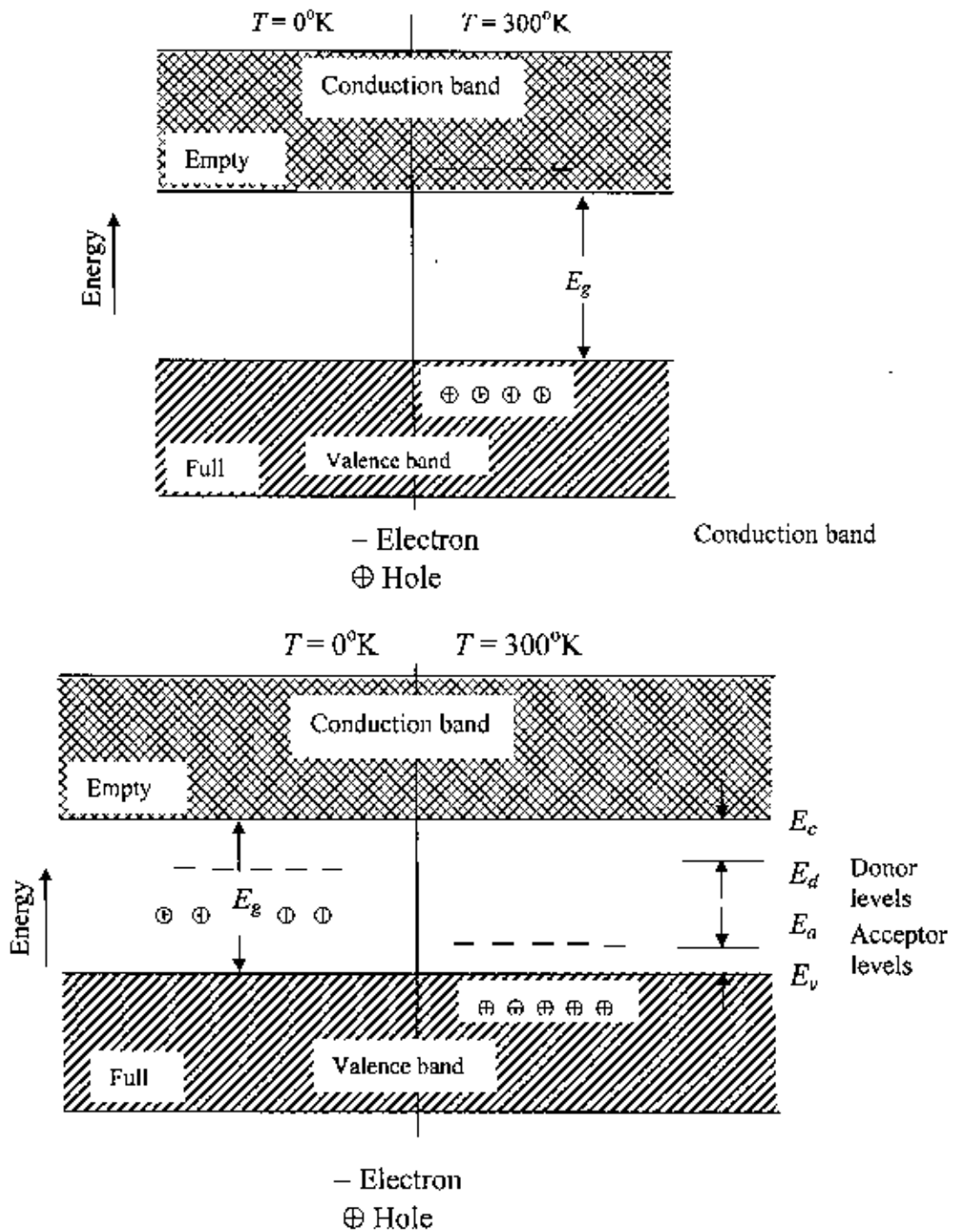
Fig. 1.3.1: A pictorial representation of an (a) intrinsic and (b) extrinsic semiconductor.

n-type semiconductors: They n-type semiconductor arises from substitution of impurity atoms having more valence electrons than Si or Ge atoms. Elements such as P, As, Sb, and Bi have five valence electrons. When such an element is substituted for a silicon atom, four of its five electrons will enter the inter-atomic bonds, but the fifth electron will be only slightly attracted by the excess of the positive charge on the nucleus. Thermal agitation even at room temperature is sufficient to transfer this electron to the conduction band. Since conductivity is due to the motion of electrons in the conduction band, this semiconductor is called n-type and the impurity is called the donor (Fig.1.3.2.b). Titanium dioxide or titania is a non-stoichiometric transition metal oxide and behaves as n-type semiconductor [7].

There are three naturally occurring crystal phases of titanium dioxide: rutile, anatase, and brookhite. Most of the electrochemical and photocatalytic work to date have been performed on rutile or anatase, or a mixture of the two. Both rutile and anatase have tetragonal unit cells, and both structures contains slightly distorted TiO_6 octahedral. Rutile is thermodynamically more stable than anatase at room temperature; the free energy change for antatase to rutile is −5.4 kJ/mol [8].

The absorption and reflection properties of rutile have been studied extensively. At 4K, the short wavelength absorption edge for rutile is 410 nm (bandgap energy = 3.05 eV) [9-10]. The lowest energy electronic absorption at 3.05 eV is an indirect transition. On the other hand, the bandgap of anatase is reported as 3.2 eV [11]. The absorption coefficients for both crystal phases are reported as ~10^5 cm^{-1} at 340 nm [12].
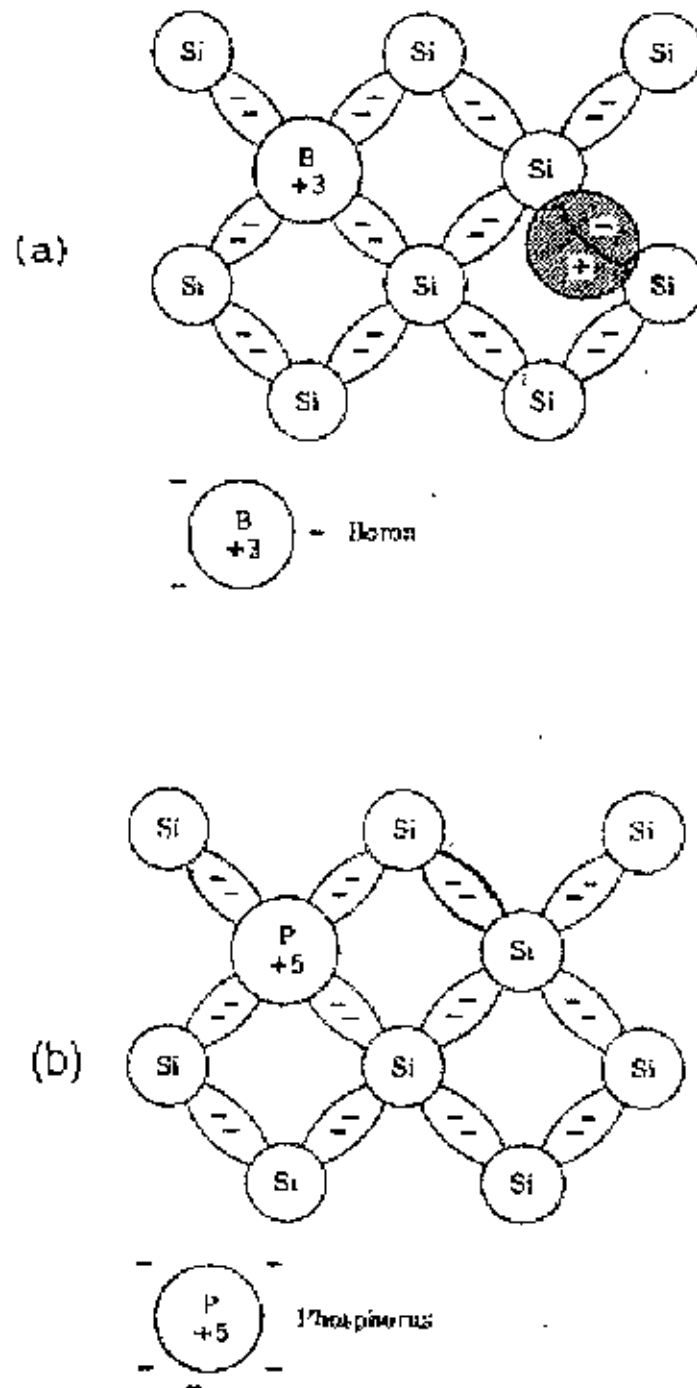
Fig. 1.3.2: Types of impurity semiconductors (a) *p*-type (b) *n*- type.

Ultraviolet radiation below ~390 nm stimulates valence-band electrons in TiO_2 particles that are suspended in contaminated water. These electrons are promoted to the conduction band (e^-_{cb}), creating holes in the valence band (h^+_{vb}). These electron / hole pairs can either recombines, producing thermal energy, or interact with the external environment to perform oxidation and reduction reactions.

$$TiO_2 \xrightarrow{h\nu} TiO_2\ (e^-_{cb},\ h^+_{\ vb})$$
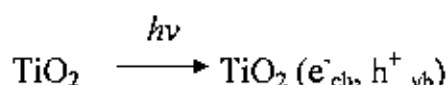
1.3.3 Inorganic Oxides

An oxide is a chemical compound containing at least one oxygen atom as well as at least one other element. Most of the Earth's crust consists of oxides. Oxides result when elements are oxidized by oxygen in air. Virtually all elements burn in an atmosphere of oxygen. In the presence of water and oxygen (or simply air), some elements - lithium, sodium, potassium, rubidium, caesium, strontium and barium - react rapidly, even dangerously to give the hydroxides. In part for this reason, alkali and alkaline earth metals are not found in nature in their metallic, i.e., native, form. The surface of most metals consist of oxides and hydroxides in the presence of air. A well known example is aluminium foil, which is coated with a thin film of aluminium oxide that passivates the metal, slowing further corrosion. Due to its electronegativity, oxygen forms chemical bonds with almost all elements to give the corresponding oxides. So-called noble metals (common examples: gold, platinum) resist direct chemical combination with oxygen, and substances like gold (III) oxide must be generated by indirect routes.

The oxide class of minerals is a rather diverse class. It includes minerals that are quite hard (corundum) and some that are quite soft such as psilomelane. It has metallic minerals such as hematite and gemstones such as corundum, chrysoberyl and spinel. Many oxides are black but others can be very colorful. The large diversity of oxides can be partially attributed to the extreme abundance of oxygen in the Earth's crust. Oxygen comprises over 45% of the Earth's crust by weight. Most of this is locked up in more complex minerals based on chemical complex anions such as CO_3^{2-}, BO_3^{3-}, SO_4^{2-}, NO_3^-, SiO_4^{4-}, PO_4^{3-} and others. But great opportunities exist for single oxygen ions to combine with various elements in many different ways. In a strict sense, minerals that belong to the more complex mineral classes such as the silicates are really oxides. But this would be cumbersome for mineralogists to be able to deal with only the four different classes of the elements class, the halides class, the sulfides class and finally the extremely large oxides class with all of its many subclasses and over 90% of all known minerals. By convention therefore, the oxides are limited to non complex minerals containing oxygen or hydroxide. Oxides also contain mostly ionic bonds and this helps distinguish members from the more complex mineral classes whose bonds are typically more covalent in nature. Quartz, SiO_2, would be considered an oxide, and still is in some mineral guides and texts, except for its covalent silicon oxygen bonds and its structural similarity to the other Tectosilicates.

There are varoius types of oxides in nature. Oxides of more electropositive elements tend to be basic. They are called basic anhydrides; adding water, they may form basic hydroxides. For example, sodium oxide is basic; when hydrated, it forms sodium hydroxide. Oxides of more electronegative elements tend to be acidic. They are called acid

anhydrides; adding water, they form oxoacids. For example, dichlorine heptoxide is acid; perchloric acid is a more hydrated form. Some oxides can act as both acid and base at different times. They are amphoteric. An example is aluminium oxide. Some oxides do not show behavior as either acid or base

Inorganic oxides are one of the most important materials for science and technology. Especially transition metal oxides have characteristics surface. It has drawn great attention to researchers. Metal oxide has been used as catalyst, sensor, and adsorbent for removal of toxic chemical, electrode material as well as used in electro chromic device and solar cell etc.
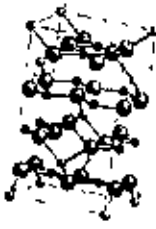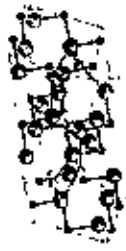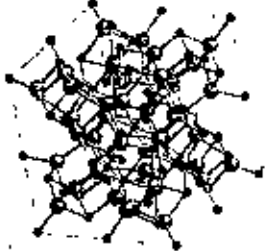
Nowadays nano metal oxide is one of the promising materials for scientists. The applications of nano oxide particles are increasing day by day. The most commonly used transition metal oxides are titania, manganese oxide, zinc oxide, cobalt oxide, nickel oxide, iron oxide etc.

1.3.4 Oxides of Manganese

Manganese is the tenth most abundant element in the earth's crust [13] and occurs in nature in the +2, +3, and +4 oxidation states. Manganese oxides are commonly used in a wide range of applications including dry-cell batteries [14], pigments [13], catalysts [15-19], and water-purifying agents [13]. The greatest percentage of the world's manganese production is consumed in steel production, where it is added for increased strength [13]. Manganese oxides are active catalysts in several oxidation and reduction reactions, including oxidation of methane and carbon monoxide and selective reduction of nitrobenzene [20]. Chang and McCarty found

the oxygen absorption and desorption behavior of manganese oxide as an oxygen storage component to be superior to that of cerium oxide [21]. Manganese forms the stable oxides MnO, Mn_3O_4, Mn_2O_3, and MnO_2 as well as the metastable Mn_5O_8. The structural properties of these oxides are listed in Table 1. Reduction and oxidation of manganese oxides are reversible up to Mn_2O_3; formation of MnO_2 in pure oxygen requires pressures greater than 3000 bar [13].

Table 1.3.1 Manganese Oxides Structural Data

Oxide	MnO	α-Mn_3O_4	Mn_5O_8	α-Mn_2O_3	β-MnO_2
JCPDS	71-1177	24-0734	39-1218	41-1442	43-1455
Mineral Name	Manganosite	Hausmannite	n/a	Bixbyite	pyrolusite
Valence	+2	+2, +3	+2, +4	+3	+4
Crystal Structure	Cubic	Tetragonal	Monoclinic	Cubic	Tetragonal/ rutile
Space group	I m$\bar{3}$m	I4$_1$/amd	C2/m	I a$\bar{3}$	P4$_2$/mnm
Lattice Parameter (Å)	a = 4.446	a = 5.7621 c = 9.4696	a = 10.392, b = 5.730 c = 4.866, β = 109.62	a = 9.4091	a = 4.3999 c = 2.8740
Unit Cell Model					
Formula units/ unit cell	4	4	4	16	2

Manganese(IV) oxide is the chemical compound MnO_2, commonly called manganese dioxide. This blackish or brown solid occurs naturally as the mineral pyrolusite, which is the main ore of manganese. It is also present

in manganese nodules. The principal use for MnO_2 is for dry-cell batteries, such as the alkaline battery and the zinc-carbon battery.

Manganese dioxide is used as an oxidant in organic synthesis. The effectiveness of the reagent depends on the method of preparation, a problem that is typical for other heterogeneous reagents where surface area, among other variables, is a significant factor [22]. The mineral pyrolusite makes a poor reagent. Usually, however, the reagent is generated by treatment of an aqueous solution $KMnO_4$ with a Mn(II) salt, typically the sulfate at various pH's.

The predominant application of MnO_2 is for the oxidation of allylic alcohols to the corresponding aldehydes:

$$cis\text{-}RCH=CHCH_2OH + MnO_2 \rightarrow cis\text{-}RCH=CHCHO + MnO + H_2O$$
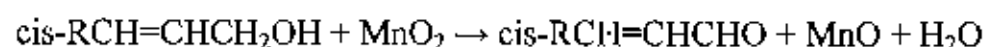
The configuration of the double bond is conserved in the reaction. The corresponding acetylenic alcohols are also suitable substrates, although the resulting propargylic aldehydes can be quite reactive. Benzylic and even unactivated alcohols are also good substrates. 1,2-Diols are cleaved by MnO_2 to dialdehydes or diketones. Otherwise, the applications of MnO_2 are numerous, being applicable to many kinds of reactions including amine oxidation, aromatization, oxidative coupling, and thiol oxidation.

Some examples of the use of MnO_2 are given below [23]:

- MnO_2 is used as a catalyst in the classical laboratory preparation of oxygen from potassium chlorate. A mixture of potassium chlorate and manganese dioxide is heated in a hard glass container and the oxygen gas collected over water.

- MnO_2 is used in combination with anthracite, sand, and gravel in industrial water treatment plants.
- Manganese dioxide also catalyses the decomposition of hydrogen peroxide to oxygen and water:

$$2\ H_2O_2(aq) \rightarrow O_2(g) + 2\ H_2O(l)$$
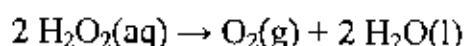
- Eighteenth-century British chemists referred to MnO_2 simply as *manganese*. Elemental manganese was known as *regulus of manganese*.
- Ancient cave painters used MnO_2 as a black or brown pigment.
- MnO_2 was used for production of chlorine in the eighteenth century, before being displaced by electrolytic methods. The manganese dioxide was subsequently recovered by the Weldon process.

Manganese(VII) oxide is the chemical compound with the formula Mn_2O_7. This volatile liquid is highly reactive and more often discussed than observed or intentionally prepared. It is a dangerous oxidizer that was first described in 1860 [24].

Mn_2O_7 arises as a dark red oil by the addition of H_2SO_4 to $KMnO_4$. The reaction initially produces permanganic acid, $HMnO_4$ (also described with the formula $HOMnO_3$). Permanganic acid spontaneously loses water to form its anhydride, Mn_2O_7.

$$2\ KMnO_4 + 2\ H_2SO_4 \rightarrow Mn_2O_7 + H_2O + 2\ KHSO_4$$
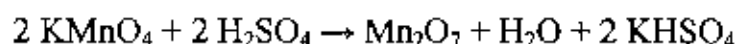
Mn_2O_7 can react further with sulfuric acid to give the remarkable cation MnO_3^+, which is isoelectronic with CrO_3:

$$Mn_2O_7 + 2\ H_2SO_4 \rightarrow MnO_3^+, HSO_4^- + H_2O$$
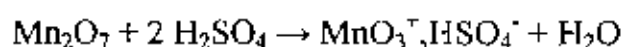
Mn_2O_7 decomposes near room temperature, explosively so at >55 °C. The explosion can be initiated by striking the sample or by its exposure to oxidizable organic compounds. The products are MnO_2 and O_2 [25].

The manganese oxide Hausmannite, Mn_3O_4, is usually not a beautiful mineral; however some specimens are truly wonderful. It can have a bright metallic luster and form well-shaped crystals. The crystals are tetragonal dipyramids, an eight faced form that looks psuedo-octahedral. Indeed at first look, good crystals of hausmannite appear to be octahedrons like those formed by the spinel group of minerals. Hausmannite is a complex oxide of manganese containing both di- and tri-valent manganese. The formula of hausmannite, $(Mn^{+2})(Mn^{+3})_2O_4$, would also seem to place it in the spinel group. Their general formula is AB_2O_4, where A can be a manganese with a positive two charge and B can be a manganese with a positive three $(+3)$ charge. However, those A and B positions are filled with other elements when either one has a manganese ion present. Both sites can not accommodate a manganese ion at the same time and still preserve the isometric structure. Ergo, hausmannite has a distorted spinel structure that produces a tetragonal symmetry and a basal cleavage not possible in the spinel group of minerals. At much higher temperatures, the structure of hausmannite converts to the isometric spinel structure. Hausmannite is an interesting, and can be (when well-formed) a first-rate mineral specimen.

Mn_3O_4 is known to be a good candidate as an active catalyst for the decomposition of waste gases [26], as a corrosion-inhibiting pigment [27, 28], and as an intercalation compound, such as in lithium manganese oxide, which is an electrode material for rechargeable lithium batteries [29]. Bulk Mn_3O_4 undergoes a ferrimagnetic transition at 42 K [30], but Mn_3O_4 nanoparticles exhibit a size-dependent Curie temperature (TC) [31, 32].

1.4 Conductive Polymers

During the last two decades, a new class of organic polymers is synthesized which conduct electrical current. These polymers are called conducting polymers [33]. In general polymers are insulating materials having conductivities ranging from 10^{-10} Scm^{-1} for polyvinyl chloride to 10^{-18} Scm^{-1} for polytetrafluro-ethylene, which are many orders of magnitude below compare to the conductivities associated with metals ($>10^6$ Scm^{-1}). As a result polymers have found wide spread acceptance in a myriad of insulating and structural applications through out the electronic industry. One of the earliest approaches to make polymers conducting is to prepare a composite of polymers and conductive filler, such as metal powder, graphite powder, flake or wire etc. Conductive fillers remain embedded more or less evenly dispersed in the polymer matrix and conduct electric current. But these composites can not be regarded as conducting polymers because the polymers present in such composites are non-conducting [34-37]. When anions like Cl$^-$, ClO$_4^-$, BF$_4^-$ etc. are doped chemically to organic polymers, their electrical conductivity increases. Again when silicon dioxide is dopped in to these plymers, their stability is increased although its electrical conductivity may be decreased.

1.4.1 Brief History of Conductive Polymers

The discovery in 1973 that poly sulfur nitride (SN)$_x$ was intrinsically conducting provided a proof that polymers could be conducting and thus greatly stimulated the search for other conducting polymer [38]. During the last two decades, a new class of organic polymers has been devised

with the remarkable ability to conduct electrical current. These class of materials are called conducting polymers [39].

One of the earliest approaches to make the polymers conductive is to prepare a composite of polymers and conductive filler, such as, metal powder, graphite powder, flake or wire etc. Conductive fillers remain embedded more or less evenly dispersed in the polymer matrix and conduct electric current. But these composites cannot be regarded as conducting polymers because the polymers presents in such composites are non-conducting [40-43].

In 1964, W. A. Little [44] synthesized a superconductor at room temperature with polymeric backbone and large polarizable side groups which led the discovery of new organic compounds with high electrical conductivity.

In the early 1980s, excitement ran high when several prototype devices based on conductive polymers, such as rechargeable batteries and current rectifying *p-n* junction diodes [45] were announced. Among the many polymers known to be conductive, polyacetylene (PAT), polyaniline (PANI), polypyrrole (PP) and polythiophene (PT) have been studied most intensively [46-52]. However, the conductive polymer that actually launched this new field of research was PAT.

Research has been expanded into the studies of heteroatomic conductive polymers because of their better chemical stability and the interest in the polaron and bipolaron conduction mechanism [53, 54]. Among the heteroatomic polymers PP, PT and PANI have been studied extensively.

In 1968, Dall'Olio *et. al.* [55] published the first report of analogous electrosynthesis in other system. They had observed the formation of brittle, film like pyrrole black on a Pt electrode during the oxidation of pyrrole in dilute sulfuric acid. Conductivity measurements carried out on the isolated solid state materials gave a value of 8 Scm^{-1}. In addition, a strong ESR signal was evidenced of a high number of unpaired spin. Earlier, in 1961, H. Lund [56] had reported in a virtually unobtainable publication that PP can be produced by electrochemical polymerization.

In 1979, Diaz *et. al.* [57] produced the first flexible and stable PP film with high conductivity (100 Scm^{-1}). The substance was polymerized on a Pt electrode by anodic oxidation in acetonitrile. The known chemical methods of synthesis [58-60] usually produced low conductivity powders from the monomers. PP formed at the electrode surface and could be peeled off as a flexible, relatively dense and shiny blue-black film. This polymer is characterized not only by its high conductivity but also by its high stability.

During the 1980s, PANI was subjected to intense structural, physical, and electrical characterization, using modern experimental techniques. A brief survey, out of numerous features and studies made on PANI is presented below:

1.4.2 Structural Features of PANI

Organic conducting polymer, PANI, is being studied more and more, and up to the recent years has been the centre of considerable scientific interest. However, PANI is not really a new material and its existence has been known for the past 150 years or over, since it had already been made by Runge in 1834.

PANI has been described in many papers [61] usually as ill-defined forms such as 'aniline black' emeraldine, nigraniline, *etc.* synthesized by the chemical or electrochemical oxidation of aniline. Figure 1.4.1 shows the idealized oxidation state of PANI: leucoemeraldine, emeraldine, pernigraniline and emeraldine salt. Different structures result in different electrical behaviours of the material. Emeraldine salt is a partially oxidized compound, protonated, with electrical conducting characteristics. Leucoemeraldine is a fully reduced compound with electrical insulating characteristics. There are no double bonds between the aromatic rings and the N-H groups. Emeraldine base is an insulating compound, partially oxidized with few N-H groups in the main chain. Emeraldine changes from insulator to conductor when it is protonated with proton donor acids, such as, hydrochloric acid. This change is one of the most interesting properties of PANI.
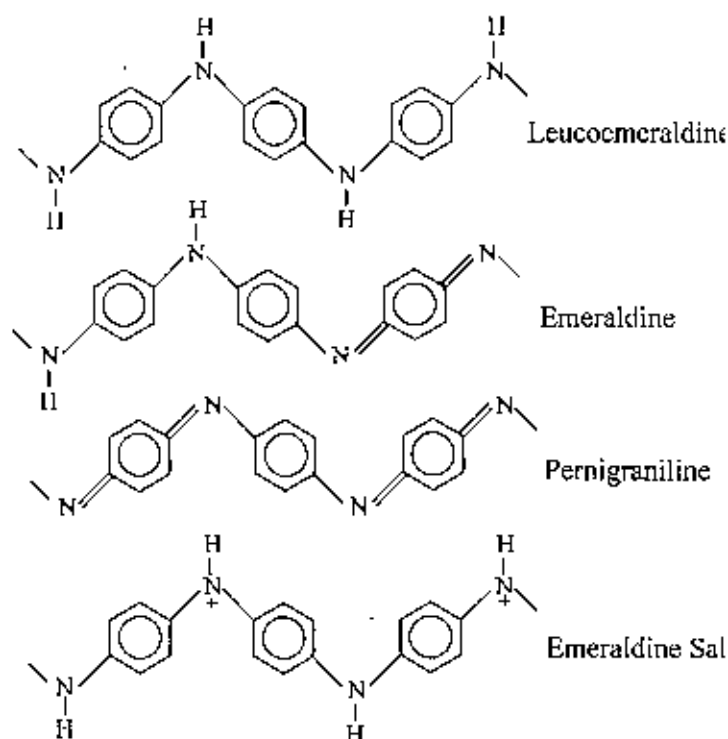
Fig. 1.4.1: Representation of idealized oxidation states of PANI.

The structure of emeraldine PANI can be changed to emeraldine salt by removing an electron from the N-H group. Pernigraniline is a fully oxidized compound without conducting characteristics. There are no N-H groups in the structure. The level of protonation in the structure causes dramatic changes in the conductivity. The base form of the polymer in the emeraldine oxidation state (y = 0.5)
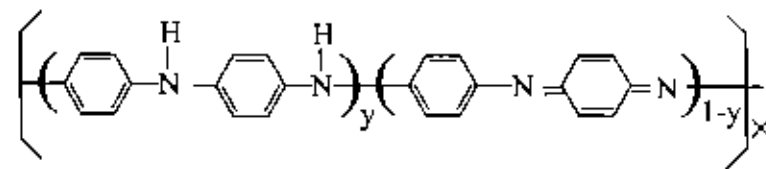
which contains equal number of alternating reduced,

 and oxidized
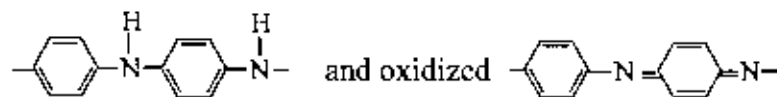
repeating units can be protonated by dilute aqueous acid to produce the corresponding salt (A=anion)
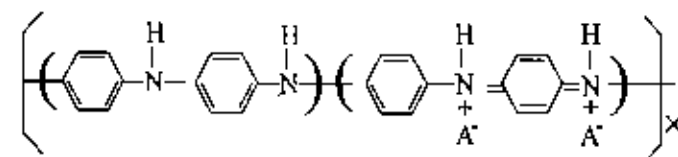
which is believed to exist as polysemiquinone radical cation [39-40].
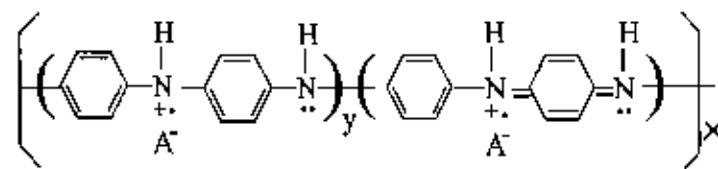
The polymer exhibits conductivities of ~ 1-5 S cm^{-1} when approximately half of its nitrogen atoms are protonated as shown above.

1.4.3 Methods of Preparation

PANI is generally prepared by direct oxidation of aniline using an appropriate chemical oxidant or by electrochemical oxidation on different electrode materials.

Various chemical oxidizing agents have been used by different authors: potassium dichromate [62, 63], ammonium persulfate or peroxydisulfate [64, 65], hydrogen peroxide, ceric nitrate and ceric sulfate [66, 67]. The reaction is mainly carried out in acid medium, in particular sulfuric acid, at a pH between 0 and 2 [53, 54]. However, MacDiarmid *et al.* [67, 68] used hydrochloric acid at pH 1. Genies *et al.* [68] used a eutectic mixture of hydrofluoric acid and ammonia, the general formula of which is NH_4F: 2.3 HF, for which the pH is probably less than 0.

When aniline is mixed with the chemical oxidant in a reaction vessel and left for a certain period of time (the duration of which depends on the temperature and the concentration of active species), the solution gradually becomes colored and a black precipitate appears [69]. The coloration of the solvent is possibly due to the formation of soluble oligomers.

Anodic oxidation of aniline on an inert metallic electrode is the most current method for the electrochemical synthesis of PANI. This method offers the possibility of coupling with physical spectroscopic technique such as visible, IR, Raman, ellipsometry and conductimetry, for *in situ* characterization.

The anodic oxidation of aniline is generally effected on an inert electrode material which is usually Pt [70, 71]. However, several studies have been

carried out with other electrode materials: iron [72], copper [73], zinc and lead, chrome-gold [74], palladium [75] and different types of carbon vitreous, pyrolic or graphite [76] or on semiconductor [77, 78]. When the polymerization is carried out at constant current, a maximum current density of 10 mA cm $^{-2}$ is rarely exceeded.

The conducting polymers, CH$_3$-PANI, PP, and the copolymers as well as the composites can also be prepared by both chemical (79-92) and electrochemical polymerization (93-125).

1.4.4 Reaction Mechanism for Polymerization of Aniline

The efficient polymerization of aniline is achieved only in an acidic medium. The mechanism of this reaction is shown in Fig 1.3.3. The first five steps involve the establishment of the anilinium radicals and the possible reactions between the anilinium radicals themselves or with each other, and finally the oxidation of ADPA by the peroxide to form PBQI. Step 6 is the most important one, because it shows that the catalytic action of the acidic reaction medium accelerates the coupling of aniline (or, more precisely anilinium radical 2) with existing dimmers and higher oligomers (step 6b). Moreover step 6b also supplies a reasonable explanation for the different oxidation states in PANI powders prepared under similar conditions.

Step 1: Formation of the aniliniumradicalcation 1

$$2\,\langle\bigcirc\rangle\text{-NH}_2 \;+\; \begin{matrix} \text{O-SO}_3^- \\ | \\ \text{O-SO}_3^- \end{matrix} \;\rightleftharpoons\; 2\,\langle\bigcirc\rangle\text{-}\overset{+\bullet}{\text{N}}\text{H}_2 \;+\; 2\,\text{SO}_4^{2-}$$
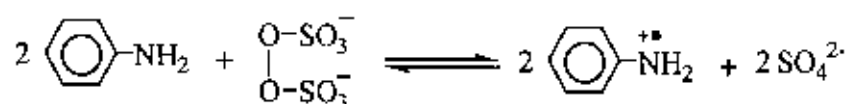
Step 2: Formation of the aniliniumradical 1
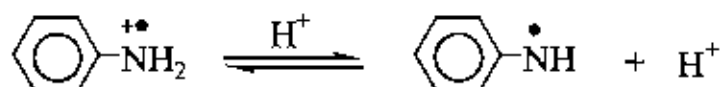
Step 3: Formation of the aniliniumradical 2
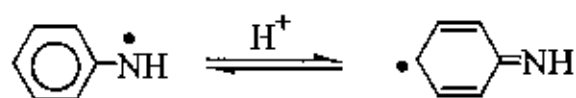
Step 4: Coupling of the aniliniumradicals 1 and 2 (Generation of
p-aminodiphenylamine)
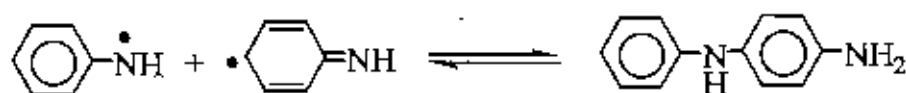
Step 5: Generation of N-phenyl-1,4-benzoquinone diimine from
p-aminodiphenylamine
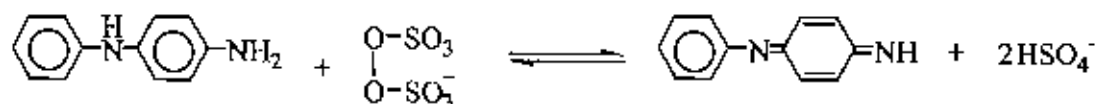
Step 6: Growth of aniline oligomers and polymers

(a) Growth via *p*-aminodiphenylamine and aniliniumradical 2
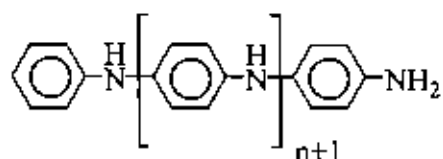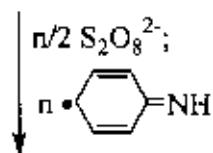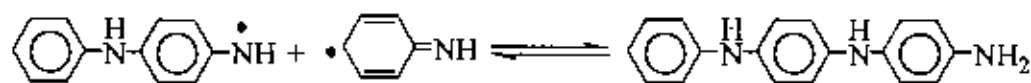
(b) Growth via N-phenyl-1,4-benzoquinone diimine and aniliniumradical 2, catalyzed by the acid HX
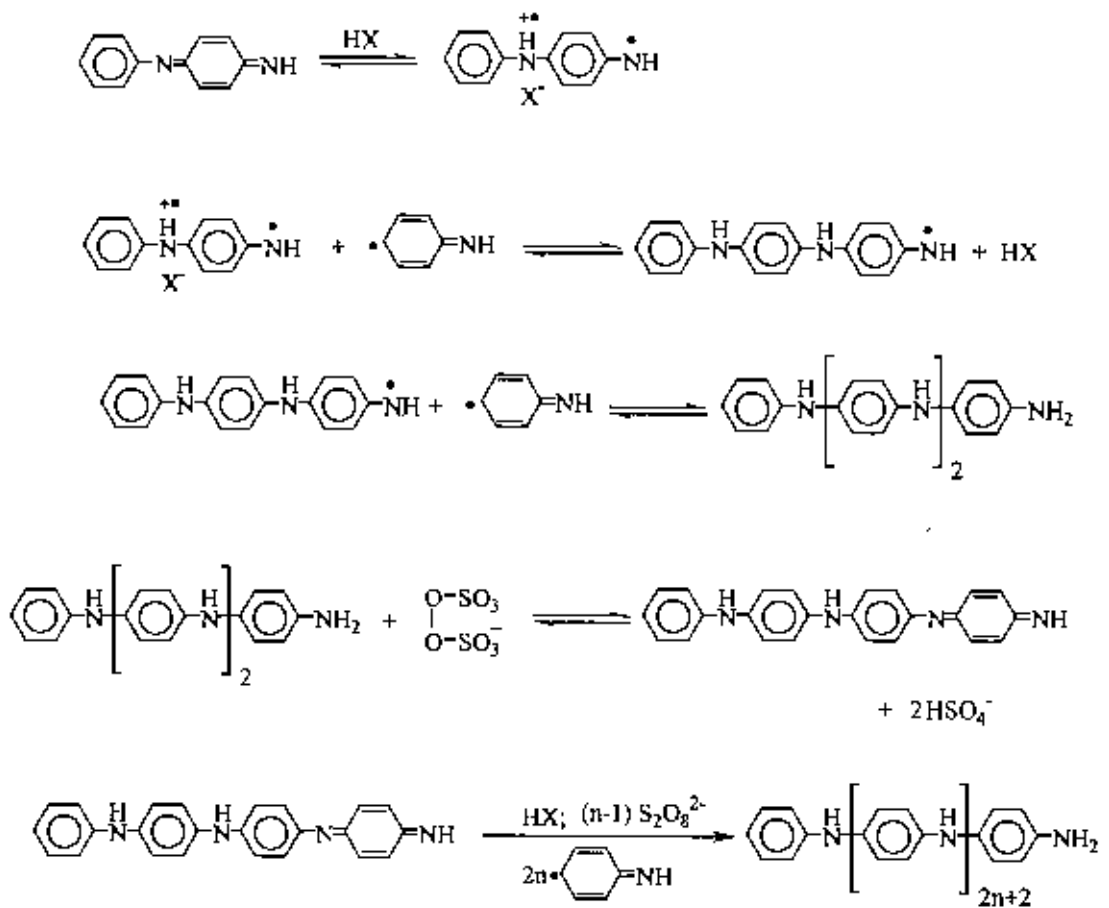
Fig. 1.4.3: Mechanism for the polymerization of aniline

1.4.5 Application of Conducting Polymer

Conducting polymeric materials prepared by electrochemical polymerization of a number of monomers have recently received considerable attention because of the large variety of their potential applications such as in energy storage [126], batteries [127,128],

electrocatalysis [129,130], gas sensors [131-135], and biosensors [136-141].

PANI can be used as material for modified electrodes [76, 142], as a corrosion inhibitors for semiconductors in photoelectrochemical assemblies [143], in microelectronics [144, 145] and as electrochromic material [146]. The application which has inspired most interest is in the area of electrochemical batteries. The possible use of PANI as active anodic material is in rechargeable batteries [61].

More recent systematic studies have been undertaken by numerous groups [47, 65, 143] on the possible use of PANI as an active electrode material. These investigations deal with the behavior of PANI in aqueous and organic media as a function of the mode of synthesis.

1.5 Composites

Since 1965 a distinct discipline and technology of composite materials have been begun to emerge. That is 80% of all research and development on composites have been done since 1965 when the Air Force launched its-all out development program to make high performance fiber composites a practical reality. There are two major reasons for the revived interest in composite materials. One is that the increasing demands for higher performance in many product areas especially in the aerospace, nuclear energy and aircraft fields is taxing to the limit our conventional monolithic materials. The second reason, the most important for the long run is that the composites concept provides scientists and engineers with a promising approach to designing, rather than selecting, materials to meet the specific requirements of an application.

The term 'composite' refers to something made up of various parts or elements. In definition of composite depends on the structural level of the composite we are thinking about. At the submicroscopic level that of simple molecules and crystal cells all materials composed of two or more different atoms or elements would be regarded as composites. This would include compounds, alloys plastics and ceramics. Only the pure elements would be excluded. At the microscopic level (or microstructural level) that of crystals, polymers, and phases a composite would be a material composed of two or more different crystals, molecular structures, or phases. By this definition most of our traditional materials, which have always been considered monolithic, would be classified as composites. At the macro structural level which is most useful for composites, the definitions of composites is that they are a mixture of macro constituent phase composed of materials which are in a divided state and which generally differ in form and/or chemical composition. Note that, contrary to a widely held assumption, this definition does not require that a composite be composed of chemically different materials, although this usually the case. The more important distinguishing characteristics of a composite are its geometrical features and the fact that its performance is the collective behavior of the constituents of which it is composed. A composite material can vary in composition, structure, and properties from one point to the next inside the material.

The major constituents used in structuring composites are fibers, particles, laminas, flakes, filters and matrix. The matrix, which can be thought of as the body constituent, gives the composite its bulk form. The other four, which can be referred to as structural constituents, determine the character of the composite's internal structure. A special type of

composite, fiberglass embedded in a polymer matrix is a relatively recent invention but has in a few decades, become a commonplace material. Characteristic of good composites, fiberglass, provides the 'best of both worlds', it carries along the superior properties of each component, producing a product that is superior to either of the components separately. The high strength of the small diameter glass fibers is combined with the ductility of the polymer matrix to produce a strong material capable of withstanding the normal loading required of a structural material.

1.6 Dyes

A dye can generally be described as a colored substance that has an affinity to the substrate to which it is being applied. The dye is generally applied in an aqueous solution, and may require a mordant to improve the fastness of the dye on the fiber.

Both dyes and pigments appear to be colored because they absorb some wavelengths of light preferentially. In contrast with a dye, a pigment generally is insoluble, and has no affinity for the substrate. Some dyes can be precipitated with an inert salt to produce a lake pigment.

Archaeological evidence shows that, particularly in India and the Middle East, dyeing has been carried out for over 5000 years. The dyes were obtained from animal, vegetable or mineral origin, with no or very little processing. By far the greatest source of dyes has been from the plant kingdom, notably roots, berries, bark, leaves and wood, but only a few have ever been used on a commercial scale.

1.6.1 Organic Dyes

An organic dye consists of a color producing structure, the chromogen (electron acceptor), and a part to regulate the solubility and dying properties, the auxochrom (electron donor). Without both parts, the material is simply a colored body.

The Chromogen is an aromatic body containing a color-giving group, called the chromophore. Chromophore groups cause color by altering absorption bands in the visible spectrum. Common chromophores are: nitroso group (- NO), nitro group (-NO_2), azo group (- N=N -), ethylene group (>C = C <), carbonyl group (>C = O), carbon nitrogen groups (>C=NH and –CH =N-), carbon sulphur groups (>C = S and $\rightarrow$C– S-S-C$\leftarrow$) etc.

Theses groups add color to aromatic bodies by causing displacement of, or an appearance of absorption bands in the visible spectrum. In modern point of views, these groups place the ground and excited state in the range that corresponds to the visible range of the spectrum.

The auxochrome, an essential part of a dye molecule, cause the dye to adhere to the material which it colors, enhance the color of dye, improve solubility in the solvent which is important for application on the materials.

Common auxochrome are: - NH_2, - OH, -NR_2, -COOH, - SO_3H etc.

1.6.2 Classification of Dyes

The first human-made (synthetic) organic dye, mauveine, was discovered by William Henry Perkin in 1856. Many thousands of synthetic dyes have since been prepared. Synthetic dyes quickly replaced the traditional

natural dyes. They cost less, they offered a vast range of new colors, and they imparted better properties upon the dyed materials [147]. Dyes are now classified according to how they are used in the dyeing process.

Acid dyes are water-soluble anionic dyes that are applied to fibers such as silk, wool, nylon and modified acrylic fibers using neutral to acid dyebaths. Attachment to the fiber is attributed, at least partly, to salt formation between anionic groups in the dyes and cationic groups in the fiber. Acid dyes are not substantive to cellulosic fibers.

Basic dyes are water-soluble cationic dyes that are mainly applied to acrylic fibers, but find some use for wool and silk. Usually acetic acid is added to the dyebath to help the uptake of the dye onto the fiber. Basic dyes are also used in the coloration of paper.

Direct or **substantive dyeing** is normally carried out in a neutral or slightly alkaline dyebath, at or near boiling point, with the addition of either sodium chloride (NaCl) or sodium sulfate (Na_2SO_4). Direct dyes are used on cotton, paper, leather, wool, silk and nylon. They are also used as pH indicators and as biological stains.

Mordant dyes require a mordant, which improves the fastness of the dye against water, light and perspiration. The choice of mordant is very important as different mordants can change the final color significantly. Most natural dyes are mordant dyes and there is therefore a large literature base describing dyeing techniques. The most important mordant dyes are the synthetic mordant dyes, or chrome dyes, used for wool; these comprise some 30% of dyes used for wool, and are especially useful for black and navy shades. The mordant, potassium dichromate, is applied as an after-treatment. It is important to note that many mordants, particularly those in the heavy metal category, can be hazardous to health and extreme care must be taken in using them.

Vat dyes are essentially insoluble in water and incapable of dyeing fibres directly. However, reduction in alkaline liquor produces the water soluble alkali metal salt of the dye, which, in this leuco form, has an affinity for the textile fibre. Subsequent oxidation reforms the original insoluble dye. The color of denim is due to Indigo, the original vat dye.

Reactive dyes utilize a chromophore attached to a substituent that is capable of directly reacting with the fibre substrate. The covalent bonds that attach reactive dye to natural fibers make them among the most permanent of dyes. "Cold" reactive dyes, such as Procion MX, Cibacron F, and Drimarene K, are very easy to use because the dye can be applied at room temperature. Reactive dyes are by far the best choice for dyeing cotton and other cellulose fibers at home or in the art studio.

Disperse dyes were originally developed for the dyeing of cellulose acetate, and are substantially water insoluble. The dyes are finely ground in the presence of a dispersing agent and then sold as a paste, or spray-dried and sold as a powder. Their main use is to dyepolyester but they can also be used to dye nylon, cellulose triacetate, and acrylic fibres. In some cases, a dyeing temperature of 130 °C is required, and a pressurised dyebath is used. The very fine particle size gives a large surface area that aids dissolution to allow uptake by the fibre. The dyeing rate can be significantly influenced by the choice of dispersing agent used during the grinding.

Azo dyeing is a technique in which an insoluble azoic dye is produced directly onto or within the fibre. This is achieved by treating a fibre with both diazoic and coupling components. With suitable adjustment of dyebath conditions the two components react to produce the required insoluble azo dye. This technique of dyeing is unique, in that the final color is controlled by the choice of the diazoic and coupling components.

Sulfur dyes are two part "developed" dyes used to dye cotton with dark colors. The initial bath imparts a yellow or pale chartreuse color. This is aftertreated with a sulfur compound in place to produce the dark black we are familiar with in socks for instance. Sulfur Black 1 is the largest selling dye by volume.

Food dyes are another class which describes the role of dyes, rather than their mode of use. Because food dyes are classed as food additives, they are manufactured to a higher standard than some industrial dyes. Food dyes can be direct, mordant and vat dyes, and their use is strictly controlled by legislation. Many are azoic dyes, although anthraquinone and triphenylmethane compounds are used for colors such as green and blue. Some naturally-occurring dyes are also used.

1.6.3 Methylene Blue

Methylene blue is a heterocyclic, cationic aromatic dye with molecular formula: $C_{16}H_{18}ClN_3S$ and its IUPAC name is 3,7-bis(Dimethylamino)-phenazathionium chloride Tetramethylthionine chloride.
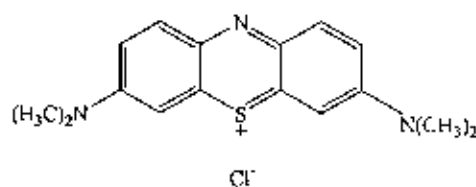
Fig. 1.6.1: Chemical Structure of Methylene Blue

It has many uses in a range of different fields, such as biology or chemistry. At room temperature it appears as a solid, odorless, dark green powder, that yields a blue solution when dissolved in water. Methylene blue is widely used as a redox indicator in analytical chemistry. Solutions of this substance are blue when in an oxidizing environment, but will turn colorless if exposed to a reducing agent. In biology methylene blue is used as a dye for a number of different staining procedures, such as Gram's stain, Wright's stain, and Jenner's stain. Since it is a temporary staining technique, methylene blue can also be used to examine RNA or DNA under the microscope or in a gel: as an example, a solution of methylene blue can be used to stain RNA on hybridization membranes in northern blotting to verify the amount of nucleic acid present. Owing to its reducing agent properties, methylene blue is employed as a medication for the treatment of methemoglobinemia, which can arise from ingestion of certain pharmaceuticals or broad beans. Basically, methylene blue acts to reduce the heme group from methemoglobin to hemoglobin.

In the human body, methylene blue is highly stable; if ingested, it resists the stomach's acidic environment as well as the many hydrolytic enzymes present. Methylene blue also has some other adverse reactions in human body that can be stated below [148, 149]:

Table 1.6.1: Some adverse effects of methylene blue in human body

Cardiovascular	Central Nervous System	Dematologic	Gastrointestinal	Genitourinary	Hematologic
•Hypertension •Precordial pain	•Dizziness •Mental confusion •Headache •Fever	•Staining of skin •Injection site necrosis (SC)	•Fecal discoloration •Nausea •Vomiting •Abdominal pain	•Discoloration of urine •Bladder irritation	•Anemia

1.6.4 Procion Red

Procion red (PR) is common textile organic monoazo dye and anionic in nature. It is a heterocyclic aromatic chemical compound with molecular formula: $C_{19}H_{10}Cl_2N_6Na_2O_7S_2$. Molecular weight of PR is 615.38 and λ_{max} is 538 nm. Its chemical structure is shown in Fig. 1.6.2.
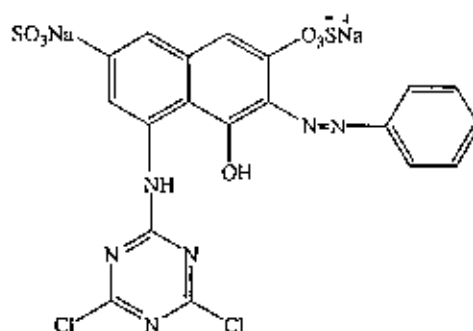
Fig. 1.6.2: Chemical structure of PR.

1.7　Theoretical Aspects of Experimental Techniques

1.7.1　Infrared Spectroscopy

Emission or absorption spectra arise when molecules undergo transition between quantum states corresponding to two different internal energies. The energy difference ΔE between the states is related to the frequency of the radiation emitted or absorption by the quantum relation

$$\Delta E = h\nu \tag{1.7.1}$$

where $h \rightarrow$ Planck's constant, and $\nu \rightarrow$ frequency.
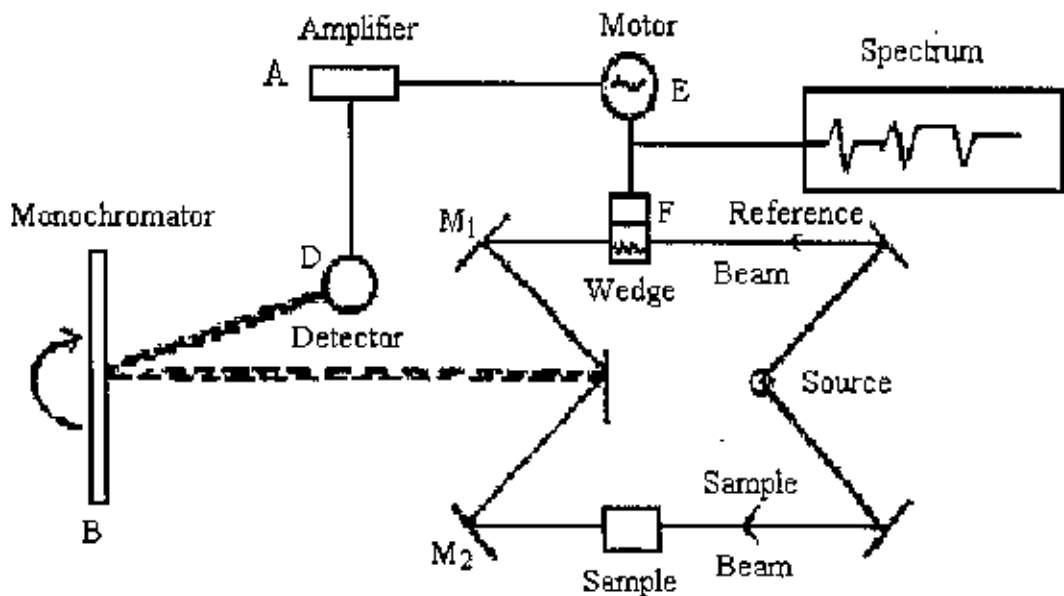
Fig.1.7.1:　A block diagram of an IR spectrophotometer.

Infrared (IR) frequencies have the wave length range from 1 μm to 50 μm are associated with molecular vibration and vibration-rotation spectra. Detection of chemical groups and bonding are done by the typical spectra.

In polymer, the IR absorption spectrum is often surprisingly simple, if one considers the number of atoms involved. This simplicity results first from the fact that many of the normal vibrations have almost the same frequency and therefore appear in the spectrum as one absorption band and second, from the strict selection rules that prevent many of the vibrations from causing absorptions. In our experiment, we tried to observe the change in frequency of different samples cobalt oxide, nickel oxide, cobalt-nickel mixed oxide and detection of cobalt oxide, nickel oxide, mixed oxide by following the Co-O or Ni-O frequencies. IR spectrums of all the compounds were recorded on IR spectrophotometer in the region of 4000-400 cm^{-1}. Samples were introduced as KBr pellets. A block diagram of an IR spectrophotometer is shown in Fig. 1.7.1.

1.7.2 Ultraviolet-Visible Spectroscopy

Electromagnetic radiation of suitable frequency can be passed through a sample so that photons are absorbed by the samples and changes in the electronic energies of the molecules can be brought about. So it is possible to effect the changes in a particular type of molecular energy using appropriate frequency of the incident radiation. When a beam of photons passes through a system of absorbing species, then we can write

$$-\frac{dI}{dx} = \alpha I \tag{1.7.2}$$

where, $I \rightarrow$ intensity of photon beam

$dI \rightarrow$ reduction of intensity

$dx \rightarrow$ rate of photon absorption with distance (x) traversed

$\alpha \rightarrow$ absorption co-efficient of the material

Now if I_o is the initial intensity at thickness $l = 0$ and I is the transmitted radiation at $x = 1$, then by integration, we can write

$$ ln\frac{I_0}{I} = \alpha l \tag{1.7.3} $$

For polymers and polymeric composites, Ultraviolet – Visivle (UV-Vis) spectrum is taken to measure the impurity level, band gap energy etc. The electrode spectra of the prepared compounds were recorded on a UV-Vis recording spectrophotometer in the wavelength range 300-800 nm. A schematic diagram of UV-Vis spectrophotometer is shown iu Fig. 1.7.2.

Fig. 1.7.2: A block diagram of an UV-Vis spectrophotometer.

1.7.3 X-Ray Diffraction

The X-ray diffraction (XRD) provides substantial information on the crystal structure. This method is applied for the investigation of orderly arrangements of atoms or molecules through the interaction of electromagnetic radiation to give interface effects with structures comparable in size to the wavelength of the radiation. Studies on the crystal structures developed based on methods using single crystals after the discovery of X-ray diffraction by crystals made by the Von Laue [150]. Nowadays XRD is used not only for the determination of crystal structure but also chemical analysis, such as chain conformations and packing for polymers, for stress measurements and for the measurement of phase equilibria and the measurement of particle size, for the determination of the orientation of the crystal and the ensemble of orientations in a polycrystalline material.

X-rays are the electromagnetic radiation whose wavelength is in the neighborhood of 1 Å. The wave length of an X-ray is thus of the same order of magnitude as the lattice constant of crystals, and it is this which makes X-rays so useful in structures analysis of crystals whenever X-ray are incident on a crystal surface they are reflected. The reflection abides by the celebrated Bragg's law as given below:

$$2d\,Sin\theta = n\lambda \qquad\qquad (1.7.4)$$

where d is distance between crystal planes, θ is the incident angle, λ is the wave length of X-ray and n is a positive integer. The diffracted X-ray may be detected by their action on photographic films or plates or by means of a radiation counter or electronic equipment feeding data to a computer [151].

The main purpose of using this technique for the analysis of the studied polymeric samples is to observe, from the X-ray diffraction pattern, the change in crystallinity in the series upon same condition.

1.7.4 SEM Technique

The Scanning Electron Microscope (SEM) uses a finely focused beam of electrons to scan over the area of interest. The beam-specimen interaction is a complex phenomenon. The electrons actually penetrate into the sample surface, ionizing the sample and cause the release of electrons from the sample. These electrons are detected and amplified into a SEM image that consists of Back Scattered Electrons and Secondary Electrons. Since the electron beam has a specific energy and the sample a specific atomic structure, different image will be collected from different samples, even if they have the same geometric appearance.

The specimen stage allows movement of the specimen along five axes as indicated in Fig.1.7.3 (a) & (b). The basic stage is controlled manually by micrometers and screw-type adjusters on the stage door. The motorized stage has motors driving the X, Y, Z and rotation controls, all with manual override.

The stage can be tilted over 90°. The tilt axis always intersects the electron optical axis of the column at the same height (10 mm). When the specimen positioned at this height, the specimen can be tilted in the eucentric plane. This means that during tilt, almost no image displacement occurs. The tilting mechanism can be locked for more stability at high magnification.

Rotation in the tilted plane

Y ± 75 mm in the plane of tilt, perpendicular to the tilt axis

X ± 75 mm along the tilt axis

Z 37 mm

Tilt range −30° to +60°
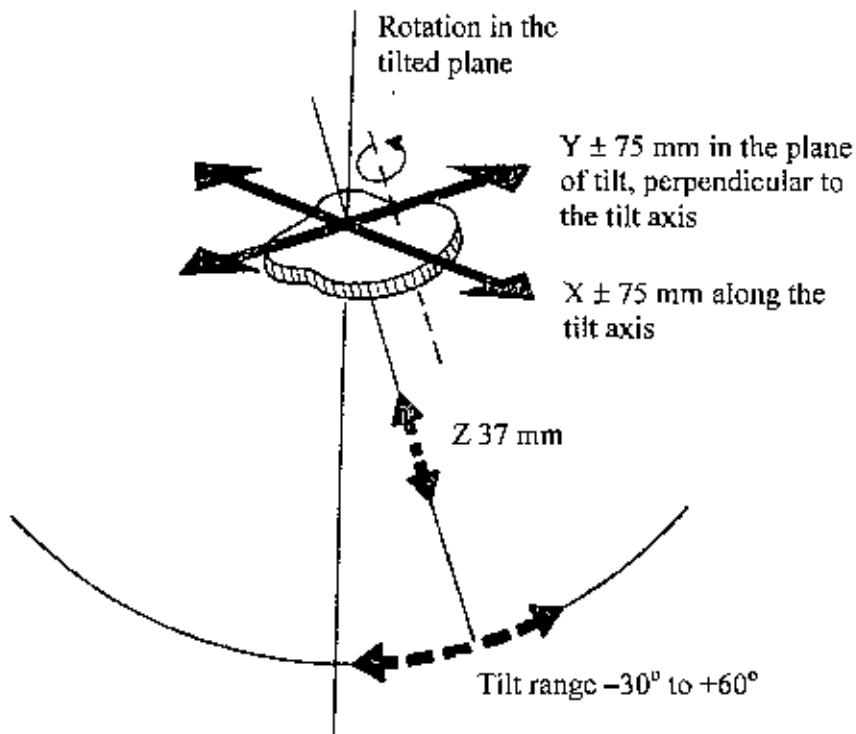
Fig. 1.7.3 (a): Illustration of specimen stage movement in SEM arrangements.
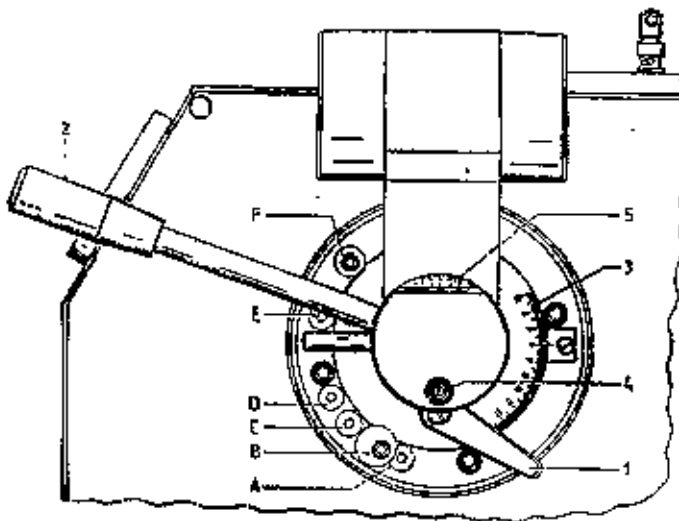
Fig. 1.7.3 (b): Mechanical controls and tilt stops on the stage door of SEM.

1.7.5 Energy Dispersive X-ray (EDX) Microanalysis

EDX is a microanalytical technique that uses the characteristic spectrum of x-rays emitted by the specimen after excitation by high-energy electrons to obtain information about its elemental composition. An electron beam strikes the surface of the sample. The energy of the beam is 120 keV. This causes X-rays to be emitted. The energy of the X-rays emitted depends on the material under examination. The X-rays are generated in the whole section. The detector used in EDX is the Lithium drifted Silicon detector. This detector must be operated at liquid nitrogen temperatures. When an X-ray strikes the detector, it will generate a photoelectron within the body of the Si. As this photoelectron travels through the Si, it generates electron-hole pairs. The electrons and holes are attracted to opposite ends of the detector with the aid of a strong electric field. The size of the current pulse thus generated depends on the number of electron-hole pairs created, which in turn depends on the energy of the incoming X-ray, which depends on the composition of the sample. Thus, an X-ray spectrum can be acquired giving information on the elemental composition of the material under examination. By moving the electron beam across the material an image of each element in the sample can be acquired.

If an electron beam strikes the surface X-rays (hv) were emitted [Fig. 1.7.4], which energy depends on the elemental compostion of the sample. Vice versa the energy of the electrons is reduced. Analysis of these emitted X-rays gives a spectrum, EDX.
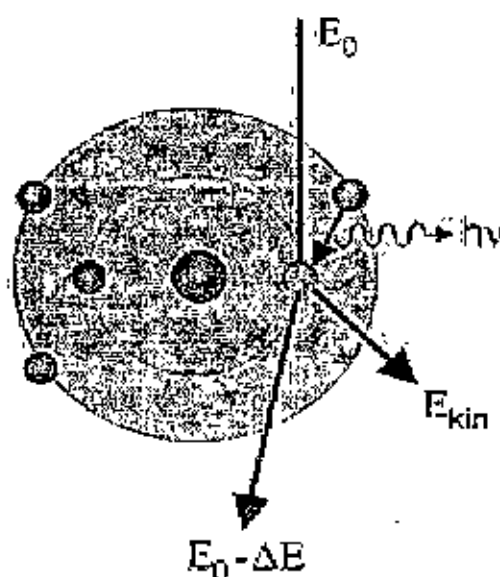
Fig. 1.7.4   Schematic diagram of emission of X-ray due to electron
beam interaction with a solid

1.7.6 Cyclic Voltammetry

Electrochemical process is widely used in the polymerization of organic
polymer. Most of the system for electrochemical polymerization consists
of compartment where three electrodes are dipped into the solution
containing monomer and electrolyte solution. Appropriate potential is
applied to the working electrode for polymerization of the monomers.
The potential of the working electrode, where deposition of the polymer
film takes place, is controlled versus the reference electrode using a feed-
back circuit or a potentiostat. Feed-back circuit drives the circuit between

the working and counter electrode ensuring that none can pass through the reference electrode circuit.

The nature of the working electrode is a critical consideration for the preparation of these films. Since the films are produced by an oxidative process, it is important that the electrode is not oxidized concurrently with the aromatic monomer. For this reason, most of the available films have been prepared using a platinum or a gold electrode.

Potentiostatic, galvanostatic and potential sweep techniques such as cyclic voltammetry are widely used for electrochemical polymerization of aromatic compounds. In potentiostatic technique, a constant potential is applied to the working electrode which is sufficient to oxidize the monomers to be polymerized on the electrode. In galvanostatic process, a constant current density is maintained to polymerize the monomers while film thickness can be monitored in the similar way as described for potentiostatic technique. On the other hand, cyclic voltammetry involves sweeping the potential between potential limits at a known sweep rate. On reaching the final potential limit, the sweep is reversed at the same scan rate to the initial potential and the sweep may be halted, again reversed, or alternatively continued further. In such experiments, cell current is recorded as a function of the applied potential.

1.7.7 Electrical Conductivity

The conductivity of polymer or polymeric composites depends on dopant level, protonation level of oxidation morphology and moisture content of the sample. Electrical resistivity of the polymer samples may be

measured by two probe and four probe techniques. The electrical conductivity may be measured by using ohm's law

$$E/I = R \qquad\qquad 1.7.6$$

where I is the current in amperes, E is the potential difference in volts, R is the resistance in ohms. The reciprocal is termed the conductance, this is measured in Siemens (S) which is reciprocal of ohms (ohm^{-1}). The resistance of a samples of length L, and cross-sectional area A, is given by

$$R = \rho L/A \qquad\qquad 1.7.7$$

where ρ is a characteristic property of the material termed the resistivity. If L and A will be measured respectively in cm and then ρ refers to cm cube of the material and

$$\rho = RA/L \qquad\qquad 1.7.8$$

The reciprocal of resistivity is the conductivity, (formerly specific conductance)

$$K = 1/\rho \quad\text{or}\quad K = L/RA \qquad\qquad 1.7.9$$

which is SI units is the conductance of a one cm cube of substance and has the units ohm^{-1} cm^{-1} or S cm^{-1}.

In this experiment, the powdered samples were pressed to rigid solid mass by pressing from the both sides of the mass. The two electrodes of microvolt were then connected with solid mass and resistance was measured directly from the microvolt.

1.8 Literature Review and Plan of the Present Research

Nanostructured materials have attracted the attention of researchers during the last decades, not only for their fundamental scientific interest, but also for many technological applications. For many of these applications, the synthesis of uniform-sized nanoparticles is of key importance. The electrical, optical, and magnetic properties of these nanoparticles depend strongly on their dimension. For example, uniform-sized magnetic nanoparticles have attracted a lot of attention because of their broad range of applications, which include magnetic storage media, ferrofluids, magnetic resonance imaging (MRI), and magnetically guided drug delivery [153-159]. Recently, one-dimensional (1-D) nanostructured materials, including nanorods, nanowires, and nanotubes, have received a tremendous amount of attention because of their unique properties. These properties are derived from their low dimensionality, and their potential use in the interconnects and functional blocks that are used for fabricating nanoscale devices [160-166]. Manganese oxides have found wide applications as catalysts and electrode materials [167-170]. Very recently, several groups reported the synthesis of nanoparticles of manganese oxides, characterization, variety of applications, and their dispersion into a polymeric matrix. Some of them are cited below:

Tokeer Ahmad et al. [171] introduced nanorods of manganese oxalate as a single source precursor to different manganese oxide nanoparticles. Nanorods of anhydrous manganese oxalate were prepared by the reverse-micellar method using CTAB as the surfactant. This precursor was then used to synthesize single phase nanoparticles of various manganese oxides such as MnO, Mn_2O_3 and Mn_3O_4 under specific reaction conditions. Both MnO

(28 nm) and α-Mn₂O₃ (50 nm) were stabilized as cubic phase. α-Mn_2O_3 showed a weak antiferromagnetic transition (TN = 80 K), while the spinel Mn_3O_4 (100 nm) particles showed a ferrimagnetic transition at 43 K.

A low temperature synthesis of Mn_3O_4 nanoparticles using manganese sulfate and hydrogen peroxide as staring materials was studied by Jin Mu et al [172]. They established a solution method for preparing Mn_3O_4 nanoparticles at 45^0 C using starch as capping agent. The distinct advantage of their method was avoiding the agglomeration of particles in high temperature treatment.

Ning Wang et al. [173] reported on the synthesis of high-quality tetragonal Mn_3O_4 nanoparticles and the large-scale assembly of the nanoparticles into a wall-like pattern by using a mild solution method at 60^0 C without any post treatment modification. This made free spatial arrangement possible. they have also investigated the magnetic properties of the as-grown Mn_3O_4 nanopatterns by using the superconducting quantum interference device (SQUID) system.

Procedures for the preparation of Mn_3O_4 nanoparticles (about 20 nm) or elongated α-MnOOH particles with length less than 2 μm and width 0.4 μm or less were described by M. Ocana [174]. Forced hydrolysis of aqueous manganese(II) acetate solutions was performed in the absence of HCl to obtain Mn_3O_4 and in the presence of HCl to obtain α-MnOOH. These solids were only produced under a very restrictive range of reagent concentrations involving solutions of 0.2-0.4 mol dm⁻³ manganese (II) acetate for Mn_3O_4 and of 1.6-2.0 mol dm⁻³ Mn(II) and 0.2-0.3 mol dm⁻³ HCl for α-MnOOH at low temperature (80 °C).

Won Seok Seo et al. [175] reported a simple, reliable synthesis of size-focused colloidal nanocrystals of two different manganese oxides,Mn_3O_4 and MnO, from thermal decomposition of a single precursor manganese acetylacetonate, $Mn(acac)_2$, in oleylamine. They also studied the size-dependent magnetic properties of colloidal Mn_3O_4 and MnO nanoparticles.

A versatile, convenient, and nontoxic solvothermal method for the synthesis of nanocrystalline iron, chromium, and manganese oxides was described by Amanda L. Willis et al. [176]. This method employed the reactions of metal acetylacetonate precursors and oxygen-containing solvents in a reaction to prepare metal oxide nanoparticles. A convenient reaction for the preparation of γ-Fe_2O_3 was discovered and had been expanded to the preparation of γ-Fe_2O_3, Mn_2O_3, Mn_3O_4, and Cr_2O_3. Characterization of these nanocrystalline materials was carried out employing transmission electron microscopy (TEM), high-resolution TEM (HRTEM), X-ray diffraction (XRD), and elemental analysis.

Weixin Zhang et al. [177] prepared Mn_3O_4 nanoparticles and MnOOH nanorods through successfully controlling a solvothermal reaction. An aqueous ethanol solution was used as the solvent and they found that the ethanol volume percent in the solvent and reaction temperature had important effects on the composition of the final products. Experiments showed that single phase of Mn_3O_4 nanoparticles can be prepared at higher reaction temperature and higher volume percent of ethanol, while single phase of MnOOH nanorods as single crystallites can be obtained at lower reaction temperature and lower volume percent of ethanol.

Z. W. Chen et al. [178] reported a simple and effective method for the generation of bulk-qnantity nanorods of manganese oxide, Mn_3O_4, under snrroundings of a suitable surfactant and alkaline solution. It was found that the Mn_3O_4 nanorod is smooth, straight, and that the geometrical shape is structurally perfect, which is produced with lengths from several hundreds nanometers to a few micrometers, and diameters range from 10 nm to 30 nm. The dripping speed of the NaOH solution was found to play an important role in formation of bulk-quantity Mn_3O_4 nanorods. The difference of dripping speed of the NaOH solution leaded to a large difference of Mn_3O_4 morphologies, which was observed in the transmission electron microscopy images.

Jenna et al. [179] prepared Mn_3O_4 nanoparticles with a faceted structure by mixing aqueous solutions of manganese nitrate and hexamethylenetetramine from 20 to 80 °C. Activation energy for the particle formation increases from 0.5 to 0.8 kJ/mol with nitrate concentration. They described synchrotron in-situ time-resolved XRD experiments in which Mn_3O_4 nanoparticles were reduced to MnO and subsequently reoxidized iu ramping temperature conditions.

Nana Zhao et al. [180] reported a two-phase route to shape- and size-controlled Mn3O4 nanocrystals that are capped with organic ligands and dissolved in a nonpolar solvent with excellent stability (at least a few months). They found that using controlled variations in the reaction conditions, the nanocrystals could be grown into either relatively monodisperse spherical shapes or almost perfect cubes.

Very recently (2008) Idalia Bilecka et al. [181] presented a broadly applicable synthesis strategy that enables the preparation of highly crystalline metal oxide nanoparticles such as CoO, ZnO, Fe_3O_4, MnO, Mn_3O_4, and $BaTiO_3$ in just a few minutes by reacting metal alkoxides, acetates or cetylacetonates with benzyl alcohol under microwave heating.

Weixin Zhang et al [182] synthesized manganese dioxide (β-MnO_2) nanorods by thermal decomposition of a template precnrsor of MnOOH, which was obtained by hydrothermal treatment of $KMnO_4$ in an aqueous ethanol solution. Through X-ray diffraction and electron microscopic characterizations, the as-prepared β-MnO_2 nanorods were shown to be phase-pure single crystallites with diameters of 30–400 nm and lengths of tens of micrometers. They demonstrated the catalytic efficiency of the as-prepared one-dimensional β-MnO_2 nanorods as catalysts in the oxidation of methylene blue dye in the presence of H_2O_2; the catalytic activity was found to be much higher than that of commercial micro-sized β-MnO_2 powders.

M.L. Singla et al. [183] prepared PANI/Mn_3O_4 composite to attain better electrical properties than individual Polyaniline and Mn_3O_4 alone whereas, re-doping with different inorganic and organic acids results in changes in electrical and thermal properties. They have also reported the behaviour of PANI/Mn_3O_4 composites doped with perchloric acid, sulphuric acid, *ortho*-phosphoric acid, acetic acid and acrylic acid for FTIR, TGA, XRD, electrical conductivity and NTC behaviour [184]. Iu a very recent study [185], they have characterized each composite sample for its behaviour toward % relative humidity (%RH) so that the composite may act as a humidity sensor.

Yi-Fan Han et al. [186] developed a new heterogeneous Fenton-like system consisting of nano-composite Mn_3O_4/SBA-15 catalyst for the complete oxidation of low concentration ethanol by H_2O_2 in aqueous solution. A novel preparation method had been developed to synthesize Nanoparticles of Mn_3O_4 by thermolysis of manganese (II) acetylacetonate on SBA-15. They found that the reaction rate for ethanol oxidation can be strongly affected by several factors, including reaction temperature, pH value, catalyst/solution ratio and concentration of ethanol.

In this study, attempt will be made to prepare manganese oxide nanoparticles having definite size and regular shape. This can be achieved by establishing a solution method at the low temperature of 80^0 C introducing starch as capping agent. The distinct advantage of this method is that it avoids the aggregation of particles in high temperature treatment, it needs only very simple equipment and the process is very facile, and it is a "green" process because no organic agent except the biodegradable starch is used.

Industrial dyestuffs constitute one of the largest groups of organic compounds that cause increasing environmental concerns and their degradation has, therefore, attracted much attention [187–189]. Although traditional physical techniques, such as adsorptiou on activated carbon and coagulation by chemical agents are generally efficient, they simply transfer organic compounds from water to another phase, and thus cause secondary pollution. The stability of modern dyes has made ineffective their biological decoloration and degradation. Advanced oxidation processes (AOPs) have emerged during the last decade as a viable strategy to degrade dyes in

aqueous media [190]. AOPs were based on the generation of very reactive species, such as hydroxy radicals ($^{\cdot}$OH) that oxidize a broad range of pollutants quickly and non selectively.

Methylene blue (MB) is a prototype of dyestuffs, which is particularly resistant to biodegradation [187, 191]. Although there have been numerous reports of photocatalytic MB degradation over the TiO2-based photocatalysts, most of the studies were performed nnder UV light irradiation [191, 192]. Recently, Zhao et al. [193] reported that some dyes could be degraded under visible light irradiation on TiO_2 by a self-photosensitized process, but MB is excluded. Up to now, only a few studies have been reported on MB dye degradation under visible light irradiation [193, 194]. Furthermore, the catalytic efficiency is limited by the light absorption characteristics of the TiO_2-based photocatalysts. In this research work, the obtained Mn_3O_4 nanoparticles are planned to be investigated for their catalytic activities in the oxidation of some organic dyes, especially MB.

For the viable technological applications, synthesis of nanoparticles having uniform size and high surface area is of key importance as the electrical, optical, and magnetic properties of these particles arc strongly depend on their dimension and effective surfacc area. Incorporation of nanoparticles into the porous polymeric matrix would facilitate the formation of regular dimension and greater surface area of the nanoparticles. In this work, catalytically important manganese oxide is planned to be incorporated into polyaniline (PANI) to develop a new matrix having interesting physico-chemical, electrical and surface properties. In doing so, it may be possible:

i) to establish a facile chemical and/or electrochemical route for the preparation of the catalytically active manganese oxide nanoparticles.

ii) to investigate the catalytic efficiency of the nanoparticles thus prepared for the dye degradation

iii) to establish a technique for the dispersion of manganese oxide nanoparticles into the polymeric matrix

iv) to examine the chemical, electrochemical and electrical functionality of the polymer-metal oxide nano-system thus fabricated.

v) to use the nanomatrix for electrode modification and catalytic process.

Reference

1. Fahlman, B. D. *Materials Chemistry*; 1, 282-283, (2007)

2. *Buffat, Ph. & Burrel, J.-P.*, "Size effect on the melting temperature of gold particles", *Physical Review A, 13 (6): 2287 – 2298*, (1976).

3. M. A. Agam and Q. Guo, "Electron beam modification of polymer nanospheres", *J. Nanosci. Nanotech.*, 7, 3615-3619, (2007).

4. Choy J H, Jang E S, Won J H, Chung J H, Jang D J, and Kim Y W. "Hydrothermal route to ZnO nanocoral reefs and nanofibers", *Appl. Phys. Lett.*, 84, 287, (2004).

5. Yugang Sun and Younan Xia Science *298*, 2176, (2002).

6. Catherine Murphy, *Science*, 298, 2139, (2002)

7. L. Smart and E. Moore, *Solid State Chemistry*, 126, (1992).

8. Samsonov, G. V. Ed.; IFI / Plennm, *The Oxide Handbook*, New York, 23, (1982)

9. F. A. Grant., *Riv. Modern Phys.*, 31, 646 (1959).

10. D.C. Cronemeyer, *Phys. Rev.*, 87, 876 (1952).

11. R. I. Bickley, *Chem. Phys. of Solids and Their Surface* 7, 118, (1978).

12. P. Salvador, *Solar Energy Matter.*, 6, 241, (1982)

13. Post, J. Manganese oxide minerals: crystal structures and economic and environmental significance. *Proc. Natl. Acad. Sci.* U.S.A. 96 (7), 3447-3454, (1999).

14. Thackeray, M. M. Manganese oxides for lithium batteries. *Prog. Solid State Chem.*, 25, 1-71, (1997).

15. A. Maltha, T. L. F. Favre, H. F. Kist, A. P. Zuur, V. Ponec, Mangauese oxides as catalysts for the selective reduction of nitrobenzene to nitrosobenzene. *J. Catal., 149*, 364-374, (1994).

16. M. Baldi, E. Finocchio, F. Milella, G. Busca, Catalytic combustion of C3 hydrocarbons and oxygenates over Mn3O4. *Appl. Catal. B: Environ., 16*, 43-51, (1998).

17. T. Yamashita, A. Vannice, Temperature-programmed desorption of NO adsorbed on Mn₂O₃ and Mn₃O₄. *Appl. Catal. B: EnViron., 13*, 141-155, (1997).

18. M. Baldi, E. Finocchio, C. Pistarino, G. Bnsca, Evaluation of the mechanism of the oxy-dehydration of propane over manganese oxide. *Appl. Catal. A, 173*, 61-74, (1998).

19. M. Te, H. C. Foley, Intrinsic reactivities of manganese oxides for carbon monoxide hydrogenation catalysis. *Appl. Catal. A, 119*, 97-106, (1994).

20. E. R. Stobbe, Boer, B. A. d.; Geus, J. W. The reduction and oxidation behavior of manganese oxides. *Catal. Today, 47*, 161-167, (1999).

21. Y.-F. Chang, J. G. McCarty, Novel oxygen storage components for advanced catalysis for emission control in natural gas fueled vehicles. *Catal. Today, 30*, 163-170, (1996).

22. J. Attenburrow; A. Cameron, F. B.; Chapman, J. H.; Evans, R. M.; Hems, B. A.; Jansen, A. B. A.; Walker, T., *J. Chem. Soc.,* 1094, (1952).

23. N. N Greenwood, & A. Earnshaw, *Chemistry of the Elements* (2nd Edn.). Oxford: Butterworth-Heinemann, (1997).

24. H. Aschoff, Ann., *Phys. Chem.* Ser. 2, 111, 217 and 224, (1860).

25. A. F. Holleman, E. Wiberg, "Inorganic Chemistry" Academic Press: San Diego, (2001).

26. T. Yamashita,, A. Vannice, *J. Catal.*, 163,158 –168, (1996).

27. I. Metil, *Mod. Paint Coat.*, 72, 49 – 52, (1982).

28. C. H. Hare,M. G. Fernald, *Mod. Paint Coat.*, 74, 40 –44, (1984).

29. L. Sanchez,J. Farcy,J. P. Pereira-Ramos,L. Hernan, J. Morales, J. L. Tirado, *J. Mater. Chem.*, 6, 37 – 42, (1996).

30. K. Dwight,N. Kenyuk, *Phys. Rev.*, 119,1470 –1479, (1960).

31. T. Ahmad, K. V. Ramanujachary, S. E. Lofland,A. K. Ganguli, *J. Mater. Chem.*, 14, 3406 –3409, (2004).

32. E. Winkler,R. D. Zysler, D. Fiorani, *Phys. Rev.* B, 70, 174406– 174410, (2004).

33. A. J. Heeger, G. B. Street and G. Tourillon, *Hand Book of Conducting Polymers* (T. A. Skotheim, ed) Marcel Dekker, Inc. New York, 1, 265, 293, 729, (1986).

34. R. B. Seymour, *Conducting polymers*, Plenum Press, New York, 23, (1981).

35. E. K. Sickel, *Carbon Black Polymer Composites*, Marcel Dekker, New York, (1982).

36. A. Malliaris, *J. App. Phys.*, 42, 614 (1972).

37. W. A. Little, *Phys. Rev.*, 134, 1416 (1964).

38. V. V. Walatka, M. M. Labes and J. H. Perlstein, *J. Phys.Rev. Lett.*, 31, 1139 (1973).

39. A. J. Heeger, G. B. Street and G. Tourillon, *Hand Book of Conducting Polymers* (T. A. Skotheim, ed.), Marcel Dekker, Ine., New York, vol. 1, 265, 293, (1986).

40. R. B. Seymour, *Conducting Polymers*, Plenum Press, New York, 23, (1981).

41. E. K. Sickel, *Carbon Black Polymer Composites*, Marcel Dekker, New York, (1982).

42. A. Malliaris and D. T. Turner, *J. Appl. Phys.*, 42, 614 (1971).

43. H. Inokushi and H. Akamatu, *Solid State Physics*, 12, 93 (1955).

44. W. A. Little, *Phys. Rev.* 134, 1416 (1964).

45. C. K. Chiang, A. J. Hegger and MacDarmid, *Ber. Bunsenges. Phys. Chem.*, 83, 407 (1979).

46. R. de Surville, M. Jozefowicz, L. T. Yu, J. Perichon and R. Buvet, *Electrochim. Acta.*, 13, 1451 (1968).

47. A. G. MacDiarmid, J.-C. Chiang, M. Halpen, W.-S. Huang, S.-L. Mu, N. L. D. Somasiri, W. Wu and S. I. Yaniger, *Mol. Cryst. Liq. Cryst.*, 121, 173 (1985).

48. E. M. Geuies, A. A. Syed and C. Tsintavis, *Mol. Cryst. Liq. Cryst.*, 121, 181 (1985).

49. E. W. Paul, A. J. Ricco and M. S. Wrington, *J. Phys. Chem.*, 89, 1441 (1985).

50. P. M. McManus, S. C. Yang and R. J. Cushman, *J. Chem. Soc., Chem Commun.*, 1556, (1985).

51. D. McInnes, M. A. Druy, P. J. Nigrey, D. P. Nairns, A. G. McDiarmid and A. J. Hegger, *J. Chem. Soc., Chem. Commun.*, 317, (1981).

52. A. G. Hegger, G. B. Street and G. Tourillon, in *Hand Book of Conducting Polymers* (T. A. Skotheim, ed.), Marcel Dekker, Inc., New York, vol 1 46, 51, (1986).

53. J. L. Bredas, G. B. Street, *Acc. Chem. Res.*, 18, 309, (1985).

54. M. G. Kanatzldls, *Chemical Engineering News,* Dec. 03, 38- 42, (1990).

55. A. Dall'Olio, Y. Dascola, V. Varacca and V. Bocchi, *Hebd. Seances. Acad. Sci. Ser.*, 267, 433, (1968).

56. H. Lund, *Elektrodenreaktioner i Organsik Polarografi og Voltammetri*, Aarhaus Stiftsbogtrykkorie, Aarhus, (1961).

57. A. F. Diaz, K. K. Kanazawa and G. P. Gardini, *J. Chem. Soc. Chem. Commun.*, 635, (1979).

58. A. Angeli, *Gazz. Chim. Ital.*, 46, 279 (1916).

59. G. P. Gardini, *Adv. Heterocycl. Chem.*, 15, 67 (1973).

60. P. Kovacic and M. B. Jones, *Chem. Rev.*, 87, 357 (1987).

61. A. G. Green and A. E. Woodhead, *J. Chem. Soc.*, 2388, (1910); R. de Surville, M. Josefowicz, L. T. Yu, J. Perichon and R. Buvet, *Electrochem. Acta*, 13, 1451 (1968); F. Cristofini, R. de Surville, M. Josefowicz, L. T. Yu and R. Buvet, *C. R. Acad. Sci. Paris, Ser.C*, 268 (15), 1346 (1969); A. F. Diaz and J. A. Logan, *J. Electroanal. Chem. Interfacial Electrochem.*, 111, 111 (1980); R. Noufi and A. J. Nozic, *J. Electrochem. Soc.*, 129, 2261 (1982).

62. E. M. Genies and C. Tsintavis and A. A. Syed, *Mol. Cryst. Liq.Cryst.*, 121, 181 (1985).

63. J. P. Travers, J. Chroboczek, F. Devreux, F. Genoud, M. Nechtschein, A. A. Syed, E. M. Genies and Tsintavis, *Mol. Cryst. Liq. Cryst.*, 121, 195 (1985).

64. A. G. MacDiarmid, J. C. Chiang, M. Halpern, W. S. Huang, S. L. Mu, N. L. D. Somasiri, W. Wu and S. I. Yaniger., *Mol. Cryst. Liq. Cryst.*, 121, 173 (1985).

65. A. G. MacDiarmid, N. L. D. Somasiri, W. R. Salaneck, I. Lundstrom, B. Liedberg, M. A. Hasan, R. Erlandsson and P. Konrasson, *Springer Series in Solid State Sciences*, 63, 218, (1985).

66. R. L. Hand and R. F. Nelson, *J. Electrochem. Soc.*, 125, 1059 (1978).

67. R. L. Hand and R. F. Nelson, *J. Am. Chem. Soc.*, 96, 850 (1974).

68. *Fr. Patent No. EN* 8307958 (1983); *U.S. Patent No.* 698 183 (1985).

69. L. T. Yu, M. S. Borredon, M. Jozefowicz, G. Belorgey and R. Buvet., *J. Polym. Sci.*, 10, 2931 (1987).

70. D. M. Mohilucr, R. N. Adams and W. J. Argersinger, *J. Am. Chem. Soc.*, 84, 3618 (1962).

71. J. Bacon and R. N. Adams, *J. Am. Chem. Soc.*, 90, 6596 (1968).

72. G. Mengoli, M. T. Munari, P. Bianco and M. M. Musiani, *J. Appl. Polym. Sci.*, 26, 4247 (1981).

73. G. Mengoli, M. T. Munari and C. Folonari, *J. Electroanal. Chem.*, 124, 237 (1981).

74. E. W. Paul, A. J. Ricco and M. S. Wrighton, *J. Phys. Chem.*, 89, 1441 (1981).

75. B. Pfeiffer, A. Thyssen, M. Wolff and J. W. Schultze, *Int. Workshop – Electrochemistry of Polymer Layers, Duisburg, F. R. G., Sept.* 15-17, (1986).

76. C. M. Carlin, L. J. Kepley and A. J. Bard, *J. Electrochem. Soc.*, 132, 353 (1985).

77. R. Noufi, A. J. Nozik, J. White and L. F. Warren, *J. Electrochem. Soc.*, 129, 226 (1982).

78. B. Aurian-Blajeni, I. Taniguchi and J. O'M. Bockris, *J. Electroanal. Chem.*, 149, 291 (1983).

79. M. A. M. Cordeiro, D. Goncalves, L. O. S. Bulhoes and J. M. M. Cordeiro, *Materials Research*, 8, 5 (2005).

80. H. John, R. M. Thomas, K. T. Mathew and R. Joseph, *J. Appl. Polym. Sci.*, 92, 592 (2004).

81. G. Zhang, X. Bi and G. Peng, *J. Appl. Polym. Sci.*, 56, 1683 (1995).

82. K. Mallick, M. J. Witcomb and M. S. Scurrell, *European Polymer Journal*, 42, 670 (2006).

83. T. Abdiryim, Z. Xiao-Gang and R. Jamal, *J. Appl. Polym. Sci.*, 96, 1630 (2005).

84. R. C. Patil, T. Aoyanagi, M. Nakayama and K. Ogura, *J. Appl. Polym. Sci.*, 81, 2661 (2001).

85. R. Anbarasan, T. Vasudevan and A. Gopalan, *European Polymer Journal*, 36, 1725 (2000).

86. Y. Wei, R. Hariharan and S. A. Petal, *Macromolecules*, 23, 758 (1990).

87. L. H. C. Mattoso, O. N. Oliveira, R. M. Faria, S. K. Manohar, A. J. Epstein and A. G. Macdiarmid, *Polym. Int.*, 35, 89 (1994).

88. S. Maeda and S. P. Armes, *Synth. Met.*, 73, 151 (1995).

89. A. –N. Chowdhury, J. M. A. Rahman and M. A. Rahman, *Indian Journal of Chemistry*, 41, 1789 (2002).

90. A. –N. Chowdhury and J. M. A. Rahman, *J. Electrochem Soc. India*, 51, 66 (2002).

91. M. Omastova, J. Pavlinec, J. Pionteck and F. Siomn, *Polym. Int.*, 43, 109 (1997).

92. B. Sari, A. Gok and D. Sahin, *J. Appl. Polym. Sci.*, 101, 241 (2006).

93. D. D. Borole, U. R. Kapadi, P. P. Mahulikar and D. G. Hundiwale, *Designated Monomers and Polymers*, 7, 45 (2004).

94. D. D. Borole, U. R. Kapadi, P. P. Mahulikar and D. G. Hundiwale, *Materials Letters*, 57, 3629 (2003).

95. D. Kumar, *European Polymer Journal*, 37, 1721 (2001).

96. E. Ekinci, *Polymer Bulletin*, 42, 693 (1999).

97. M. Ozden, E. Ekinci and E. Karagozler, *J. Appl. Polym. Sci.*, 71, 2141 (1999).

98. A. Buzarovska, I. Arsova and L. Arsov, *J. Serb. Chem. Soc.*, 66, 27 (2001).

99. P. Savitha and D. N. Sathyanarayana, *Polym. Int.*, 53, 106 (2004).

100. M. R. Huang, X. G. Li, Y. L. Yang, X. S. Wang and D. Yan, *J. Appl. Polym. Sci.*, 81, 1838 (2001).

101. P. S. Rao and D. N. Sathyanarayana, *J. Polym. Sci., Polym. Chem. Ed.*, 40, 4065 (2002).

102. S. H. Jang, M. G. Han and S. S. Im, *Synth. Met.*, 110, 17 (2000).

103. M. ITA, Y. Uchida and K. Matsui, *Journal of Sol-Gel Science and Technology*, 26, 479 (2003).

104. S. Asavapiriyanont, G. K. Chandler, G. A. Guawardena and D. Pletcher, *J. Electroanal. Chem.*, 177, 229 (1984).

105. M. Zhou and J. Heinze, *J. Phys. Chem. B*, 103, 8443 (1999).

106. M. Zhou and J. Heinze, *J. Phys. Chem. B*, 103, 8451 (1999).

107. S. E. Bae, S. H. Pack and Y. S. Kim, *Mol. Crys. Lett.*, 349, 359 (2000).

108. Y. C. Liu and L. Y. Jang, *Chem. Phys. Lett.*, 349, 363 (2001).

109. F. Y. Song and K. K. Shiu, *J. Electronal. Chem.*, 498, 161 (2001).

110. B. J. Hwang, R. Santhanam and Y. L. Lin, *Electrochim. Acta*, 46, 2843 (2001).

111. P. G. Pickup and R. A. Osteryoung, *J. Am. Chem. Soc.*, 106, 2294 (1984).

112. G. Cakmak, Z. Kucukyavuz and S. Kucukyavuz, *Synth. Met.*, 151, 10 (2005).

113. A. M. Fenclon and C.B. Greslin, *Electrochim. Acta*, 47, 4467 (2002).

114. N. R. Detacconi, Y. Son and K. Rajeshwar, *J. Phys. Chem.*, 97, 1042 (1993).

115. B. Zaid, S. Aeiyach, P. C. Lacaze and H. Takeuouti, *Electrochem. Acta.*, 43, 2331 (1998).

116. S. Aeiyach, B. Zaid and P. C. Lacaze, *Electrochim.Acta.*, 44, 2889 (1999).

117. A. De Brync, J. L. Delplancke and R. Winand, *J. Appl. Electrochem.*, 27, 867 (1997).

118. K. Idla, O. Inganas and M. Strandberg, *Electrochim. Acta.*, 45, 2121 (2000).

119. S. B. Saidman and J. B. Bessne, *J. Electroanal. Chem.*, 87, 521 (2002).

120. T. Zalewska, A. Lisowska-Oleksiak, S. Biallozor and V. Jasulaitiene, *Electrochim. Acta.*, 45, 4031 (2000).

121. A. C. Cascalheira, S. Aeiyach, P. C. Lacaze and L. M. Abrantes, *Electrochim. Acta.*, 48, 2523 (2003).

122. G. Appel, D. Schmeisser, J. Bauer, M. Bauer, H. J. Egelhaaf and D. Oelkrug, *Synth. Met.*, 99, 69 (1999).

123. M. Karakisla and M. Sacak, *J. Polym. Sci., Polym. Chem. Ed.*, 38, 51 (2000).

124. B. Sari and M. Talu, *Synth. Met.*, 94, 221 (1998).

125. R. Rajagopalan and J. O. Iroh, *Electrochim. Acta.*, 47, 1847 (2002).

126. T. Mustang, H. Difulen, T. Nakajima and T. Eawage, *Polym. Adv. Technol.*, 1, 33 (1990).

127. N. Mermillod, J. Tanguy and F. Petiot, *J. Electrochem. Soc.*, 133, 947 (1986).

128. T. Osaka, K. Naoi, S. Ogano and S. Nakamura, *J. Electrochem. Soc.*, 134, 2096 (1987).

129. R. A. Bull, R. R. Fan and A. J. Bard, *J. Electrochem. Soc.*, 130, 1636 (1983).

130. R. A. Saraceno, J. G. Pack and A. G. Ewing, *J. Electroanal. Chem.*, 197, 265 (1986).

131. M. Josowicz, J. Janata, K. Ashley and S. Pons, *Anal. Chem.*, 59, 253 (1987).

132. A. Boyle, E. M. Genies and M. Lapkowski, *Synth. Met.*, 28, 769 (1989).

133. P. N. Bartlett and S. K. Ling-Chung, *Sensors Actuators*, 20, 287 (1989).

134. S. Dogan, U. Akbulut, T. Yalcin, S. Suzer and L. Toppare, *Synth. Met.*, 60, 27 (1993).

135. F. Selampinar, L. Toppare, U. Akbulut, T. Yalcin and S. Suzer, *Synth. Met.*, 68, 109 (1995).

136. E. Ekinci, M. Ozden, A. A. Karagozler, H. M. Turkdemir and A. E. Karagozler, *Tr. J. Chem.*, 19, 170 (1995).

137. E. Ekinci, A. A. Karagozler and A. E. Karagozler, *Electroanalysis*, 7, 1 (1995).

138. E. Ekinci, A. A. Karagozler and A. E. Karagozler, *Synth. Met.*, 79. 57 (1996).

139. E. Ekinci, S. T. Ogunc and A. E. Karagozler, *J. Appl. Polym. Sci.*, 68, 145 (1998).

140. M. Ozden, E. Ekinci and A. E. Karagozler, *J. Appl. Polym. Sci.*, 68, 1941 (1998).

141. P. N. Bartlett and R. G. Whitaker, *Biosensors*, 3, 359 (1988).

142. A. F. Diaz and J. A. Logan, *J. Electroanal. Chem.*, 111, 111 (1980).

143. E. M. Genies, M. Lapkowski, C. Santier and E. Vicil, *Synth. Met.*, 18, 631 (1987).

144. E. P. Lofton, J. W. Thackeray and M. S. Wrighton, *J. Phys. Chem.*, 90, 6080 (1986).

145. S. Chao and M. S. Wrighton, *J. Am. Chem. Soc.*, 109, 6627 (1987).

146. Katerina Ch. Akvatopulu, Christos Kordulis and Alexis Lycourghiotis, Effect of Temp. on the Point of Zero Charge and Surface Charge of TiO_2, *J. Chem. Soc. Faraday Trans.*, 80(20) 3437-3440, (1990).

147. Simon Garfield (2000). *Mauve: How One Man Invented a Color That Changed the World.* Faber and Faber. ISBN 0-393-02005-3.

148. Mokhlesi B. "Adult Toxicology in Critical Care: Part II: Specific Poisonings". *Chest,* 123: 897, (2003).

149. Harvey J W. "Studies of the Efficacy and Potential Hazards of Methylene Blue Therapy in Aniline-Induced Methaemoglobinaemia". *Br J Haemotol* 54: 29, (1983).

150. M. Ozden, E. Ekinci and A. E. Karagozler, *J. Appl. Polym. Sci.*, 68, 1941 (1998).

151. P. N. Bartlett and R. G. Whitaker, *Biosensors*, 3, 359 (1988).

152. B. G. Yacobi, D. B. Holt, *An Introduction to Microanalysis of Solids*, Plenum Press, New York, 87, (1994)

153. T. Hycon, *Chem. Comm.* 2003, 927. (b) S. Sun, C. B. Murray, D. Weller, L. Folks, A. Moser, *Science*, 287, 1989, (2000).

154. F. X. Redl, K.-S. Cho, C. B. Murray, S. O'Brien, *Nature*, 423, 968, (2003).

155. F. Dumestre, B. Chaudret, C. Amiens, P. Renaud, P. Fejes, *Science*, 303, 821, (2004).

156. K. Jacobs, D. Zaziski, E. C. Scher, A. B. Herhold, A. P. Alivisatos, *Science*, 293, 1803, (2001).

157. P. Michler, A. Imamoglu, M. D Mason, P. J. Carson, G. F. Strouse, S. K. Buratto, *Nature*, 406, 968, (2000).

158. S. Sun, C. B. Murray, *J. Appl. Phys.*, 85, 4325, (1999).

159. S. Sun, H. J. Zeng, *Am. Chem. Soc.*, 124, 8204, (2002).

160. Y. Xia, P. Yang, Y. Sun, Y. Wu, B. Mayers, B. Gates, Y. Yin, F. Kim, H. Yan, *Adv. Mater.*, 15, 353, (2003).

161. Special issue on nanowires, *Adv. Mater.*, 15, 351, (2003).

162. J. T Hu, T. W. Odom, C. M Lieber, *Acc. Chem. Res.*, 32, 435, (1999).

163. S.-J. Park, S. Kim, S. Lee, Z. G Khim, K. Char, T. Hyeon, *J. Am. Chem. Soc.*, 122, 8581, (2000).

164. F. Dumestre, B. Chaudret, C. Amiens, M. Respaud, P. Fejes, P. Renaud, P. Zurcher, *Angew. Chem., Int. Ed.*, 42, 5213, (2003).

165. F. Dumestre, B. Chaudret, C. Amiens, M.-C. Fromen, M.-J. Casanove, M. Respaud, P. Zurcher, *Angew. Chem., Int. Ed., 41*, 4286, (2002).

166. J. Park, B. Koo, Y. Hwang, C. Bae, K. Au, J.-G. Park, H. M. Park, T. Hyeon, *Angew. Chem., Int. Ed., 43*, 2282, (2004).

167. S. H. Kim, S. J. Kim, S. M. Oh, *Chem. Mater., 11*, 557., (1999)

168. S. K. Nayak, P. Jena, *J. Am. Chem. Soc., 121*, 644, (1999).

169. J. Li, Y. J. Wang, B. S. Zou, X. C. Wu, J. G. Lin, L. Guo, Q. S. Li, *Appl. Phys. Lett., 70*, 3047, (1997).

170. J. C Nardi,. *J. Electrochem. Soc., 132*, 1787, (1985).

171. T. Ahmed, K. V. Ramanujachary, S. E. Lofland and A. K. Ganguli, *J. Mater. Chem.*, 14, 3406–3410, (2004).

172. Jiu Mu, Zhenfang Gu, Hua Sun, and Qinglian Wei, Journal of Dispersion Science and Technology, 27, 307–309, (2006).

173. Ning Wang, Lin Guo, Lin He, Xia Cao, Chinping Chen, Rongming Wang, and Shihe Yang, *small*, 3, No. 4, 606 – 610, (2007)

174. M. Ocana, *Colloid Polym Sci*, 278, 443-449 (2000)

175. W. S. Seo, H. H. Jo, K. Lee, B. Kim, S. J. Oh, and J. T. Park, Angew. *Chem. Int.*, 43, 1115 –1115, (2004)

176. A. L. Willis, Z. Chen, J. He, Y. Zhu, N. J. Turro, and S. O'Brien, *Journal of Nanomaterials*, p- 7, (2007),

177. W. Zhang, Z. Yang, Y. Liu, S. Tang, X. Han, M. Chen, *J. Crystal Growth*, 263 394–399, (2004).

178. Z. W. Chen,a! J. K. L. Lai, and C. H. Shek, *App Phys Lett*, **86**, (2005), 181911.

179. J. Pike, J. Hanson, L. Zhang,§ and S. W. Chan, *Chem. Mater.*, *19*, 5609-5616, **(2007)**.

180. N. Zhao, W. Nie, X. Liu, S. Tian, Y. Zhang, and X. Ji, *small*, 4, No. 1, 77–81, (2008).

181. I. Bilecka, I. Djerdj and M. Niederberger, *Chem. Commun.*, 886–888, (2008).

182. W. Zhang , Z. Yang, X. Wang, Y. Zhang, X. Wen, S. Yang, *Catalysis Communications*, 7, 408–412, (2006)

183. K. Majid, S. Awasthi, M.L. Singla, Low temperature sensing capability of polyaniline and Mn_3O_4 composite as NTC material, *Sens. Actuators* A 135, 113–118, (2007)

184. M.L. Singla, S. Awasthi, A. Srivastava, D.V.S. Jain, Effect of doping of organic and inorganic acids on polyaniline/Mn_3O_4 composite for NTC and conductivity behavior, *Sens. Actuators* A 136, 604–612, (2007).

185. M.L. Singla, S. Awasthi, A. Srivastava, *Sens. Actuators* B 127 (2007) 580–585

186. Y.-F. Han, F. Chen, K. Ramesh, Z. Zhong, E. Widjaja, L. Chen, *Applied Catalysis B: Environmental* 76, 227–234, (2007).

187. R. Asahi, T. Morikawa, T. Ohwaki, K. Aoki, Y. Taga, Science 293 269, (2001).

188. I.K. Konstantinou, T.A. Albanis, *Appl. Catal.* B 49, 1, (2004).

189. J.W. Tang, Z.G. Zou, J.H. Ye, *Chem. Mater.* 16, 1644, (2004).

190. S.F. Yin, B.Q. Xu, C.F. Ng, C.T. Au, *Appl. Catal.* B 48, 237, (2004).

191. T.Y. Zhang, T. Oyama, A. Aoshima, H. Hidaka, J.C. Zhao, N. Serpone, J. Photochem. Photobiol. A 140, 163, (2001).

192. A. Houas, H. Lachheb, M. Ksibi, E. Elaloui, C. Guillard, J.M. Herrmann, *Appl. Catal.* B 31, 145, (2001).

193. W. Zhao, C. Chen, X. Li, J. Zhao, H. Hidaka, N. Serpone, *J. Phys. Chem.* B 106, 5022, (2002).

194. X.Z. Li, F.B. Li, *Environ. Sci. Technol.* 35, 2381, (2001).

Chapter 2

EXPERIMENTAL

2.1 Materials and Probes

2.1.1 Chemicals

The chemicals and reagents used in this work are listed below. These were analytical grade and used without further purification except aniline which was distilled twice prior to use. Doubly distilled water was used as solvent to prepare most of the solution of this work.

(i)   Manganese acetate [Merck,India]

(ii)   Starch [Merck, India]

(iii)   Aniline [E. Merck, Germany]

(iv)   Ammonium peroxydisulfate [Merck, India]

(v)   Potassium permanganate [Merck, India]

(vi)   Potassium dichromate [Merck, India]

(vii)   Sulfuric acid [Merck, India]

(viii) Hydrochloric acid (32%) [E. Merck, Germany]

(ix)   Sodium hydroxide [E. Merck, Germany]

(x)   Sodium chloride [Uni-chem, China]

(xi)   Methylene blue [E. Merck, Germany]

(xii)   Procion red [E. Merck, Germany]

2.1.2 Instruments

Analysis of the samples performed in this work employed the following devices:

(i)   Infrared spectrophotometer [IR-470, Shimadzu, Japan]

(ii)   UV-visible spectrophotometer [UV-1601 PC, Shimadzu, Japan]

(iii)   Scanning electron microscope [Philips XL30, Holland]

(iv)   X-raydiffractometer [Philips, Expert Pro, Holland]

(v)   pH meter [Hanna, pH 209, India]

(vi)   Condnctivity meter [WPA, Cambridge, UK]

(vii)   Centrifuge machine [Hermle, 2200 A, Germany]

(viii) Sonicator [Model 50 T, VWR Scientific, USA]

(ix)   Digital balance, [FR-200, Japan]

(x)   Furnace [DK, Chino, England]

(xi)   Microburette [China]

(xii)   Potentiostat / Galvanostat / Coulombmeter [HABF 501, Hokuto Denko, Japan]

2.2   Preparation of Mn₃O₄ Nanoparticles

Mn_3O_4 are usually prepared by heating manganese(II) salts or other manganese oxides and hydroxides at about 700 °C and about 1000 °C, repectively [1-3]. However, all these methods yield, in general, particles with irregular shape and broad size distribution. Nanoparticles of Mn_3O_4 have recently been obtained from different precursors such as manganese acetylacetonate [4], and manganese(II) acetate [5]. This work describes procednres for the low temperatnre (80 °C) preparation of Mn_3O_4 nanoparticles by forced hydrolysis of manganese acetate, $Mn(OOCCH_3)_2$, aqueous solution using starch as capping agent. In brief, the procedure is as follows:

Manganese acetate and soluble starch were commercially available and used without further purification. Double-distilled water was used as solvent. At first, saturated solution of soluble starch (0.16 wt%) was prepared in a 500 mL beaker. Calculated amount of manganese acetate crystal was dissolved in that saturated starch solution to prepare 500 mL 0.2 M solution with the help of a volumetric flask. After being shaken for

a while, the flask was placed in an oven preheated to 80 °C for 2 hours. The brown dispersions thus obtained were then taken out followed by aging for 12 hours at room temperature. The reaction mixture was concentrated with a rotary evaporator and extracted with ethanol to obtain brown precipitate. Finally, the precipitate was washed several times with ethanol and dried at 40 °C to get brown loosen powder. The dried product was then stored in a desiccator.

Same procedure was followed to carry out three preparations of such solid Mn_3O_4 nanoparticles and yields of Mn_3O_4 were found to be 252 mgL^{-1}, 265 mgL^{-1}, and 233 mgL^{-1}. So, the average yield of Mn_3O_4 was 250 mgL^{-1}.

2.3 Preparation of Polyaniline (PANI)

PANI was prepared by a chemical method at room temperature, 30 °C (±2°) following the procedure described elsewhere [6-8]. In this study polyaniline was synthesized by using potassium dichromate, $K_2Cr_2O_7$, as an oxidant. 10 mL of distilled aniline. 20.0 mL of concentrated sulfuric acid (H_2SO_4) and 10.0 g $K_2Cr_2O_7$ were added to double distilled water maintaining the total volume of the mixture 400 mL. The reaction mixture was turned into deep blue polymeric sediment instantaneously. However, the content was left overnight for completion of polymerization.

The deep blue sediment was then filtered and treated with 0.8 M H_2SO_4 and continued washing with acid until the supernatant shows a pH value 2.30. The content was then left overnight in 0.8 M H_2SO_4 solution. The PANI substrate thus treated was then dried in air followed by vacuum

drying. The dried mass was ground and then sieved using 100 mesh sieves and stored in a vacuum desiccator.

2.4 Dispersion of Mn_3O_4 into PANI

The method for the dispersion of Mn_3O_4 into PANI employed the following procedure. 500 mL aqueous colloidal suspension of Mn_3O_4 was prepared as described in section 2.2 and used for PANI-Mn_3O_4 matrix preparation. This nano suspension was then added to the deep blue sediment of PANI (as prepared as described in section 2.3). The dispersion system was further stirred for a while and then allowed to settle for overnight. The reaction mixture was then centrifuged for 30 minutes and then resulting deep blue sediment was redispersed in double distilled water. The centrifugation-redispersion cycle was repeated thrice in order to remove completely the excess manganese oxide particles from the PANI-Mn_3O_4 matrix.

2.5 Polymerization of Aniline Using Mn_3O_4 Nanoparticles

200 mL aqueous solution was prepared by dissolving 1.0 mL of distilled aniline and 5.0 mL 5.0 N sulfuric acid. 100 mL suspension of starch capped Mn_3O_4 nanoparticles were added to this solution. Immediately on addition of nanoparticles, the solution turned into blue color. The reaction mixture was then left overnight for completion of polymerization. The polyaniline thus obtained was then centrifuged and redispersed in double distilled water. The centrifugation-redispersion cycle was repeated thrice in order to remove starch completely from the polymer. Finally, the polymer substrates were dried in air initially and then in oven at 40°C for three hours and stored in a vacuum desiccator.

2.6 Decolorization of Dye Using Mn₃O₄ Nanoparticles

2.6.1 Decolorization of Methylene Blue

Stock methylene blue solution was prepared by dissolving 0.036g solid methylene blue to 500 mL double distilled water. In this way, 2.0×10^{-4} M MB solution was prepared which was used as stock methylene blue solution.

(i) Various concentrations of MB studied for declorization: 0.5×10^{-5} M, 1.0×10^{-5} M, 1.5×10^{-5} M, 2.0×10^{-5} M, 2.5×10^{-5} M, 3×10^{-5} M methylene blue solutions were prepared by diluting 2.5 mL, 5.0 mL, 7.5 mL, 10.0 mL, 12.5 mL, and 15.0 mL respectively of stock solution to 100 mL with double distilled water. 1.0 mL sulfuric acid and 5.0 mL suspension of Mn_3O_4 nanoparticles were added to 5.0 mL of each of these MB concentrations. After 1.0 minute, absorbance of each of the reaction mixtures was taken. Typical UV-Visible spectral feature of MB is presented in Fig. 2.6.1.

(ii) Influence of amount of Mn₃O₄ nanoparticles on MB declorization: To investigate the effect of amount of Mn_3O_4 nanoparticles on MB degradation, 3×10^{-5} M methylene blue solution was prepared by diluting 15.0 mL of stock solution to 100 mL with double distilled water. To 5.0 mL of this MB and 1.0 mL of H_2SO_4 different amount of Mn_3O_4 nanoparticles suspensions, 1.0 mL, 1.5 mL, 2.0 mL, 2.5 mL, 3.0 mL, 5.0 mL, and 7.0 mL were added.
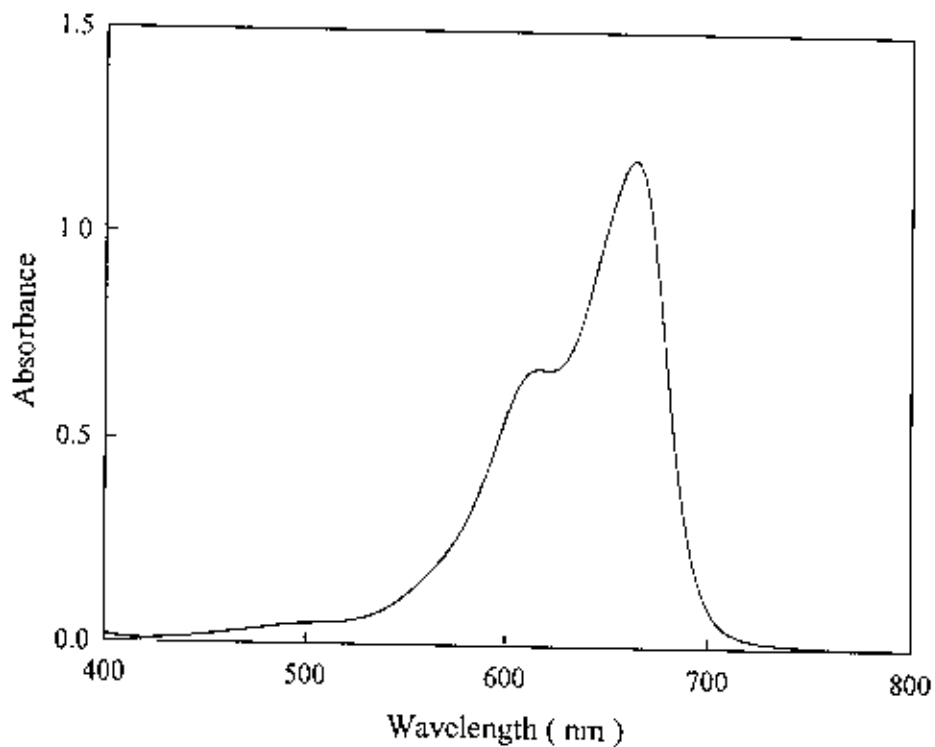
Fig. 2.6.1: Spectrum of an aqueous 2×10^{-5} M solution of MB at pH 6.86

*(iii) **Influence of acid concentration on MB declorization:*** Influence of concentration of sulfuric acid on MB degradation was studied using various concentrations of H_2SO_4, keeping the amount of nanoparticles and the concentration of MB fixed. In brief the procedure is as follows: 68.4 mL of concentrated H_2SO_4 was poured into a 250 mL volumetric flask containing distilled water. The flask was shaken carefully and total volume was maintained to 250.0 by adding distilled water to give a 5.0 M H_2SO_4 solution. 0.05 M, 0.25 M, 0.5 M, 1.0 M, 1.5 M, 2.5 M, 3.5 M acid solutions were prepared by diluting 1.0 mL, 5.0 mL, 10.0 mL, 20.0 mL, 30.0 mL, 50.0 mL, and 70.0 mL respectively of 10.0 N solution to 100 mL with double distilled water. 1.0 mL of each of these acid solutions

were added to 3×10^{-5} M methylene blue solution and 5.0 mL suspensions of Mn_3O_4 nanoparticles. Immediately after 1.0 minute, UV-Visible absorption spectrum was taken for each solution and absorbance was recorded.

(iv) MB declorization as a function of time: The performance of Mn_3O_4 nanoparticles on the degradation of MB was monitored as a function of time. The catalytic reaction was carried out in a 100 mL glass flask, which contained 50 mL of 3×10^{-5} M methylene blue solution and 10 mL of 2.5 M sulfuric acid. After adding 50 mL suspensions of starch capped Mn_3O_4 nanoparticles, the mixture was allowed to react at room temperature. For optical absorption measurements, approximately 1 mL of the mixture solution was taken out into the UV quartz cell for a given time interval: 1 minute, 2 minutes, 3 minutes, 5 minutes, 7 minutes, 10 minutes, 20 minutes, 30 minutes, 1 hour, 2 hours, 3 hours, 6 hours, 12 hours, 24 hours.

(v) MB declorization in absence of light: The efficiency of Mn_3O_4 nanoparticles on the degradation of MB was investigated in absence of light. The reaction was carried out in a 250 mL stopper bottle containing 50 mL of 3×10^{-5} M methylene blue solution and 10 mL of 2.5 M sulfuric acid. The bottle was well covered with carbon paper so that light could not pass through it. 50 mL of Mn_3O_4 nanoparticles suspension were then added to this the mixture and the stopper bottle was placed in dark place at room temperature. After 24 hours the colorless clean solution was taken out to measure the absorption spectra.

2.6.2 Declorization of Procion Red

Degradation of another textile dye, procion red (PR), by Mn_3O_4 nanoparticles was also studied. PR solution was prepared by dissolving 0.0615 g solid PR to give 50 mL solution using double distilled water. In this way, 2.0×10^{-3} M PR solution was prepared which was used as stock PR solution. 2.0×10^{-4} M PR solution was prepared by diluting 10 mL of stock solution to 100 mL with double distilled water. The degradation was carried out in a 250 mL beaker containing 50 mL of 3×10^{-4} M procion red solution and 20 mL of 2.5 M sulfuric acid. 100 mL of nanoparticles suspension were then added to this mixture allowed to react completely at room temperature. As soon as Mn_3O_4 was added, the color of the mixture turned from blue to gray rapidly. The solution was then left overnight to obtain completely colorless clear solution. This solution was used to measure the absorption spectra. Typical UV-Visible spectral feature of PR is presented in Fig. 2.6.2.
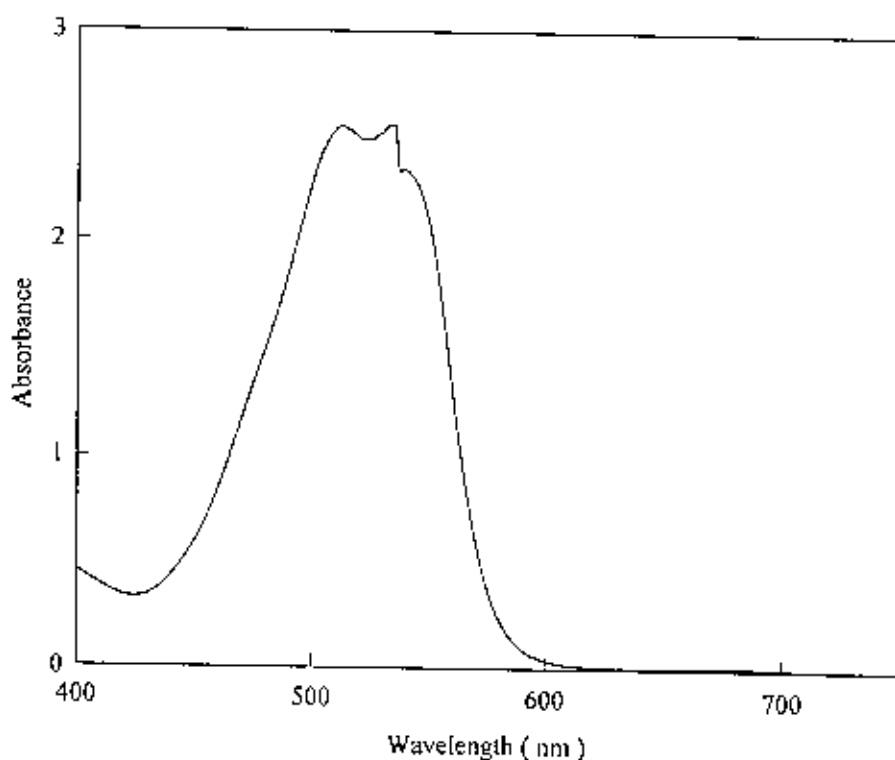
Fig. 2.6.2 : Spectrum of an aqueous 2.0×10^{-4} M solution of PR at pH 4.56

2.6.3 Decolorization of Industrial Effluent

The colored industrial effluent was collected from "Young One", Dhaka Export Processing Zone, Dhaka, Bangladesh, and successfully decolorized with the help of prepared Mn_3O_4 nanoparticles. 100 mL of the effluent was taken into a beaker, 2 mL of 2.5 M sulfuric acid was added to it followed by adding 10 mL nanoparticles suspension. The effluent was immediately turned its color and the effluent spectrum was recorded.

2.7 Sensitivity on Different Pathogenic Organisms

To test the sensitivity of the prepared Mn_3O_4 nanoparticles on some pathogenic organisms the following procedure was employed. Some bacteria such as *Vibrio cholerae, Shigella sp, Salmonella sp.*, and *Escherichi coli* were grown somehow on a Petridis. 20 µL of the Mn_3O_4 nanoparticles suspension was then absorbed into a circular soaking paper and placed into that dish. As a reference antibiotic ciprofloxacin soaked paper was also kept into that dish. The arrangements were kept for overnight and zone of inhibition for the nanoparticles and antibiotic were measured.

2.8 Spectral Analysis

2.8.1 Infrared Spectra

IR spectra of all the dried samples Mn_3O_4, PANI and PANI/Mn_3O_4 were recorded on an IR spectrometer in the region of 4000 - 400 cm^{-1}. IR spectra of the solid samples were frequently obtained by mixing and grinding a small amount of materials with dry and pure KBr crystals. Thorough mixing and grinding were done in a mortar by a pestle. The powdered mixture was then compressed in a metal holder under a pressure of 8-10 tons to make a pellet. The pellet was then placed in the path of IR beam for measurements.

2.8.2 Ultraviolet-Visible Spectra

The Ultraviolet-Visible (UV-Vis.) spectral analysis of the sample solutions employed a double beam spectrophotometer. UV-Vis spectroscopic analysis for the characterization and degradation studies

involved the DMF and aqueous solution respectively. The references in these cases were the corresponding solvents that used for preparing the solutions. The amount of dye degraded by Mn_3O_4 nanoparticles was determined spectroscopically in the visible region.

2.8.3 X-ray diffraction

Manganese oxide, Mn_3O_4, was analyzed for their X-ray diffraction pattern in the powder state. For this purpose, the samples were prepared as the procedure described in section 2.2. The powder samples were pressed in a square aluminum sample holder (40 mm × 40 mm) with a 1 mm deep rectangular hole (20 mm × 15 mm) and pressed against an optical smooth glass plate. The upper surface of the sample was labeled in the plane with its sample holder. The sample holder was then placed in the diffractometer.

2.8.4 Energy Dispersive X-ray (EDX) Spectra

Elemental analysis of the synthesized Mn_3O_4 nanoparticles was performed by EDX spectra. The dried powders of Mn_3O_4 and Mn_3O_4-polymerized PANI were dispersed on a 1 cm × 1 cm conducting steel plate. The still plates were then placed on a conducting carbon glued strip and a very thin gold layer was sputtered on the sample to ensure the conductivity of the sample surface. The sample was then placed in the main SEM chamber integrated with the EDX machine.

2.9 Surface Morphology

The dried powder of Mn_3O_4 nanoparticles, PANI and $PANI/Mn_3O_4$ composite samples were dispersed on a 1 cm × 1 cm conducting steel

plate. Mn_3O_4 nanoparticles and PANI matrices thus prepared and treated (following the methods described in section 2.2, 2.3, 2.4 and 2.5) were examined for their surface morphology. For this purpose, scanning electron microscope was adopted. The dried powders of these samples were dispersed on a conducting carbon glued strip. The sample-loaded strip was then mounted to a chamber that evacuated to $\sim 10^{-3}$ to 10^{-4} torr and then a very thin gold layer ($\sim$ few nanometers thick) were sputtered on the sample to ensure the conductivity of the sample surface. The sample was then placed in the main SEM chamber to view its surface. The system was computer interfaced and thus provides recording of the surface images in the computer file for its use as hard copy.

2.10 d. c. Conductivity

The study of electrical conductivity of the solid samples of Mn_3O_4 nanoparticles, PANI and PANI/ Mn_3O_4 composite, at room temperature was carried out by a conventional two point-probe method [6, 7]. For this purpose, the dried and powdered solids were compressed mechanically in a transparent plastic tube as illustrated in Fig. 2.9.1. A few centimeters long plastic tube having diameter 0.186 cm was taken for loading the solids in it. One end of the tube was tightly closed with a copper (Cu) wire having the same diameter as that of the tube. The sample was then pushed gradually inside the tube and compressed mechanically from the other end of the tube by another piece of same wire. Eventually the mass become tightly compressed having a very rigid structure that on further pressing did not change the length of the compressed mass. In this position, the other end of tube was made closed by the similar wire. The two Cu wires at the two ends pressed tightly in such a way that ensures an adequate contact between the sample and the wires. The wire poles were

used for electrical contact to get the voltage drop between the two ends of the sample under investigation. An auto ranging microvolt was employed for the conductivity measurements. This equipment allows reading directly the resistance of the sample. Thus, knowing the observed resistance, the specific conductance of each studied sample was calculated out by using the standard relation mentioned in chapter 1. The measurement was conducted at laboratory temperature ($\sim 30°C$).
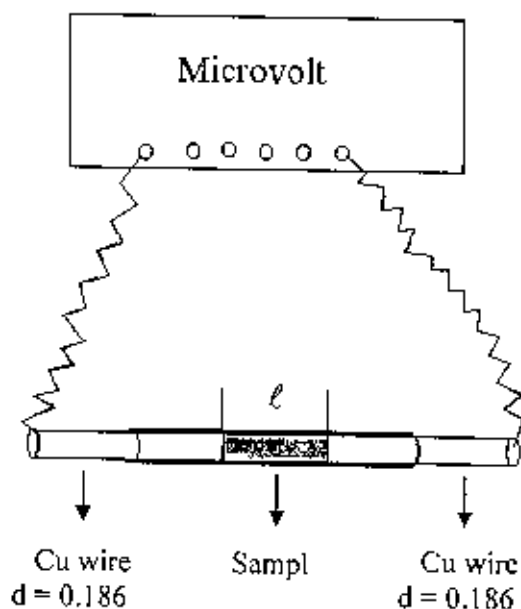

Fig. 2.9.1: The construction for the measurement of the two point-probe conductivity.

2.11 Cyclic Voltammogram

The cyclic voltammogram of methylene blue before and after degradation was examined. 50 mL of MB 6×10^{-5} M solution was acidified with 10 mL 2.5 M sulfuric acid and total volume is diluted to 100 mL solution of 6×10^{-5} M MB with double distilled water. A cell consists of Pt working

electrode was allowed to sweep between the potential -0.2 and +0.5 V at a scan rate of 100 mV sec⁻¹. This process was performed in a single compartment three-electrode cell under ambient atmosphere (Fig. 2.10.1). After degrading this MB solution with 50 inL Mn_3O_4 nanoparticles, again a CV was taken sweeping the same potential window and scan speed.
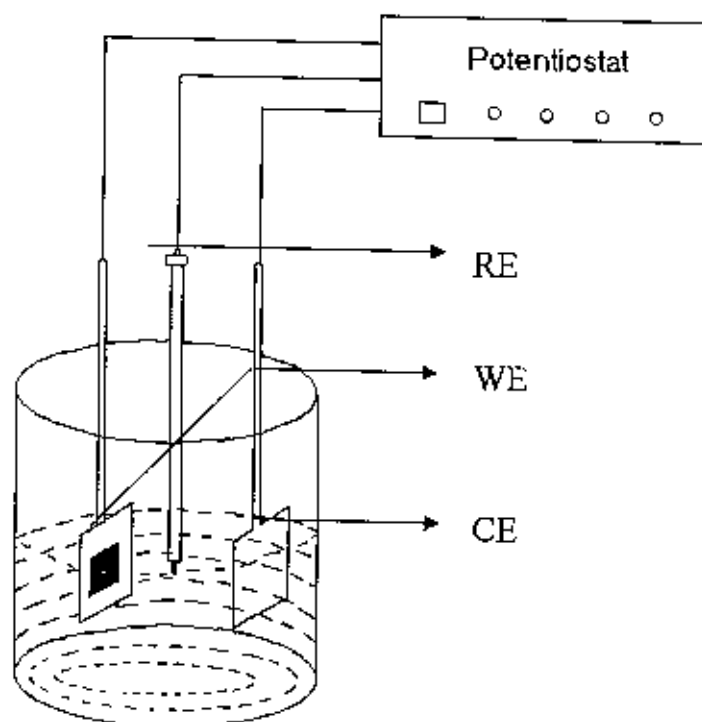

Fig. 2.10.1: Three electrode system for Cyclic Voltammogram (CV)

References

1. W C Vosburgh, *J Electrochem Soc,* 106, 839-845, (1959)

2. T E Moore, M Ellis, PW Selwood, *J Am Chem Soc,* 72, 856-866, (1950)

3. E Mendelovici, A Sagarzazu, *Thermochim Acta,* 133, 93-100, (1988)

4. M Ocana, *Colloid Polym Sci,* 278, 443-449, (2000)

5. A L Willis, Z. Chen, J. He, Y. Zhu, N. J. Turro, and S. O'Brien, *Journal of Nanomaterials,* 7, (2007)

6. T Ohsaka, Y Ohnuki, N. Oyama, G. Katagiri and K. Kamisako, *J. Electroanal, Chem.,* 161, 399, (1964).

7. A Kitani and K Sasaki, *Stud. Org. Chem.,* 30, 377, (1987).

8. E M Genies, J F Penneau, M Lapkowski and A Boyle, *J. Electroanal. Chem.,* 269, 63, (1989).

9. I J van der Pauw, *Philips Res. Repts.,* 13, 1, (1958).

10. J Lange, *J. Appl. Phys.,* 35, 2659 (1964).

Chapter 3

RESULTS AND DISCUSSION

3.1   Nano-state Mn_3O_4

Manganese oxides are important materials in many applications, such as in catalyst, electrode, sensor, and magnetic materials [1–6]. Among them, Mn_3O_4 is known to be a good candidate as an active catalyst for the decomposition of waste gases [7], as a corrosion-inhibiting pigment [8, 9], and as an intercalation compound [10]. Recognizing that dimensionality and ratio of surface area to volume are crucial factors in determining the properties of the nanomaterials, such as surface activity and catalytic efficiency, our interest was the preparation of nano-state particles of Mn_3O_4. Our focus was also to stabilize the nano-state Mn_3O_4 in solution media preventing them from agglomeration.

One of the most used methods for the preparation of particles with controlled particle size and shape is the forced hydrolysis of metal cations. It has been amply reported that the morphology of the so-precipitated particles is strongly influenced by the nature of the anions present in solution [11]. In some cases, they are incorporated into the solid phase; in others, they end up adsorbed on the particle surface and can be further eliminated by washing [11]. In the later case, the effects of the anions have been mainly attributed to the formation of soluble complexes which act as precursors to the solid-phase formation [11]. Preparations of Mn_3O_4 nanoparticles or elongated α-MnOOH particles by forced hydrolysis of aqueous $Mn(OOCCH_3)_2$ solutions were reported under certain experimental conditions and no precipitation could be detected when $Mn(OOCH_3)_2$ was substituted by otherMn(II) salts (nitrate, sulfate, chloride) and keeping constant the other experimental parameters, indicating that although the acetate anions are not incorporated to the solid phase, their presence is essential for particle formation [12]. Similar

behavior has been reported for the precipitation of small Co_3O_4 cubes from cobalt(II) acetate aqueous solutions [13].

Manganese(II) acetate, $Mn(OOCCH_3)_2$, precursor is not as common as manganese sulfate or manganese halides for the synthesis of manganese oxide nanoparticles, despite it is widely available commercially and is inexpensive. In this report it has been demonstrated that the aging of 0.4 mol dm^{-3} aqueous $Mn(OOCCH_3)_2$ solutions at 80 °C for 2 h yielded equiaxial particles with a mean diameter of 17 nm as reported by M. Ocana [12]. It was found that if heating time was increased up to 6 h and 12 h, however, more heterogeneous dispersion consisting of bigger, aggregated and fused particles were obtained. But, the nanosystem thus obtained, however, led to sedimentation producing bigger particles within 6 h to 12 h through agglomeration. To prevent the agglomeration of nanoparticles in the solution system, starch was employed as capping agent. The whole method needed only very simple equipment and the process was very facile, and it was a "green" process because no organic agent except the biodecomposible starch was used.

3.2 Characterization of Mn_3O_4 Nanoparticles

Uniform Mn_3O_4 nanoparticles were prepared at temperature, 80 °C, based on the forced hydrolysis of aqueous manganese(II) acetate solution using starch as a capping agent. The Mn_3O_4 nanoparticles were then extracted with ethanol to obtain brown precipitate and dried to get powder form. The solid was characterized in terms of their particles size and morphology (by SEM), chemical composition (by IR and EDX), crystalline structure (by X-ray), and electrical conductivity (by d. c. conductance measurement).

3.2.1 EDX Spectral Analysis

Elemental analysis of the as prepared solid Mn_3O_4 has been performed by employing Energy Dispersion X-ray (EDX) method. For this purpose, the sample used was that employed for SEM analysis which has been described in section 2.8. From elemental analysis it is possible to investigate all the elements contained in Mn_3O_4 nanoparticles. The patterns of the EDX spectra are presented in Fig. 3.2.1(a) - 3.2.1(b). The peaks observed at 5.90 and 0.64 keV were for K and L lines respectively of the manganese element; at 0.52 keV for K lines of the oxygen element and at 2.12 for M lines of the gold element (as reference). The percentages of Mn and O were determined from the intensity of the lines and the results are summarized further in Table 3.2.1.

Table 3.2.1: Elemental composition of as prepared manganese oxide

Location of sample	Manganese (%)	Oxygen (%)	Tentative formula	Chemical formula
1 (full frame)	71.85	28.15	Mn_3O_4	
2 (full frame)	71.18	28.82	Mn_3O_4	Mn_3O_4
On spot # 1	71.89	28.11	Mn_3O_4	
On spot # 2	72.10	27.90	Mn_3O_4	

Thus from the chemical composition obtained from the EDX spectra, it can be concluded that the prepared manganese oxide is Mn_3O_4 and no other phases are present.
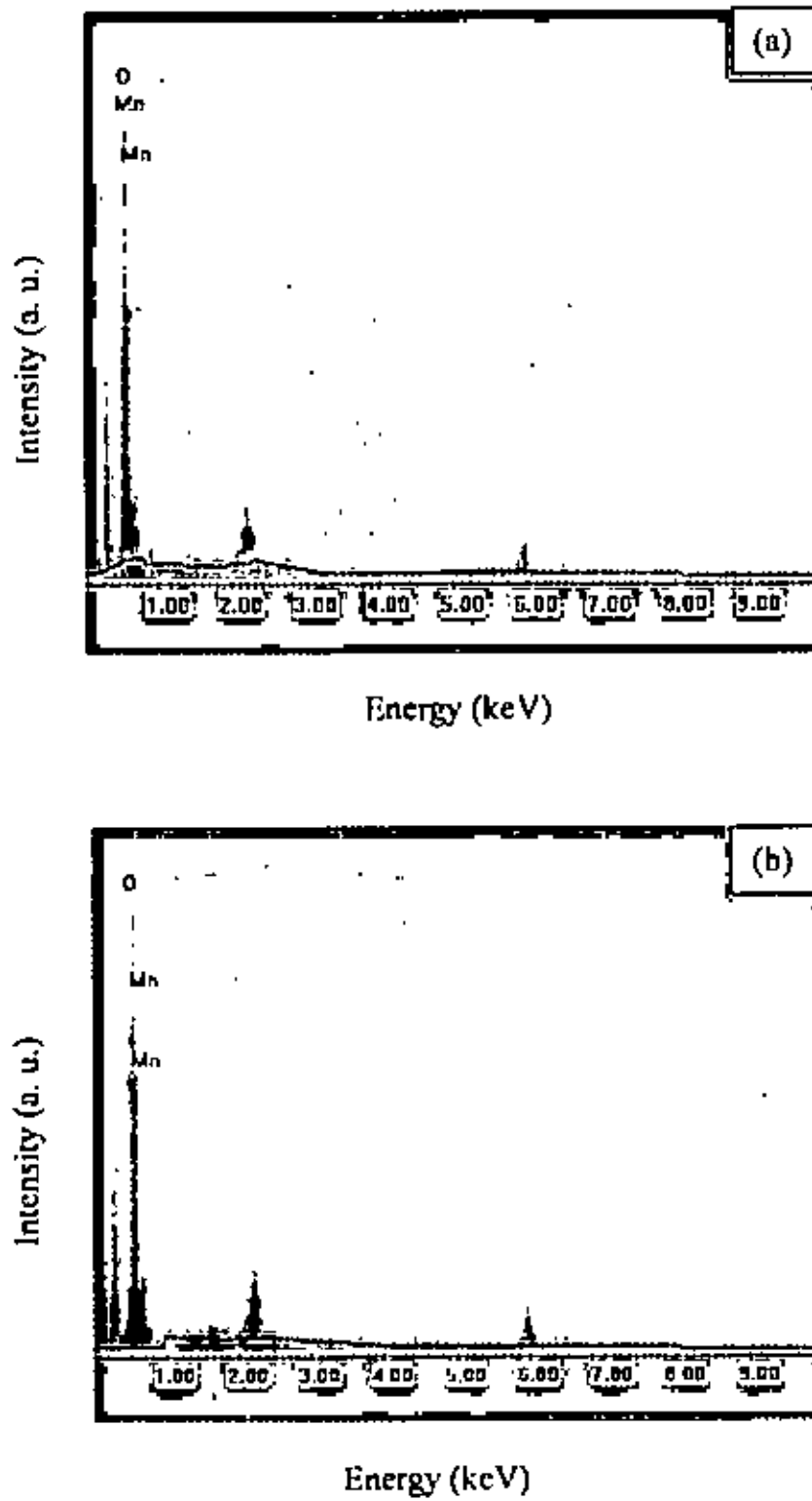
Fig. 3.2.1: Elemental analysis of Mn_3O_4 nanoparticles at sample (a) location 1 and (b) location 2.

3.2.2 Infrared Spectral Analysis

IR spectral analysis studies provide some useful qualitative information on the identification of compounds. Both organic and inorganic substances absorb IR light and thus IR active. In order to get some insight about the structure of the synthesized solid substance, IR spectra of manganese oxide sample is presented in Fig. 3.2.2.

IR spectrum of as-synthesized Mn_3O_4 nanoparticles displayed three main bands: 632.6, 528.5 and 405.0 cm^{-1} in the region 1000-400 cm^{-1}, identical to those reported for the same solid [14]. In the region from 650 to 500 cm^{-1} of the observed spectrum, two absorption bands were observed at 632.6 and 528.5 cm^{-1}. These bands may be associated with the coupling modes between the Mn−O stretching modes of tetrahedral and octahedral sites [15]. The only band in the region 500 to 400 cm^{-1} was observed at 405.0 cm^{-1}. This band is assigned as the band stretching mode of the octahedral sites; displacement of the Mn^{2+} ions in tetrahedral sites is negligible [15]. Thus, the FTIR spectra further confirm that the nanoparticles analyzed is Mn_3O_4.

Similar results have been found by M. Ocana [12]. He observed the bands for same oxide at 633, 527 and 415 cm^{-1} after heat treatment at 800 °C. They also reported that these three peaks indicated the chemical formula of corresponding manganese oxide was Mn_3O_4. W. Zhang and co-workers [16] also found the peaks at 631, 529 and 416 cm^{-1} for Mn_3O_4 nanocrystallites due to Mn−O vibrations. In the present experiment, it can be concluded that the chemical formula of manganese oxide thus obtained is Mn_3O_4. However, the weak absorptions at about 1364 and 1734 cm^{-1} suggest that the particles may also contain a very small amount of absorbed acetate [17].
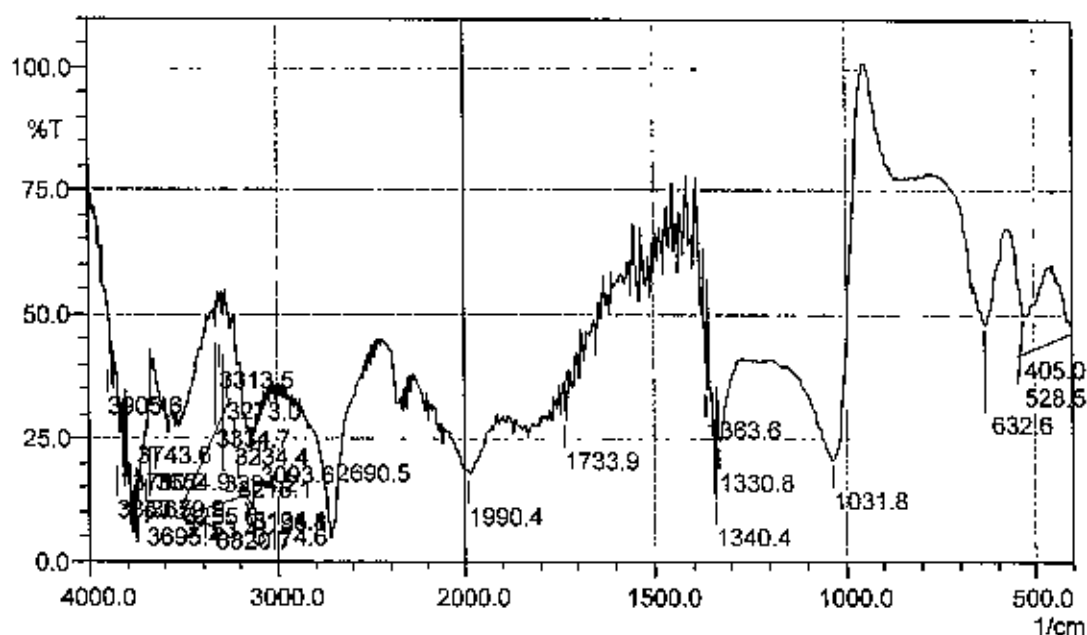
Fig. 3.2.2: IR spectrum of Mn_3O_4 nanoparticle.

3.2.3 X-Ray Diffraction

The X-ray technique is one of the powerful tools for structural analysis of solids. This can provide information on the intermolecular arrangement, i.e., the level of crystallinity of the solids. The solid manganese oxide was examined for its structural analysis in the powdered state by using wide angle X-ray diffraction. The scattering pattern as a function of Bragg angle, 2θ at $\lambda = 1.54$ Å for the studied samples powder are presented in Fig. 3.2.3.

The XRD pattern of these nanoparticles (Fig. 3.2.3) was consistent with that of Mn_3O_4 (hausmannite) [18]. All diffraction peaks can be perfectly indexed to the tetragonal hausmannite structure (space group: I41/amd) with strong ring patterns due to (101), (103), (211), (220), (224), and

(400) planes. The Mn_3O_4 lattice constants obtained by refinement of the XRD data of the nanowires are a=b=5.7630 Å and c=9.4560 Å, which are consistent with standard values for bulk Mn_3O_4 [18], although the peaks were widened as a result of the small-size effects of the nanoparticles. No characteristic peaks of impurities, such as other forms of manganese oxides, were detected.

Crystallite size was calculated by fitting the synchrotron XRD results using the Scherrer equation, $d = 0.941\gamma / (B \cos \theta_B)$, where γ is the wavelength, B is the full width at half-maximum (FWHM) of the peak, and θ_B is the Bragg angle. The crystallite sizes measured from the four peaks (112), (103), (211), and (224) were averaged to obtain the Mn_3O_4 crystallite size and found to be 10.0 nm.
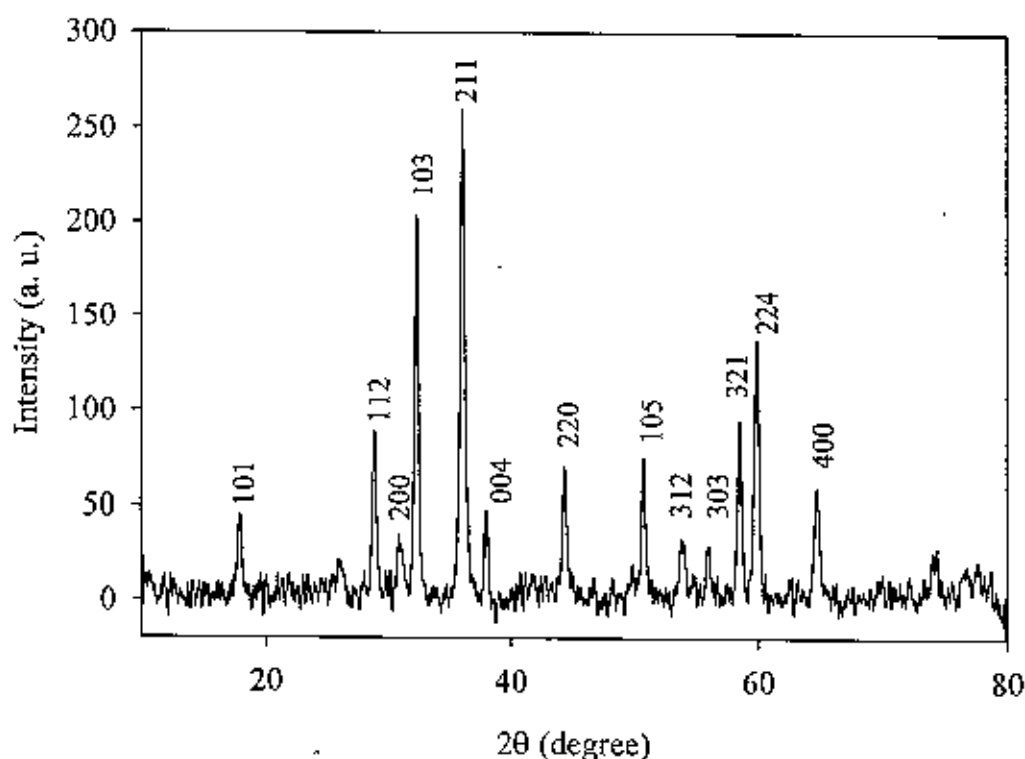

Fig. 3.2.3: XRD pattern of Mn_3O_4 nanoparticles.

3.2.4 Scanning Electron Microscopy

To get more clear insight about the surface morphology scanning electron microscopic (SEM) analysis was employed. SEM is known to the best choice because of its potential in precise analysis of a solid surface. Chemical composition and morphological structure of a material strongly depends on the mode of synthesis conditions such as temperature, pH, concentration of reactant and products, electrochemical parameters etcetera. Thus, there is a variety of morphology of a material could be possible. In the present work, Mn_3O_4 was prepared from aqueous solution of manganese acetate precursor at 80 °C extending the heating time up to 2 h, 6 h and 12 h. Effect of starch, as capping agent, on crystal growth of nanoparticles was also attempted to prevent their agglomeration in solution media. These four Mn_3O_4 samples thus obtained were layered over steel plate for its SEM analysis. All the images (Fig. 3.2.4 a-c) display well-dispersed nanoparticles, however, with different morphologies and varying uniformity.

Figure 3.2.4 (a) shows the SEM image of the Mn_3O_4 synthesized as described before (section 2.6) maintaining the heating time 2 h. From this image, it can be seen that particles exhibit very uniform and well-dispersed morphology with granular shape.

Figure 3.2.4 (b) shows the SEM image of the Mn_3O_4 sample obtained after 6 h reaction time. Here, the particles are observed to grow as the reaction time is increased. Particles get fused together and less uniformed at this stage.

SEM analysis (Fig. 3.2.4 c) of the Mn_3O_4 obtained after 12 h reaction time at 80 °C reveals that the particles are much agglomerated at this stage and least uniformed. The granular particles get clustered together to give a coarse surface.
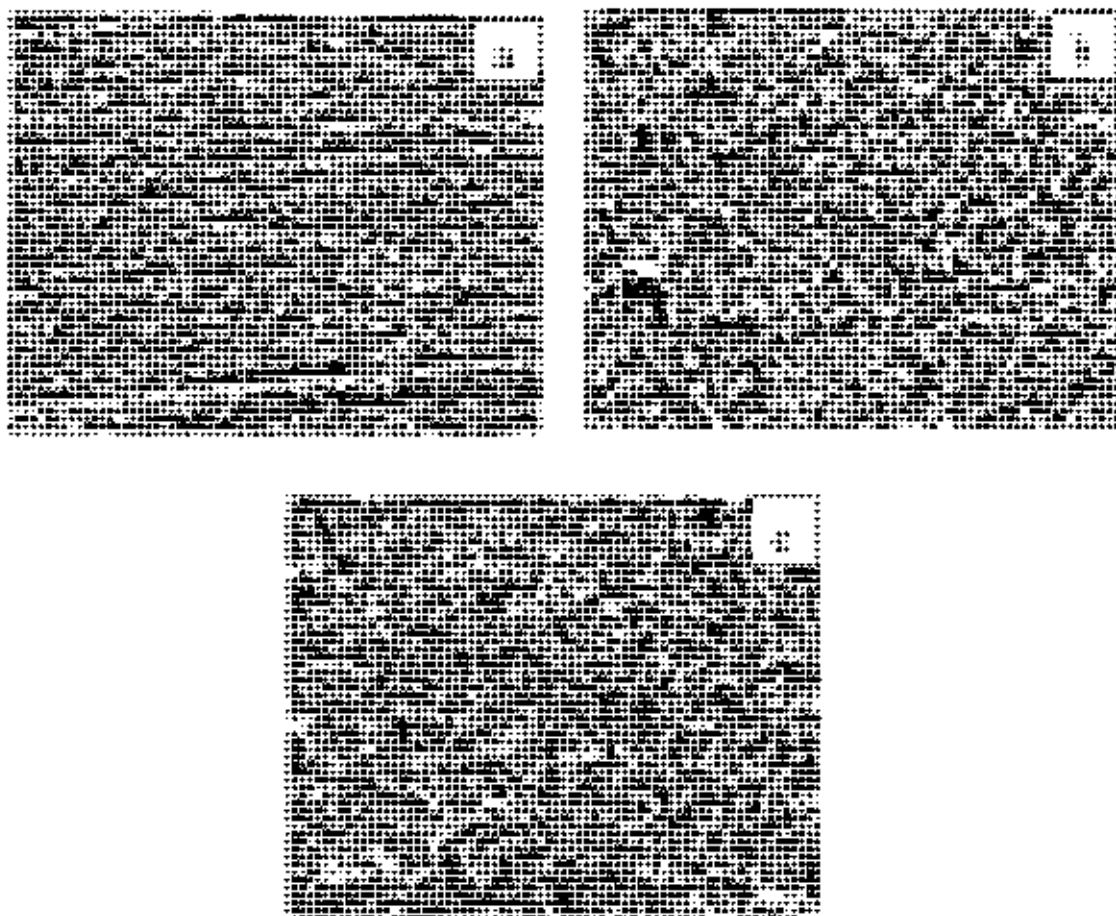
FIg.3.2.4: SEM micrographs of Mn_3O_4 prepared by heating 0.4 M aqueous manganese acetate solution at 80 °C for (a) 2 hours (b) 6 hours and (c) 12 hours

From this study of Mn_3O_4 nanoparticles synthesized at 80 ˚C for different reaction times ranging from 2 to 12 h, it can be concluded that the particle size and irregularity in morphology increase with an increase in reaction time due to agglomeration of particles in solution media.

The average particle size distribution measured from SEM may be in higher range (10 um to 100 nm) than the crystallite size measured from XRD. This is expected as the XRD measurements represent a weighted mean of the actual crystallite size. Albeit, the particles were found to be highly crystalline according to the X-ray diffraction studies but from the SEM images a thin amorphous layer surrounding each particle was observed. This observation is also in agreement with the previous reports [19].

3.2.5 d. c. Conductivity

The conductivity of studied oxide has been measured by employing couveutional two-point probe method. The length and diameter of the sample was 0.3 cm and 0.186 cm respectively.

The measured conductivity of as prepared manganese oxide nanoparticles was 4.60×10^{-8} Scm^{-1} and the corresponding resistivity was 21.74×10^6 Ω cm. The result thus shows that although the Mn_3O_4 is crystalliue, its electrical conductivity is less than that of semiconductors or metals. However, its crystalline nature could be very important for its use in technological applicatious like optoelectronic and electrochromic display devices.

3.3   Characterization of PANI

3.3.1 Ultraviolet-Visible Spectra

UV-Vis spectrum of PANI sample recorded in DMF solutions at room temperature is given in Fig. 3.3.1.
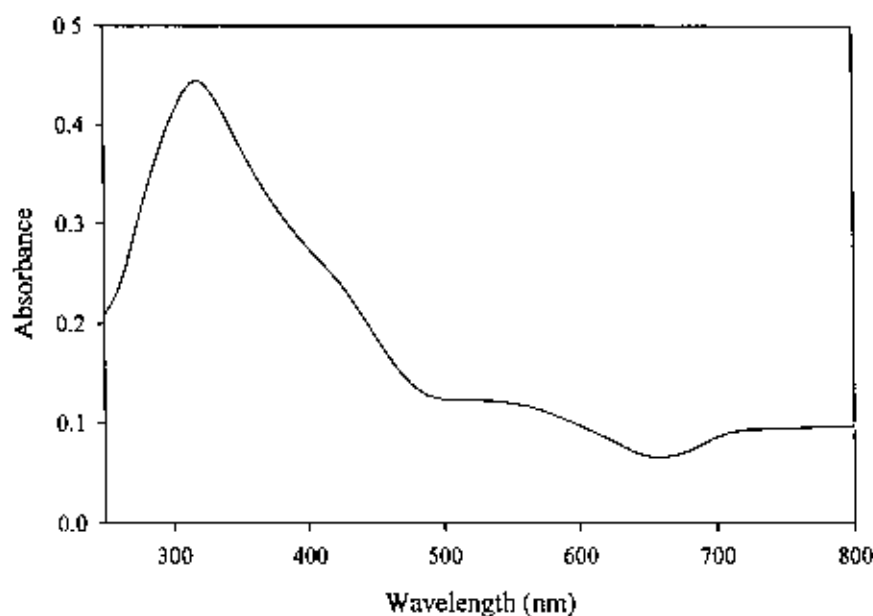

Fig. 3.3.1: UV-Vis. spectrum of PANI as prepared using $K_2Cr_2O_7$.

The absorption spectra (Fig. 3.3.1) of PANI sample shows peaks at 307 nm and a shoulder at *ca.* 663 nm. The result is similar to the studies reported for PANI by previous workers [20, 21] and suggests that the peak observed at 307 nm corresponds to the interband $\pi - \pi^*$ (valence band to conduction band) transition while the other transition observed at around 663 nm may be responsible for PANI conductivity by forming polaron and bipolaron as mid-gap state. Similar phenomeuon has also

been observed with other conducting polymers such as polypyrrole [22-24]. In fact, polaron state is a radical cation, i.e. contains one electron whereas bipolaron is a dication, *i.e.* electronless. At low doping level, polaron formation takes while at highly doped states, bipolaron formation predominates. However, because of the greater stability, a bipolaron is favored over polaron.

3.3.2 Infrared Spectral Analysis

Almost all compounds, particularly organic substances, absorb in the IR region. Although the IR spectrum is characteristic of the entire molecule, it is true that certain groups of atoms give rise to bonds at or near the same frequency regardless of the structure of the rest of the molecule. In order to get some insight about the structure of the synthesized matrices, IR spectral analysis was performed and the results are described below:

Figure 3.3.2 shows the IR spectra of PANI synthesized chemically using potassium dichromate, $K_2Cr_2O_7$, as an oxidant. It is worthwhile to mention here that the observed IR spectra are consistent with the previous studies [25, 26] and discussed below according to the frequency region:

(a)   *3500-3100 cm^{-1}*

This is the N-H stretching region. The absorption of PANI in this region is rather weak. The main absorption peaks are located at 3380 and 3310 cm^{-1}, with shoulders at 3460 and 3170 cm^{-1}.

(b)   *3100- 2800 cm^{-1}*

This is the C-H stretching region. The absorption of PANI in this region is even weaker, but it is observable at 3050 – 3030 and 2960 – 2850 cm^{-1}.

(c)   *1600-1450 cm⁻¹*

Aromatic ring breathing, N-H deformation and C=N stretching all give absorption in this region. In general, the N-H deformation band is very weak. A 1, 4- substituted benzene ring may give absorption band at 1600-1580 and 1510-1480 cm⁻¹. However, the former is very weak and even observable if the two substituents are the same and the latter is strong in the IR in this range. Therefore, it is reasonable to assign the band at 1484 cm⁻¹ mainly to benzoid ring (B) stretching in PANI. Based on the following arguments, we consider the 1591 cm⁻¹ band as a characteristic band of nitrogen quinone (Q).
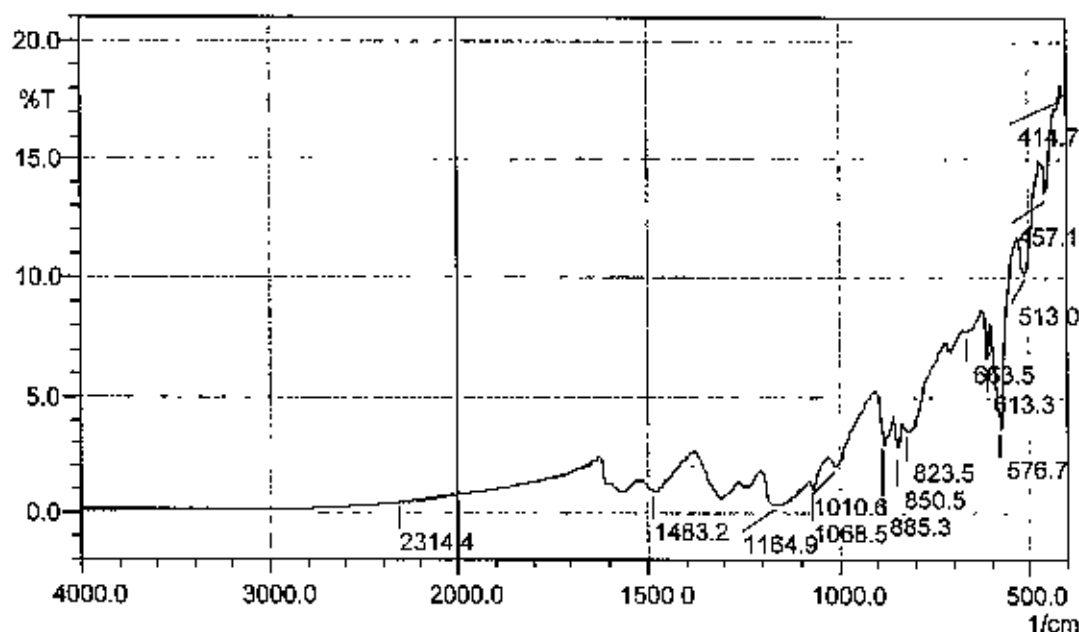

Fig. 3.3.2: IR spectrum of PANI as prepared using $K_2Cr_2O_7$.

(d)   1400-1240 cm⁻¹

This is the C-N stretching region for aromatic amines. The intrinsic PANI shows three peaks: medium absorption at 1240 cm⁻¹ and weak ones at 1380 and 1240 cm⁻¹. The band at 1160 and 1140 was referred as "electronic like band" and was considered as a measure of the degree of delocalization of electrons on PANI and thus are the characteristic peaks of PANI conductivity [14]. The band at 1160 and 1140 cm⁻¹ be assigned separately: 1160 cm⁻¹ to intrinsic structure and 1140 cm⁻¹ to the doped (acid treated) structure. The 1140 cm⁻¹ band is a vibrational mode of $B\overset{+}{-}NH{=}Q$ or $B{-}\overset{\cdot\cdot+}{N}H{-}B$ which is formed in doping reactions. This may be attributed to the existence of the positive charge and the distribution of the dihedral angle between the B and Q rings [27].

(e)   1220-500 cm⁻¹

This is the region of in-plane and out-of-plane bending of C-H bonds on aromatic rings. The main absorption bands for intrinsic PANI are located at 1160 and 830 cm⁻¹ and some weak bands can be observed. It is easy to judge the substitution pattern on the benzene ring from the frequencies of these peaks. For example, 1220, 1105, 1010 and 830 cm⁻¹ stands for 1,4-substitution, 1115, 1060, 960, 895 and 850 cm⁻¹ for 1, 2, 4-substitution and 740 and 690 cm⁻¹ for 1,2- or mono-substitution.

Peaks at 1069 and 613 cm⁻¹ are also observed in the spectra of the PANI film and correspond to the presence of SO_4^{-2} ions, which were used as an electrolytic anion in the film [28, 29].

A summary of tentative assignments of the IR spectra of intrinsic PANI are presented in Table 3.2.2.

Table 3.2.2: Tentative assignment of the IR spectra of PANI sample.

Frequency (cm^{-1})	Assignment*
3590-3710	presence of H$_2$O
3221-3436	NH$_2$ asym. str.
2850-3050	C-H str.
1577	str. of N=Q=N
1483	str. of N-B-N
1321	C-N str. in QB$_c$Q, QBB, BBQ
1165	a mode of N = Q = N
1069	
1010	C-H *ip* on 1,4-ring
824	
1069	
886	C-H *ip* on 1,2,4-ring
851	
831	C-H *op* on 1,2,4-ring

* Abbreviations: asyn = asymmetric, sym = symmetric, str = stretching, *ip* = in-plane bending, *op* = out-of-plane bending, Q = quinoid unit, B = benzoid unit, B$_t$= *trans* benzoid unit, B$_c$= *cis* benzoid unit.

3.3.3 Scanning Electron Microscopy

Figure 3.3.3 shows the SEM image of PANI. It can be seen that soil like morphology is appeared for PANI. Surface seems to be compact with spongy like soil deposit. The present observation is in good agreement with the previous work [30].
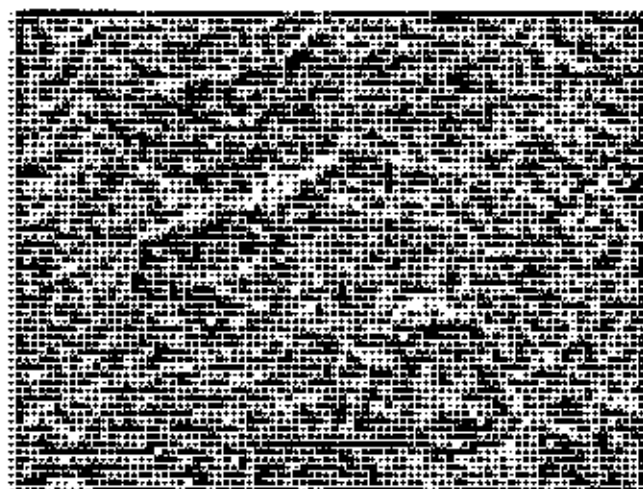

Fig. 3.3.3: SEM micrograph of PANI prepared by $K_2Cr_2O_7$.

3.3.4 d. c. Conductivity

d. c. conductivity measurement of the sample PANI was performed by employing conventional two point-probe method. The vacuum dried sample was compressed to a rigid mass and stored in vacuum desiccators till the conductance measurement commenced.

The observed conductivity of PANI was measured to be 3.72×10^{-6} S cm^{-1}. The conductivity of PANI is usually in the order of 10^{-6} to 10 S cm^{-1},

depending somewhat on the polymerization and protonation conditions [31]. Thus, the observed conductivity of the present PANI sample prepared chemically from H_2SO_4 medium seems to be consistent with the early report suggesting that less harmful $K_2Cr_2O_7$ could be an effective oxidant in preparing the PANI.

3.4   Characterization of Mn_3O_4 Dispersed PANI

Incorporation of micron or submicron sized particles of transition metal oxides in to the whole of polymer matrix of conjugated polymers (polypyrrole, polythiophene, and polyaniline) created metal oxide/polymer composites having increased conductivity with special catalytic properties [32-35]. Mn_3O_4 dispersed PANI was prepared chemically. The PANI/Mn_3O_4 has been characterized by following techniques

3.4.1 Ultraviolet-Visible Spectra

UV- Vis spectra of PANI/Mn_3O_4 sample recorded in DMF solutions at room temperature are given in Fig. 3.3.1.

The PANI/Mn_3O_4 sample (Fig. 3.4.1), shows peaks at 309 nm and a weak shoulder at *ca.* 663 nm. The peak observed at 309 nm corresponds to the interband $\pi - \pi^*$ (valence band to conduction band) transition while the other transition observed in the spectra at around 663 nm may be responsible for PANI conductivity by forming polaron and bipolaron as mid-gap state. The peaks are same as that of shown in Fig. 3.3.1.This due to the manganese oxide particles have no effect on UV-vis spertum of PANI in PANI/Mn_3O_4 and/or Mn_3O_4 particles are sediment when taking UV spectrum.
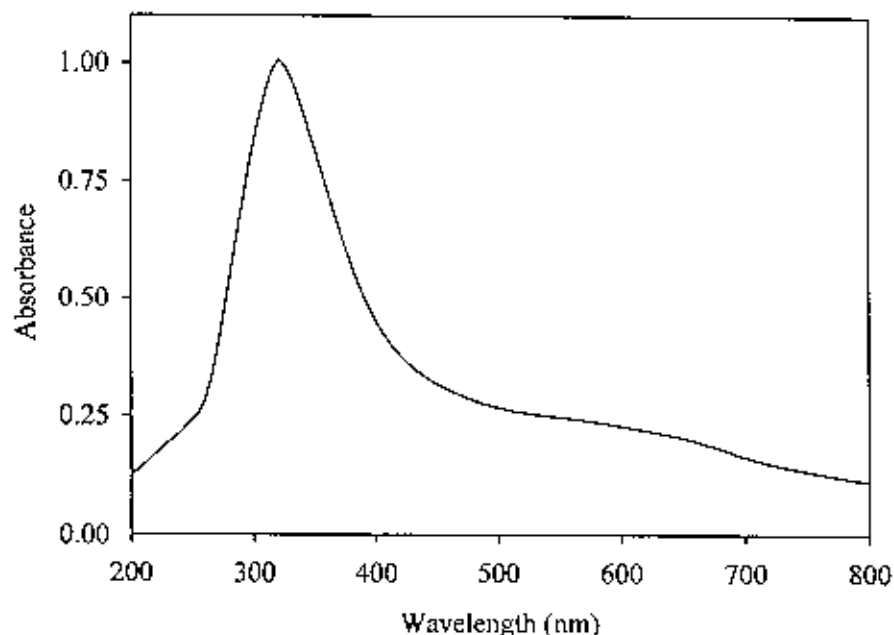
Fig. 3.4.1: UV-Visible spectrum of PANI/Mn$_3$O$_4$ matrix.

3.4.2 Infrared Spectral Analysis

Figure 3.4.2 shows the IR spectrum of Mn$_3$O$_4$ dispersed PANI. By comparing with the individual spectra of PANI with that of PANI/Mn$_3$O$_4$ matrix, three bands at 526.5, 474.5 and 410 cm^{-1} were found for the sample. These three observed bands may be compared with the characteristic bands of Mn−O stretching modes. From this obtained result it may be concluded that the prepared PANI matrix contains Mn$_3$O$_4$ nanoparticles. The characteristics band of Mn$_3$O$_4$ at 630-635 cm^{-1} (Fig. 3.2.2) is not observed in the spectrum of Mn$_3$O$_4$ dispersed PANI due to the overlaping with the band of PANI at 598 cm^{-1}.
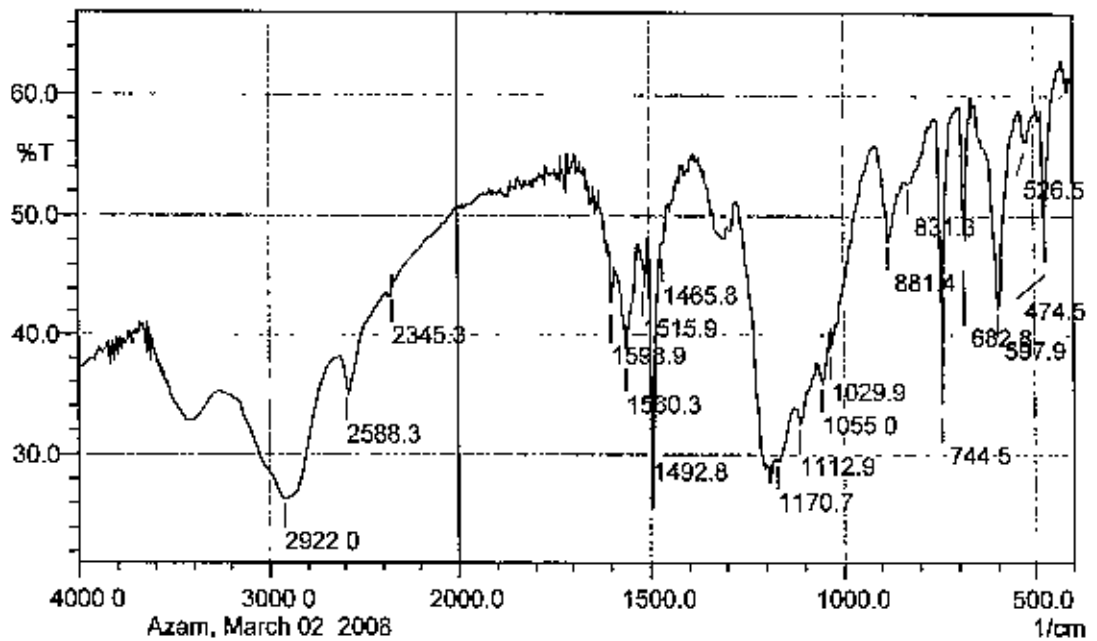
Fig. 3.4.2: IR spectrum of PANI/Mn$_3$O$_4$ matrix.

3.4.3 *Scanning Electron Microscopy*

Figure 3.4.3 (a, b) show that there is a large difference between the surface morphology of the PANI film and the PANI film containing Mn$_3$O$_4$ nanoparticles (PANI/Mn$_3$O$_4$ film). PANI surface has been changed due to the dispersion of oxide particles. The PANI/Mn$_3$O$_4$ film appears to show a number of coral-like polymer net consisting of twisted polymer deposit. From the image it seems that Mn$_3$O$_4$ nanoparticles are distributed randomly in PANI matrix.
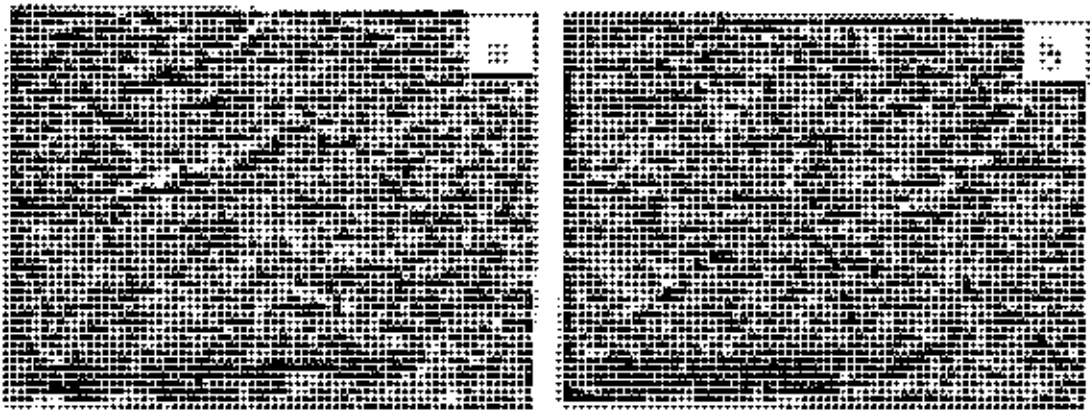
Fig. 3.4.3: SEM images of (a) a PANI film and (b) a PANI/Mn$_3$O$_4$ film

3.4.4 X-Ray Diffraction

Mn$_3$O$_4$ nanoparticles dispersed PANI was analyzed by X-ray diffraction technique which is shown in Fig. 3.4.4. It can be seen from the result that the sample show only diffuse X-ray scattering i.e. the exhibited scattering pattern consists of amorphous peaks. This observation clearly indicates that Mn$_3$O$_4$ has no influence on the structure even it incorporated to the matrix. It is also due to the large weight fraction of the amorphous polymer matrix, the amorphous contribution dominated scattering spectrum and it was not possible to clearly discern the metal oxide contribution in the overall scattering of the matrix [36].
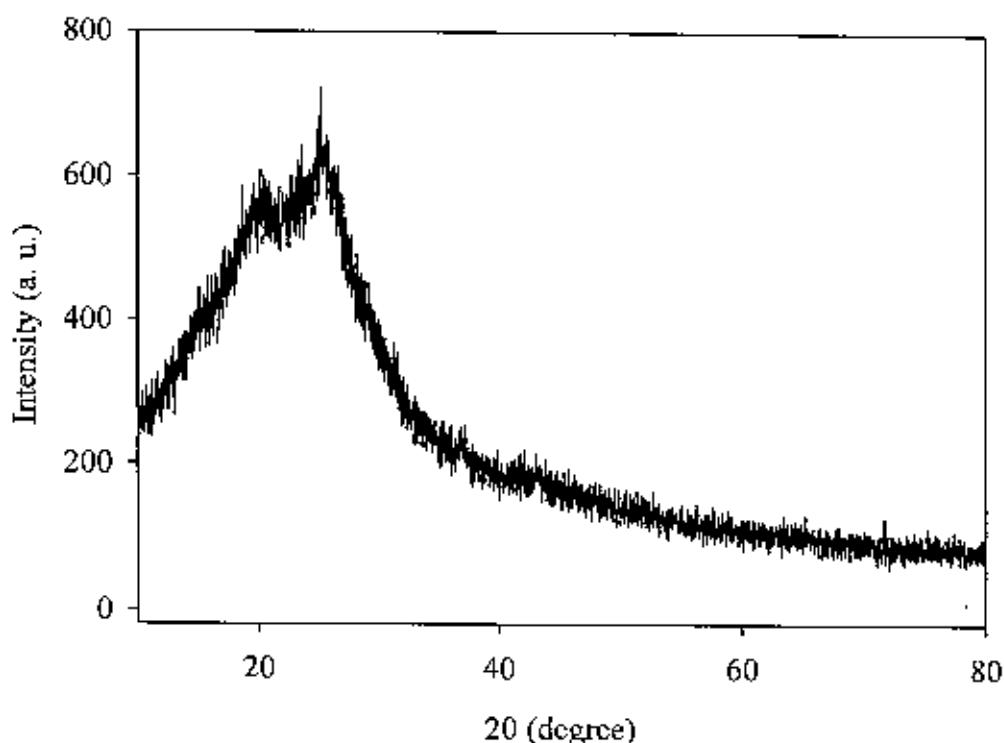
Fig. 3.4.4: XRD pattern of PANI/Mn₃O₄ matrix.

3.4.5 d. c. Conductivity

The conductivity of PANI/Mn$_3$O$_4$ has been found to be 20.82×10^{-6} S cm^{-1}. The conductivity of PANI/Mn$_3$O$_4$ matrices is 4 to 5 times higher than that of PANI. However, the increase conductivity of the PANI/Mn$_3$O$_4$ matrix seems to be reasonable, if one consider the crystalline nature of the Mn$_3$O$_4$ particles. Thus, the presence of Mn$_3$O$_4$ itself may contribute to the conductivity enhancement of the PANI/Mn$_3$O$_4$ matrix. Moreover, the presence of Mn$_3$O$_4$ colloidal particles in the synthesis may provide surface for the aniline adsorption and finally cause a massive production of PANI and thus modifying the rate of its production to yield a matrix with different morphological and electric properties. The change in

conductivity is also reported by the early workers [37-39] for surfactant incorporated conducting polymers. The results of PANI and PANI/Mn_3O_4 indicate that the conductivity of the studied sample falls in the range of semiconductor conductivity, thus may find applications in optical and electronic devices.

3.5 Applications of Mn_3O_4 Nanoparticles Tested

3.5.1 Polymerization of Aniline

PANI was prepared successfully by using Mn_3O_4 nanoparticles. Conventional chemical polymerization of aniline requires strong oxidant to polymerize the aniline monomer. In the present study, aniline was found to be polymerized in presence of nano Mn_3O_4 without addition of any oxidant. PANI thus obtained was green product similar to PANI obtained by using oxidant. The PANI film was then characterized by employing UV-Visible, Infrared spectroscopy, SEM technique and d. c. conductivity measurements.

(i) Ultraviolet-Visible Spectra

UV-Vis spectrum of PANI sample as prepared using nanoparticles of Mn_3O_4 was recorded in DMF solutions at room temperature as given in Fig. 3.5.1

A peak at 307 nm and a weak shoulder at *ca.* 663 nm were observed. The result is similar to the studies reported previously for the PANI prepared using conventional oxidant as $K_2Cr_2O_7$.
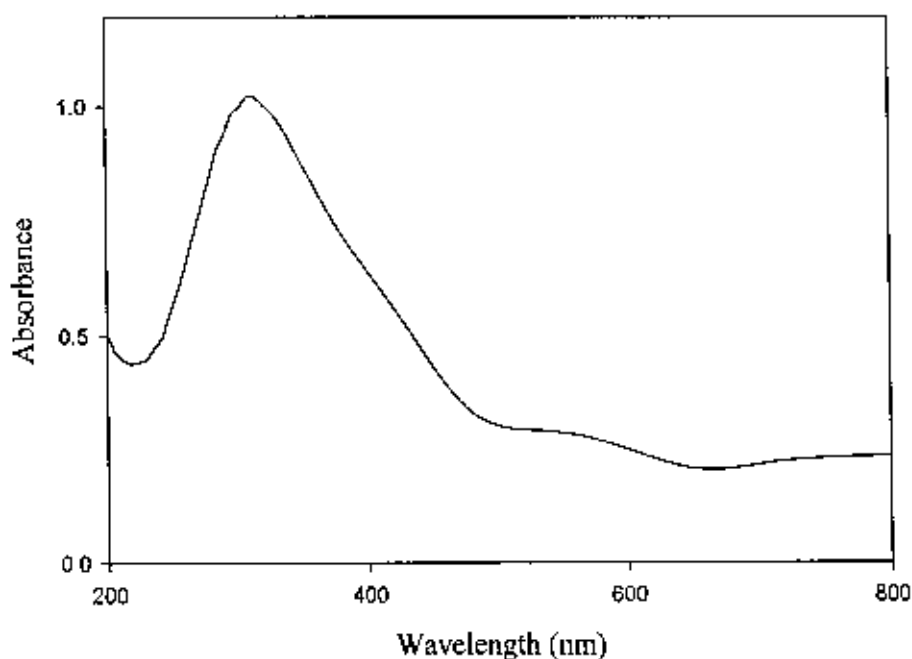
Fig. 3.5.1: UV-Vis. spectrum of PANI prepared using Mn_3O_4 nanoparticles.

(ii) Infrared Spectral Analysis

Figure 3.5.2 shows the IR spectra of PANI synthesized chemically using Mn_3O_4 nanoparticles. It is worthwhile to mention here that the observed IR spectra are consistent with the previous spectrum (Fig. 3.3.2) obtained for the PANI prepared using $K_2Cr_2O_7$.
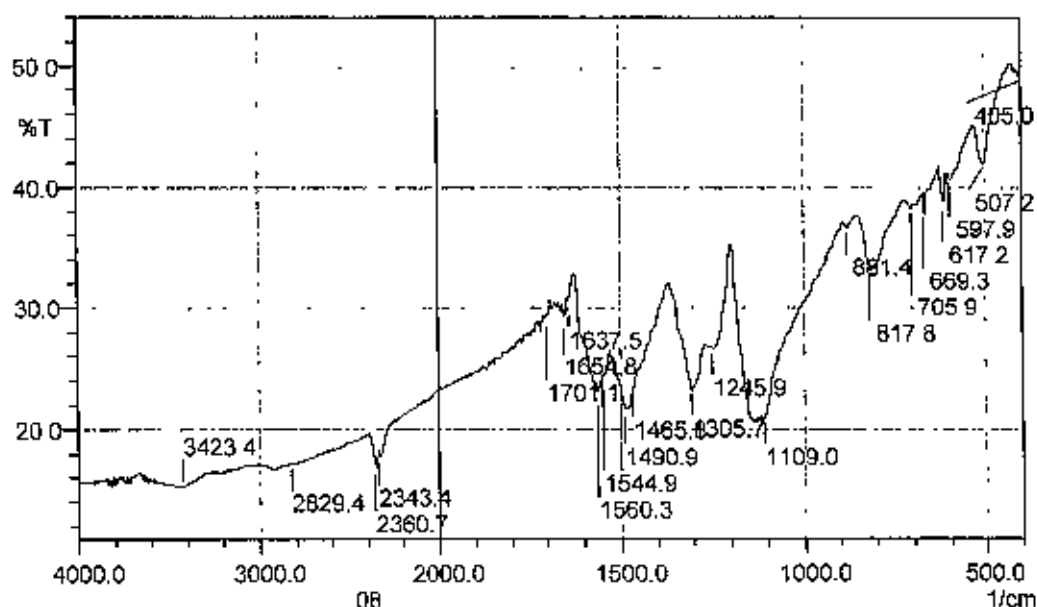
Fig. 3.5.2: IR spectrum of PANI prepared using Mn₃O₄ nanoparticles.

A summary of tentative assignments of the IR spectra of the PANI prepared using Mn_3O_4 nanoparticles are presented in Table 3.5.1.

IR spectrum of as-synthesized PANI using Mn_3O_4 nanoparticles displayed three additional main bands at 617.2, 507.2 and 405.0 cm^{-1} in the region 1000-400 cm^{-1}. These bands may be associated with the coupling modes between the Mn−O stretching modes of tetrahedral and octahedral sites [15]. Thus, the FTIR spectra suggest that there would be some manganese oxide nanoparticles in the polymer matrix.

Table 3.5.1: Tentative assignment of the IR spectra of nanoparticles assisted PANI sample.

Frequency (cm^{-1})	Assignment*
3300-3490	NH$_2$ asym. str.
2829	C-H str.
1545,1560	str. of N=Q=N
1490	str. of N-B-N
1306	C-N str. in QB$_c$Q, QBB, BBQ
1165	a mode of N = Q = N
1069	C-H *ip* on 1,4-ring
1010	
824	
1069	C-H *ip* on 1,2,4-ring
881	
851	
818	C-H *op* on 1,2,4-ring

* Abbreviations: asym = asymmetric, sym = symmetric, str = stretching, *ip* = in-plane bending, *op* = out-of-plane bending, Q = quinoid unit, B = benzoid unit, B$_t$= *trans* benzoid unit, B$_c$= *cis* benzoid unit.

(iii) Scanning Electron Microscopy

Figure 3.5.3 (a, b) show the SEM image of PANI prepared by employing Mn$_3$O$_4$ nanoparticles and by a conventional method using K$_2$Cr$_2$O$_7$ oxidant, respectively. It can be seen that there is notable differences between the surface morphology of the PANI matrices. Compared to the

spongy soil like morphology of PANI, a layer-by-layer lump morphology is observed. The PANI deposit thus produced seems to be more compact with sharp edges.
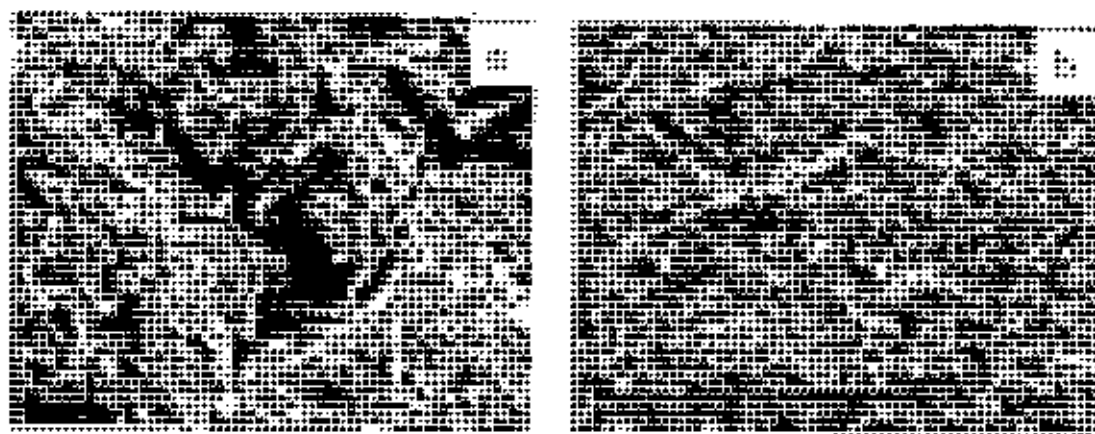

Fig. 3.5.3: SEM micrograph of PANI prepared (a) using Mn_3O_4 nanoparticles and (b) using $K_2Cr_2O_7$.

(iv) d. c. Conductivity

d. c. conductivity measurement of the sample PANI was performed by employing conventional two point-probe method. The observed conductivity of PANI as prepared using nanoparticles was measured to be 4.59×10^{-6} S cm^{-1} whereas the conductivity of PANI as prepared using $K_2Cr_2O_7$ was 3.72×10^{-6} S cm^{-1}. So, it can be seen that the conductivity of PANI increases if it is prepared using nanoparticles. It might be due to the change in the morphological nature of the PANI. In addition, during formation of the polymer some manganese oxide could be incorporated in the PANI and thus modify the surface morpholology of the PANI.

3.5.2 Decolorization of Methylene Blue (MB)

3.5.2.1 Optimization of MB decolorization

The performance of Mn_3O_4 nanoparticles on the decolorization of MB dye has been studied in the presence of sulfuric acid. Effect of MB concentration, amount of nanoparticles, influence of acid concentration, and function of time on MB degradation were also investigated to suggest an optimum condition. UV–Vis absorption spectra of MB solutions were measured in all the cases.

(i) *Various concentrations of MB studied for decolorization:* 0.5×10^{-5} M, 1.0×10^{-5} M, 1.5×10^{-5} M, 2.0×10^{-5} M, 2.5×10^{-5} M, 3×10^{-5} M methylene blue solutions were prepared and used to observe the effect of MB concentration on its removal by Mn_3O_4 nanoparticles at low pH. 5 mL of each concentration MB, 5 mL of nano Mn_3O_4 suspension and 1 mL H_2SO_4 were mixed together and after 1.0 min, absorbance of each of the reaction mixtures was taken. Figure 3.5.4 shows the UV–Vis absorption spectra of untreated 3×10^{-5} M MB solution and the spectra of every concentrations after 1 min of the reaction.
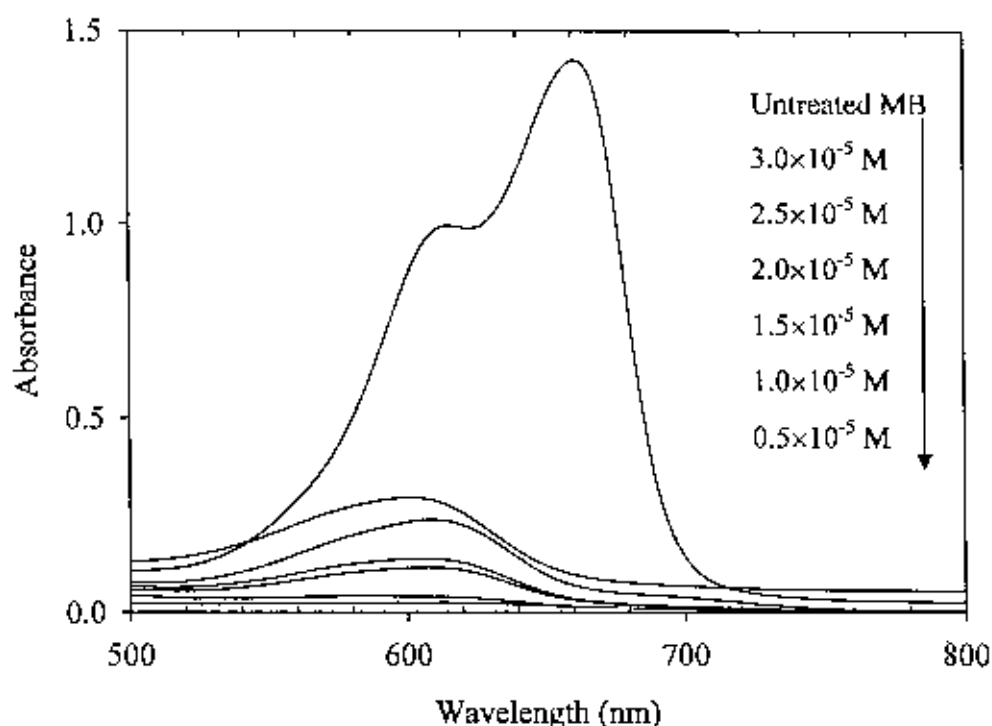
Fig. 3.5.4: UV-Vis. spectrum of untreated 3×10^{-5} M MB and various concentration of MB after treatment with Mn_3O_4 nanoparticles.

(ii) Influence of amount of Mn_3O_4 nanoparticles on MB decolorization: To investigate the effect of amount of Mn_3O_4 nanoparticles on MB decolorization, different amount of Mn_3O_4 nanoparticles suspensions (250 mgL^{-1}), *viz.*, 1.0 mL, 1.5 mL, 2.0 mL, 2.5 mL, 3.0 mL, 5.0 mL, and 7.0 mL, were added to a fixed amount (5.0 mL of 3×10^{-5} M) of methylene blue solution and allowed to react for 1 min. It was found that 5.0 mL nanoparticles suspension was enough for complete decolorization of that amount of MB. UV–Vis absorption spectra (Fig. 3.5.5) of MB solutions were measured in every case.
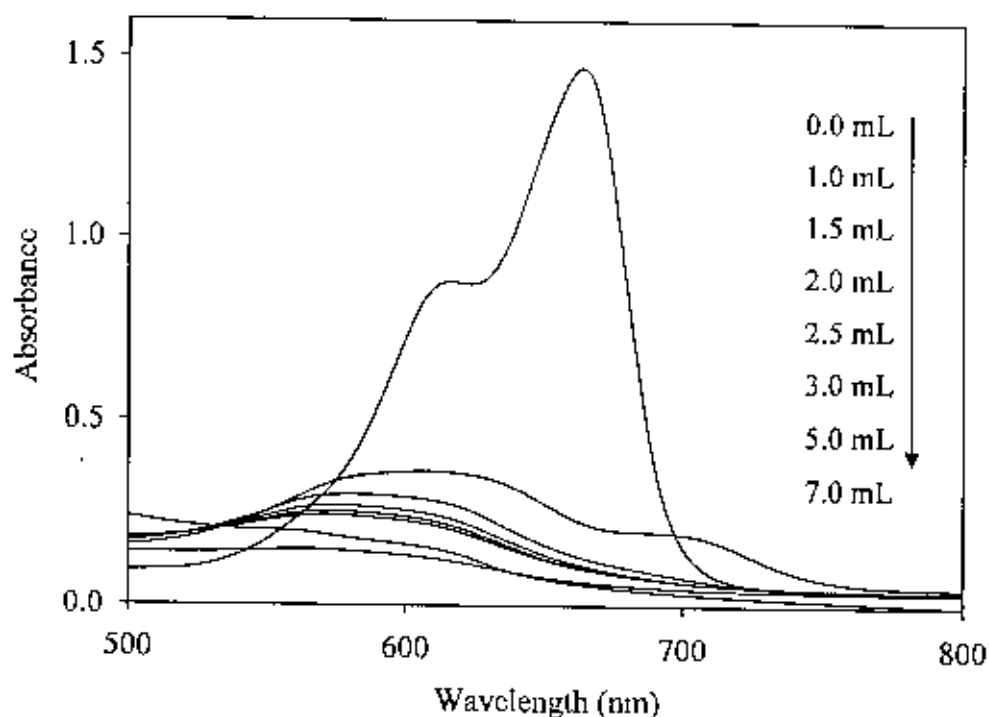
Fig. 3.5.5: UV-Vis. spectrum of 3×10^{-5} M MB after treatment with various amount of Mu_3O_4 nanoparticles.

(iii) *Influence of acid concentration on MB decolorization:* Influence of concentration of sulfuric acid on MB degradation was studied using 0.05 M, 0.25 M, 0.5 M, 1.0 M, 1.5 M, 2.5 M, 3.5 M H_2SO_4 acid solutions, 5 mL of 250 mgL^{-1} nanoparticles suspension and 5 mL of 3×10^{-5} M MB. Figure 3.5.6 shows the UV-Vis spectrum of MB after treatment with nanoparticles indicating the effect of concentration of MB degradation. It was clearly observed from this investigation that presence of 1 mL 2.5 N acid is enough to satisfactorily remove 5 mL dye by adding 5 mL nanoparticles within 1 min.
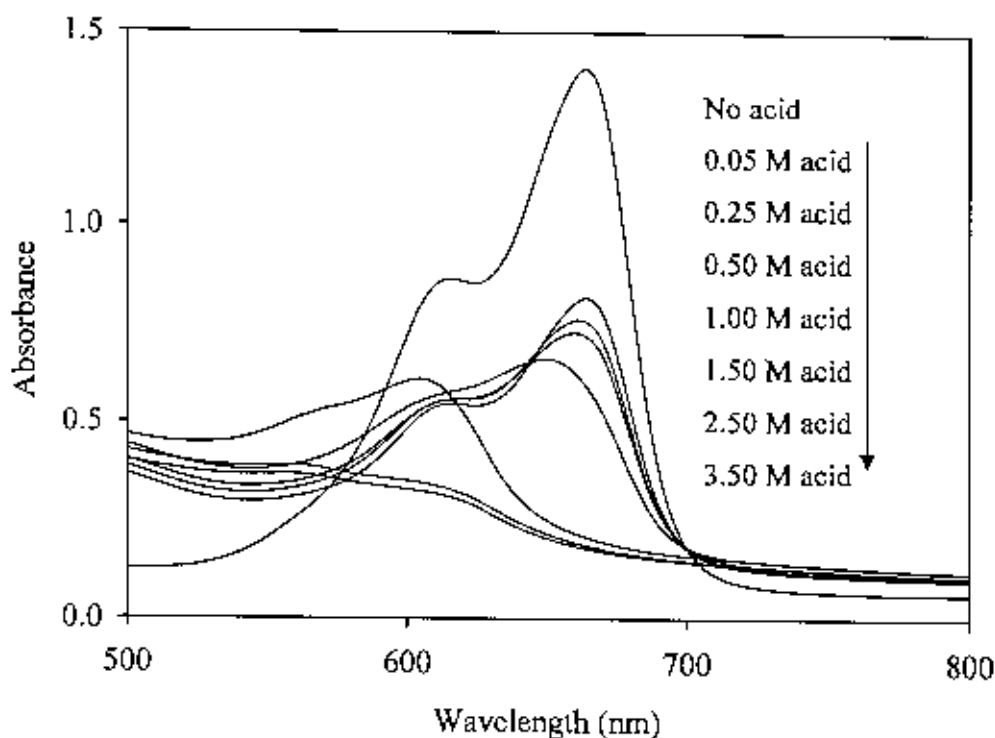
Fig. 3.5.6: UV-Vis. spectrum of 3×10^{-5} M MB after treatment with Mn_3O_4 in presence of various concentration of H_2SO_4.

(iv) ***MB decolorization as a function of time:*** The efficiency of Mn_3O_4 nanoparticles on the decolorization of MB was monitored as a function of time. Figure 3.5.7 shows the UV-Vis spectra of the nanoparticles treated MB for a given time interval: 1 minute, 2 minutes, 3 minutes, 5 minutes, 7 minutes, 10 minutes, 20 minutes, 30 minutes, 1 hour, 2 hours, 3 hours, 6 hours, 12 hours, 24 hours. The color of the mixture turned from blue to light violet and then gray quickly. Within the first minute after treatment, the 664 nm MB peak lessened sharply. With the further elapse of reaction time, the drop of the MB peaks carried on but much more slowly. Moreover, the original absorption maximum at 664 nm shifted to 618, 615, 612 and 610 nm after reaction for 1, 3, 5 and 7 minutes, respectively.

The blue shifts of the absorption band indicates the catalytic degradation of MB similar to that reported by W. Zhang et al [40], Hidaka et al. [41] and Watanabe et al. [42]. Within 30 min, the band at 610 nm became very broad and weak and no obvious new band was observed, suggesting nearly complete degradation of MB.
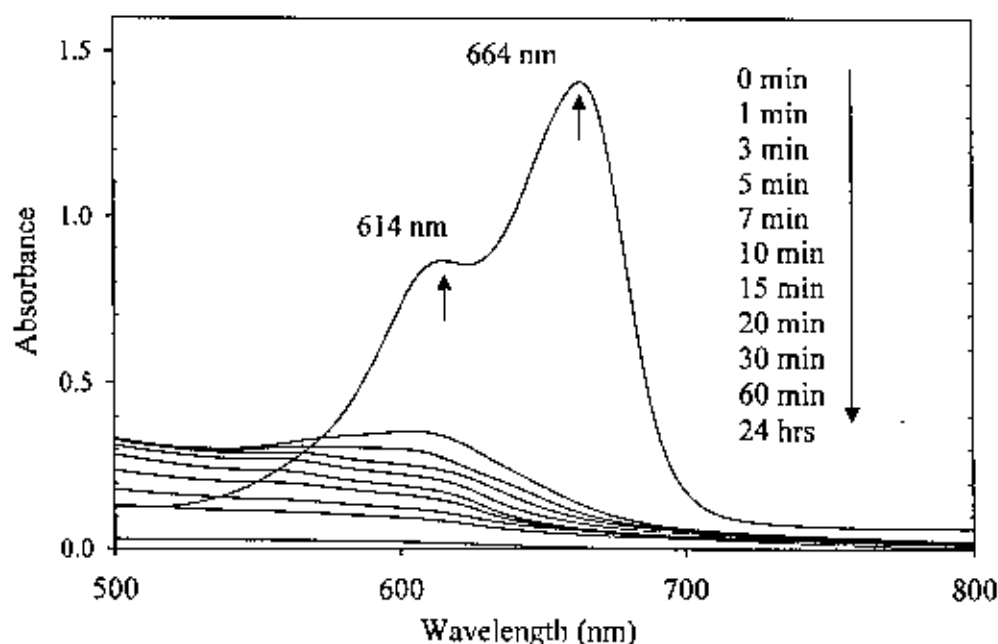
Fig. 3.5.7: UV-Vis. absorption spectra of the (MB+Mn$_3$O$_4$+H$_2$SO$_4$) solution as a function of time.

The Mn$_3$O$_4$ nanocrystal has been systematically studied on the degradation of MB under controlled conditions. By monitoring the MB absorption peak at 664 nm, we obtained results shown in Fig. 3.5.8. Now the degree of decolorization is expressed as $(I_0 - I_t)/I_0$, where I_0 is the absorption at $t = 0$ and I_t is the absorption at a given reaction time, t.

Remarkably, the use of Mn_3O_4 nanoparticles as a degrading agent allowed the degree of decoloration to reach approximately 80% within only 1 min.
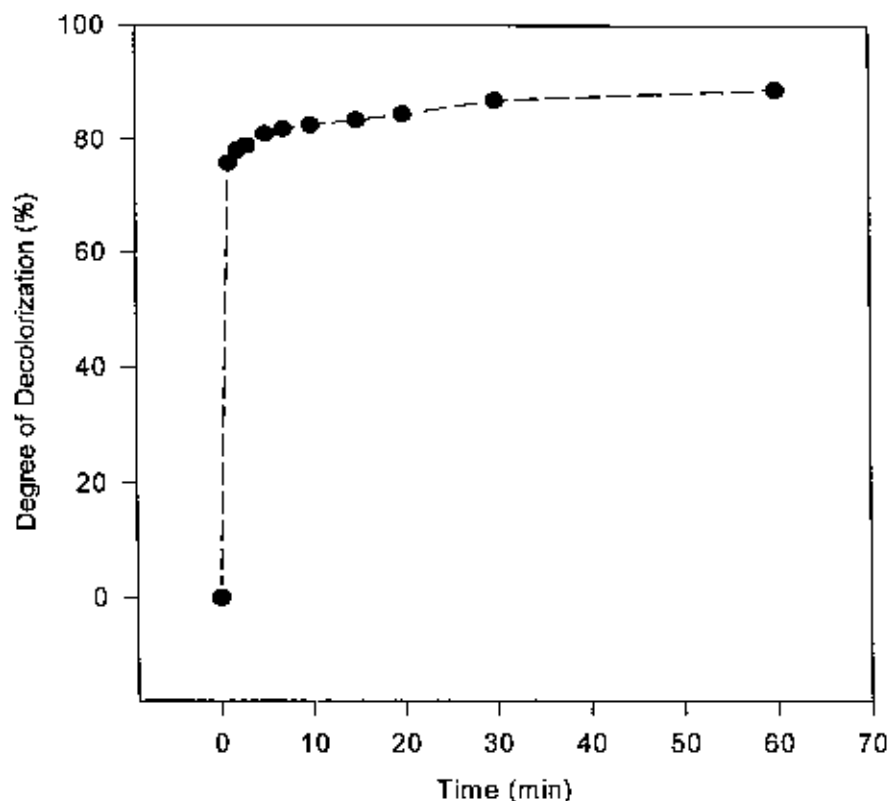

Fig. 3.5.8: Time profile of MB degradation: MB+Nanoparticles+H_2SO_4.

(v) MB decolorization in absence of light: The activity of Mn_3O_4 nanoparticles on the degradation of MB was investigated in absence of light. It was found that the nanoparticles can decolorize the MB dye even in the dark. Figure 3.5.9 shows the UV-Vis absorption spectra of MB before and after decolorization.
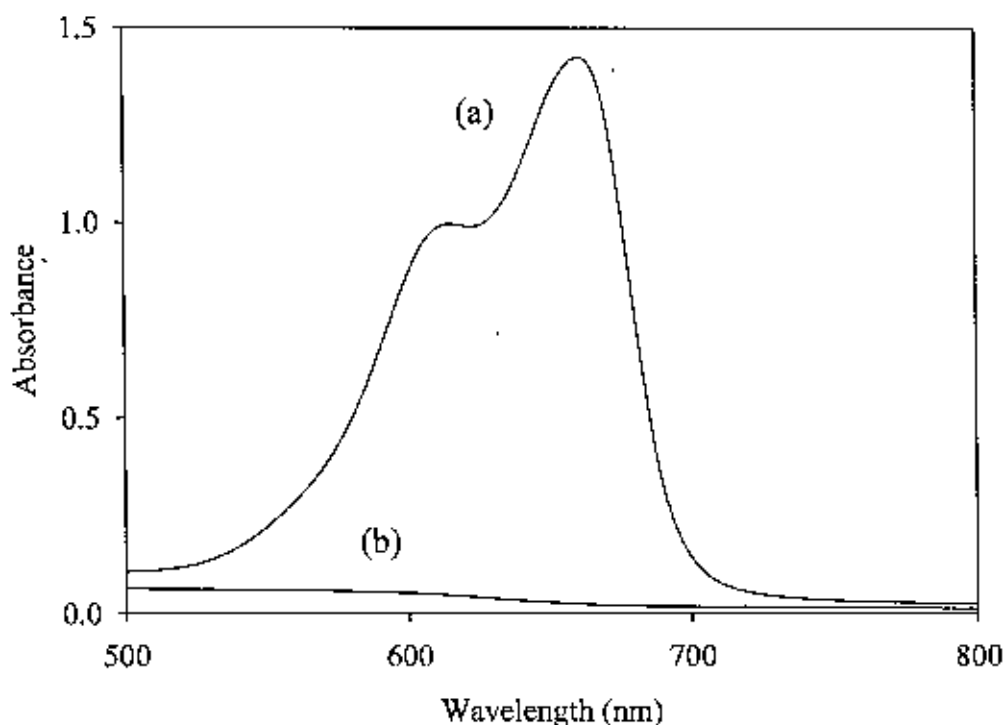
Fig. 3.5.9: UV-Vis absorption spectra of (a) 3×10^{-5} M MB before addition, (b) (MB+Mn$_3$O$_4$+H$_2$SO$_4$) after decolorization in absence of light.

3.5.2.2 *Investigation of Decolorization by Cyclic Voltammetry*

The decolorization of MB solution by nanoparticles in presence of sulfuric acid was also investigated by Cyclic Voltammetry. In Fig. 3.5.10(a), the CV shows the electrochemical behavior of the MB in H$_2$SO$_4$ solution. For this case, a cell consists of Pt working electrode was allowed to sweep between the potential -0.2 and +0.5 V at a scan rate of 100 mV sec^{-1}. The result clearly shows that the MB solution can be switched between its oxidized and reduced states. It can be seen from the CV that, it is composed of a well-defined single redox process: anodic

process at *ca.* +0.26 V and the cathodic one at *ca.* 0.21 V, suggesting the characteristic oxidation and reduction of MB under the electrochemical conditions employed. However, in the CV of MB solution after nanoparticles treatment given in Fig. 3.5.10(b), no characteristic peak of MB was observed. This modification of the voltammogram may arise as the MB degraded of MB by the Mn_3O_4 nanoparticles.
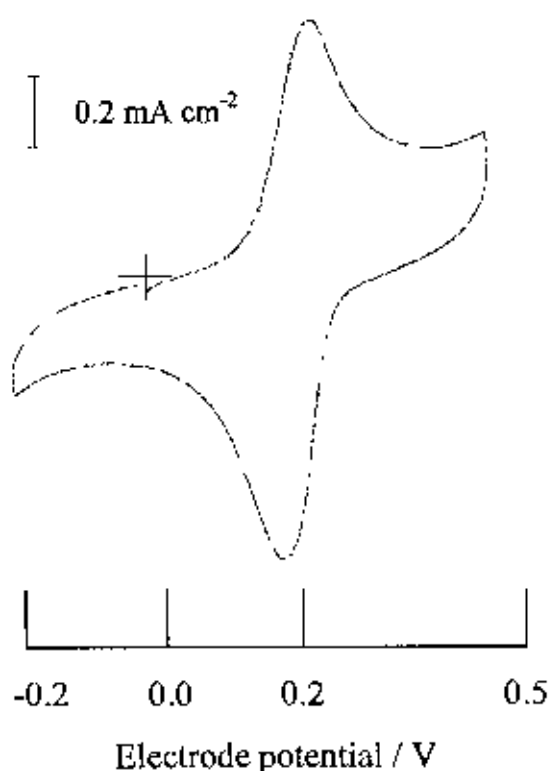

Fig. 3.5.10 (a): CV for 3×10^{-5} M MB in 0.5 N H_2SO_4 solution.

0.2 mA cm^{-2}

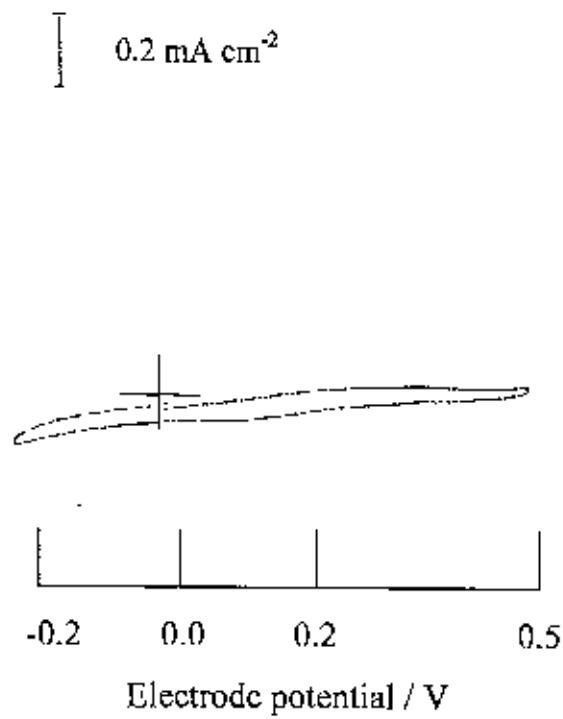-0.2   0.0   0.2   0.5

Electrode potential / V

Fig. 3.5.10 (b): CV of the mixture of 50 mL 3×10^{-5} M MB+50 mL Mn_3O_4 taken after decolorization.

3.5.3 Declorization of Procion Red

Degradation of another textile dye, procion red (PR), by Mn_3O_4 nanoparticles was also investigated. It was observed that the prepared nanoparticles can also successfully decolorize the dye, PR, within very short period of time. As Mn_3O_4 was added to the acidic solution of PR, the reddish color of the mixture turned from blue to gray rapidly. Figure 3.5.10 represents the UV-Vis spectra of PR before reaction and that of $PR+Mn_3O_4+H_2SO_4$ solution after complete decolorization.
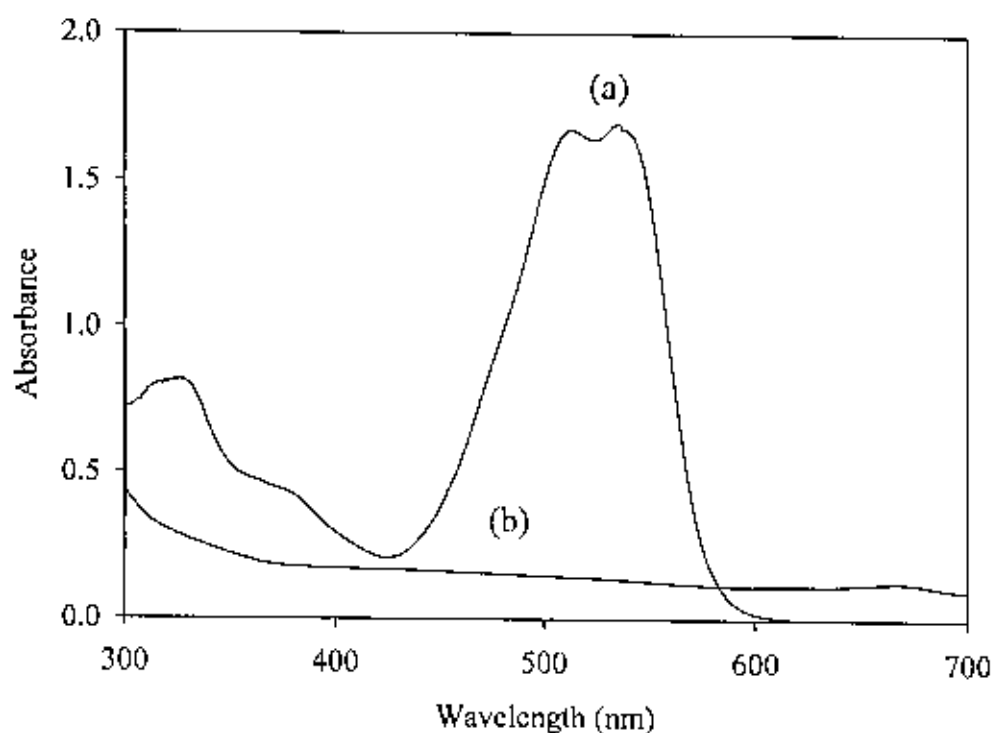

Fig. 3.5.10: UV-Vis absorption spectra of (a) 2×10^{-4} M PR before addition and (b) $(PR+Mn_3O_4+H_2SO_4)$ after decolorization.

3.5.4 Decolorization of Industrial Effluent

The colored industrial effluent was collected from "Young One", Dhaka Export Processing Zone, Dhaka, Bangladesh, and successfully decolorized with the help of prepared Mn_3O_4 nanoparticles. Only 10 mL of Mn_3O_4 suspension (250 mgL^{-1}) was found to be enough to decolorize 50 mL of that industrial effluent within 10 min. UV-Vis spectra of the effluent before addition and that of effluent+Mn_3O_4+H_2SO_4 solution after complete decolorization is represented in Fig. 3.5.11.
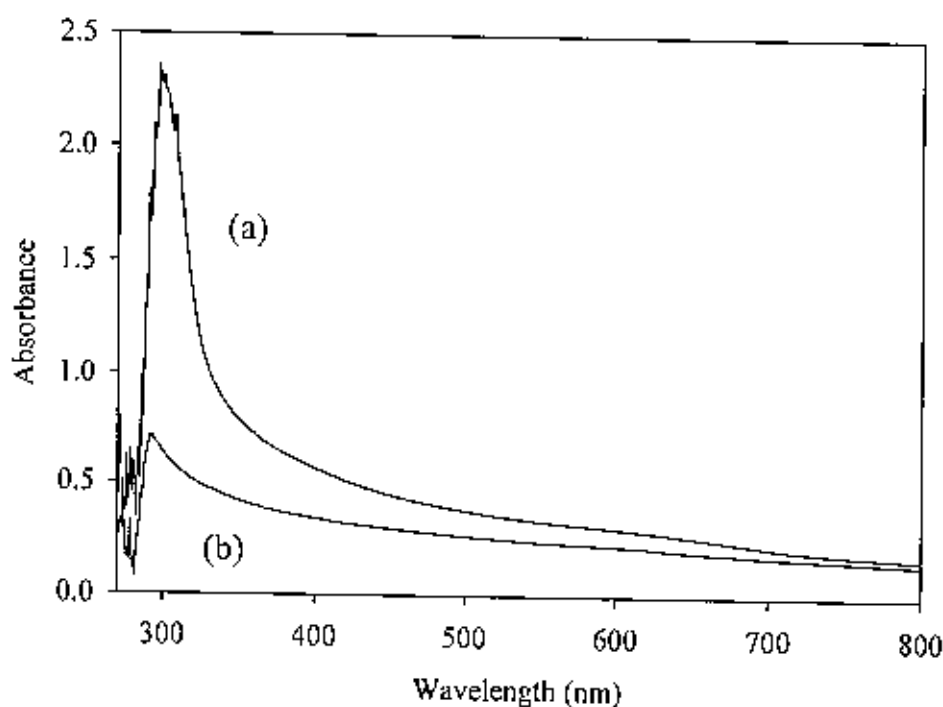

Fig. 3.5.11: UV-Vis absorption spectra of (a) the effluent before addition and (b) (effluent+Mn_3O_4+H_2SO_4) after decolorization.

3.5.5 Sensitivity on Different Pathogenic Organisms

Sensitivity of Mn_3O_4 nanoparticles suspension (250 mgL^{-1}) was tested on various pathogenic organisms at two different pH: 6.2 and 3.3. The tested bacteria are *Vibrio cholerae* (Fig. 3.5.12 a) causing cholera, *Shigella sp* (Fig. 3.5.12 b) causing dysentery, *Salmonella sp* (Fig. 3.5.12 c) causing diarrohea and enteric fever as typhoid, and *Escherichia coli* (Fig. 3.5.12 d) causing diarrhoea. Zone diameter of inhibition in millimeters were measured compared to control ciprofloxacin antibiotic and found to be moderately sensitive against those bacteria. 10^{-2} diluted suspension was also tested against those bacteria but, however, found to be resistant. The sensitivity pattern of the Mn_3O_4 nanoparticles is represented in table 3.5.3.

Table 3.5.3: Sensitivity pattern of the Mn_3O_4 nanoparticles suspension on different pathogenic organisms

pH of suspension	Bacteria/ Diseases	Zone Diameter of inhibition in mm		
		Neat Suspension	Dilution 10^{-2}	Control (Ciprofloxacin)
6.2 (sample # 1)	*Vibrio cholerae/* cholera	S* 16	R*	S* (33)
	Shigella sp/ dysentery	S* 14	R*	S* (26)
	Salmonella sp/ diarrohea and typhoid	S* 15	R*	S* (20)
	Escherichia coli/ diarrhoea	R*	R*	S* (32)
3.3 (sample # 2)	*Vibrio cholerae/* cholera	S* 16	R*	S* (30)
	Shigella sp/ dysentery	S* 14	R*	S* (30)
	Salmonella sp/ diarrohea and typhoid	S* 13	R*	S* (22)
	Escherichia coli/ diarrhoea	S* 12	R*	S* (30)

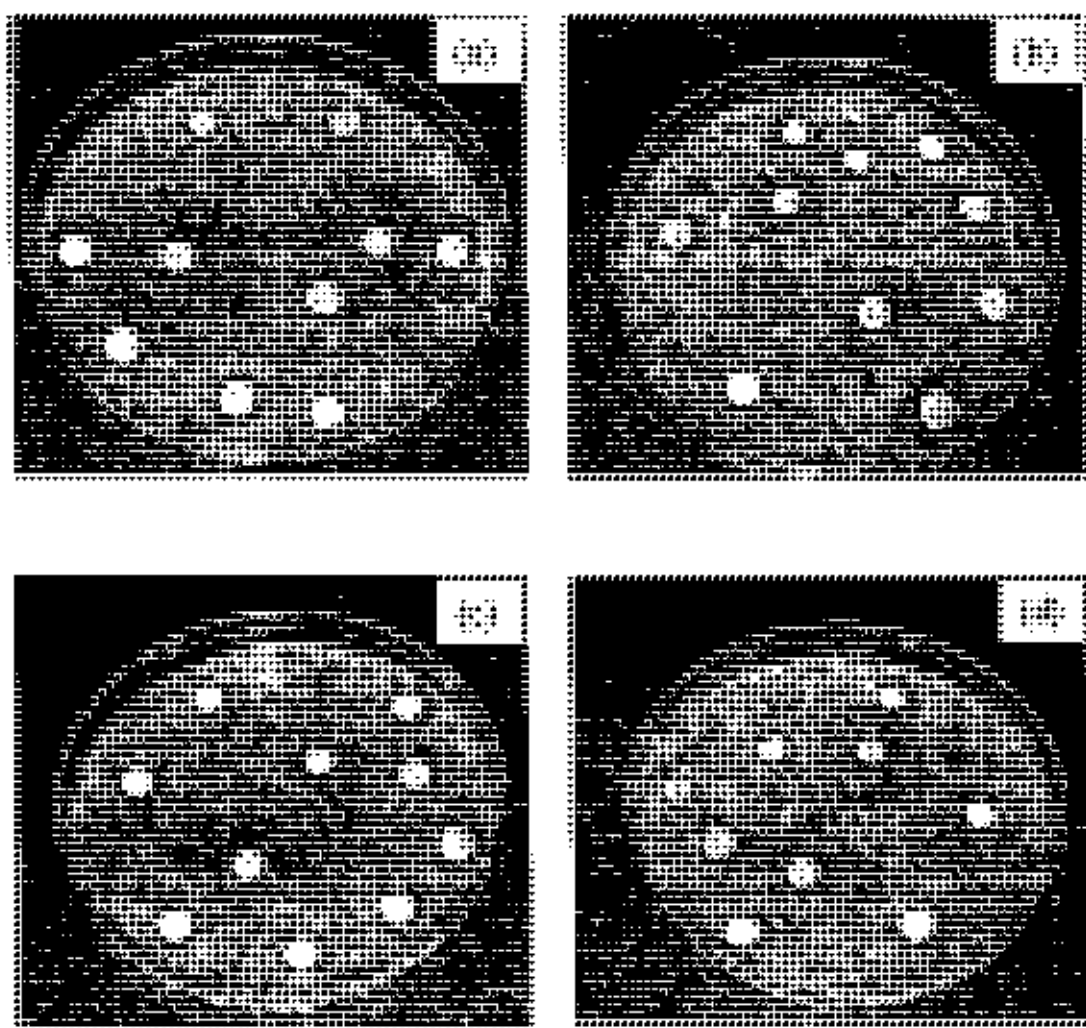- S and R stand for Sensitive and Resistant respectively

Fig. 3.5.12:   Inhibition of Mn_3O_4 nanoparticles suspension against
(a) *Vibrio cholerae* (b) *Shigella sp.* (c) *Salmonella sp.*
and (d) *Escherichia coli*

3.6 Conclusion

Uniform Mn_3O_4 nanoparticles of about 10 nm crystallite size have been prepared by a simple chemical method using manganese(II) acetate, $Mn(OOCCH_3)_2$, as precursor and starch as capping agent. 0.4 M aqueous solution of $Mn(OOCCH_3)_2$ was aged at 80 °C for 2, 6, and 12 h to yield the Mn_3O_4 nanoparticles. Reaction time was observed to have a significant effect on the uniformity and size of the resulting particles. The most isotropic particles were obtained using a heating time of 2 h, during synthesis.

PANI was prepared chemically from aniline by using as an oxidant at room temperature 30 ± 2 °C. The electrical conductivity of the as prepared PANI, 3.72×10^{-6} Scm^{-1}, is increased to 20.82×10^{-6} Scm^{-1}, when Mn_3O_4 nanoparticles were incorporated into the whole of the polymer matrix.

Applications of the Mn_3O_4 nanoparticles were tested to perform polymerization, color removal of dyes and industrial effluent, and sensitivity against different pathogenic organisms. Instead of conventional chemical polymerization of aniline using strong oxidant, in this study, polymerization was carried out in the presence of Mn_3O_4 nanoparticles without using any oxidant. The PANI deposit thus produced was found to be more compact with sharp edges. The electrical conductivity also increased from 3.72×10^{-6} Scm^{-1} (for PANI prepared by $K_2Cr_2O_7$) to 20.82×10^{-6} Scm^{-1} (for nanoparticles assisted PANI). The activity of the Mn_3O_4 nanoparticles has been demonstrated for the decolorization of an organic dye MB in presence of H_2SO_4. The degree of decolorization of MB by Mn_3O_4 nanoparticles reached more than 75%

within 1 min. Correspondingly, the color of the mixture turned from blue to grey quickly, even in the dark. The blue shifts of the absorption bands for MB after the addition of the Mn_3O_4 nanoparticles indicate the catalytic degradation of MB. It was also observed that the Mn_3O_4 nanoparticles can successfully decolorize another textile dye, PR. As Mn_3O_4 was added to the solution of PR in acidic media, the deep reddish color turned to light pink and then grey within 30 minutes. Mn_3O_4 can also effectively decolorize industrial effluent within few minutes. Only 10 mL of Mn_3O_4 nanosuspension (250 mgL^{-1}) was found to be adequate for decolorizing 50 mL of that collected effluent sample. Sensitivity of the Mn_3O_4 nanoparticles suspension (250 mgL^{-1}) was tested on various pathogenic organisms, such as *Vibrio cholerae, Shigella sp., Salmonella sp.*, and *Escherichi coli.* Zone diameter of inhibition were measured compared to control ciprofloxacin antibiotic and found to be moderately sensitive against those bacteria, responsible for cholera, dysentery, typhoid, and diarrhoea diseases.

References

1. J. Li,Y . J. Wang,B. S. Zou,X. C. Wu, J. G. Lin,L. Guo,Q. S. Li, *Appl. Phys. Lett.*, 70, 3047 –3049, (1997).

2. W. P. Tang,H. Kanoh,X. J. Yang,K. Ooi, *Chem. Mater.*, 12, 3271–3279, (2000).

3. G. H. Lee, S. H. Huh,J. W. Jeong,B. J. Choi,S. H. Kim, H.-C. Ri, *J. Am. Chem. Soc.*, 124,12 094–12095, (2002).

4. Y. Omomo,T . Sasaki, L. Z. Wang, M. Watanabe, J. Am. Chem. Soc., 125, 3568 –3575, (2003).

5. J. M. Tarascon, M. Armand, *Nature*, 414, 359 –367, (2001).

6. Y. F. Shen,R. P. Zerger, R. N. De Guzman, S. L. Suib,L. McCrudy, D. I. Potter,C. L. O'Young, *Science*, 260, 511 –515, (1993).

7. T. Yamashita,A. Vannice, *J. Catal.*, 163,158 –168, (1996).

8. I. Metil, *Mod. Paint Coat.*, 72, 49 –52, (1982).

9. C. H. Hare,M. G. Fernald, *Mod. Paint Coat.*, 74, 40 –44, (1984).

10. L. Sanchez,J. Farcy,J. P. Pereira-Ramos,L. Hernan, J. Morales, J. L. Tirado, *J. Mater. Chem.*, 6, 37 –42, (1996).

11. Matijevi E., *Langmuir*, 2, 12-20, (1986)

12. M. Ocana, *Colloid Polym Sci* 278, 443-449 (2000)

13. Sugimoto T, Matijevi E, *J Inorg Nucl Chem*, 41, 165-172, (1979)

14. Nohman AKH, Zaki MI, Mansour SAA, Fahim RB, Kappenstein C, *Thermochim Acta*, 210, 103-121, (1992)

15. M. Ishii, M. Nakahira, *Solid State Commun*, 11, 209, (1972)

16. W. Zhang, Z. Yang, Y. Liu, S. Tang, X. Han, M. Chen, *J. Cryst Growth*, 263, 394-399, (2004)

17. Nakamoto K, Infrared and Raman spectra of inorganic and coordination compounds. Wiley, New York, 232, (1986)

18. International Centre for Diffraction Data (ICDD), PDF file no. 24-0734.

19. J. Pike, J Hanson, L. Zhang, and S-W Chan, *Chem. Mater.*, *19*, 5609-5616, (2007)

20. F. Wudl, R. O. Angus, F. L. Lu, P. M. Allemand, D. J. Vachon, M. Nowak, Z. X. Liu and A. J. Heeger, *J. Am. Chem. Soc.*, 109, 3677, (1987).

21. M. Angelopoulos, G. E. Asturias, S. P. Ermer, A. Roy, E. M. Scherr, A. G. MacDiarmid, A. Akhter and Z. Kiss, *Mol. Liq. Cryst.*, 160, 151, (1988).

22. F. Genoud, M. Guglielmi, M. Nechtschein, E. Genice and M. Salmon, *Phys. Rev. Lett.*, 55, 118, (1985).

23. E. M. Genics and J. M. Pernaut, *Synth. Met.*, 10, 117, (1984).

24. J. H. Kaufman, N. Colaneri, J. C. Scott and G. B. Street, *Phys. Rev. Lett.*, 53, 10005, (1984).

25. W. R. Salaneck, B. Liedberg, O. Inganas, R. Erlandsson, I. Lundstrom, A. G. MacDiarmid, M. Halpern and N. L. D. Somasiri, *Mol. Cryst., Lig. Cryst.*, 121, 191 (1985).

26. J. Tang, X. Jing, B, Wang and F. Wang, *Synth. Met.*, 24, 231 (1988).

27. S. Stafstrom and B. Sjogren, *Synth. Met.*, 16, 31 (1986).

28. D. Dolphiue and A. Wick, *Tabulation of Infrared Spectral Data*, John Wiley & Sons, New York, London, Sydney, Toronto, (1977)

29. A. D. Cross and R. A. Jones, *An Introduction to Practical Infrared Spectroscopy, 3rd edn., Butterwarth*, London, (1969).

30. E. M. Genies, S. C. Tsintavis and A. A. Syed, *Mol. Cryst. Liq. Cryst.*, 121, 181, (1985).

31. F. Lux, *Polymer*, 35, 2936, (1994).

32. N. Endo, Y. Miho, K. Ogura, *J. Mol. Catal.A: Chem*, 127, 49, (1997)

33. K. Pielichowski, M. Hasik, *Synth. Met.*, 89, 1999, (1997)

34. P. Wang, Y. F. Li, *J. Electroanal. Chem.*, 408, 77, (1996)

35. M. Barth, M. Lapkowski, W. Turek, J. Muszynski, S. Lefrant, *Synth. Met.*, 84, 111, (1997)

36. Sofi, R. Ahmed, Peter Kofinas; *J. of Magnetism and Magnetic Materials*, 288, 219-223 (2005).

37. R. B. Bjorklund and B. Liedberg, *J. Chem Soc., Chem. Commun.*, 1293 (1986).

38. C. DeArmitt and S. P. Armes, *J. Colloidal Interface Sci.*, 150, 134 (1992).

39. C. DeArmitt and S. P. Armes, *Langmuir*, 9, 652, (1993).

40. W. Zhang, Z. Yang, X. Wang, Y. Zhang, X. Wen, S. Yang, *Catalysis Communication*, 7, 408-412, (2006)

41. T.Y. Zhang, T. Oyama, A. Aoshima, H. Hidaka, J.C. Zhao, N. Serpone, *J. Photochem. Photobiol.* A 140, 163, (2001)

42. T. Watanabe, T. Takizawa, K. Honda, J. Phys. Chem. B 81, 1845, (1977).